

Office of Naval Research
Ocean Engineering Division
Arlington, Virginia 22217-5000

# Basic Studies of the Liquid State of Matter: Electrical Properties and Laser Interactions N00014-89-J-1990 and N00014-92-3-1606

Final Report
by

L. G. Christophorou and H. Faidas
Department of Physics, The University of Tennessee
Knoxville, Tennessee 37996

July 1993





CONTENTS

# I. INTRODUCTION

This report covers the period June 1989 through May 1993 of Contract 00014-89-J-1990 and the period June 1992 through December 1992 of Contract N00014-92-J-1606. The research sponsored by the Office of Naval Research (ONR) under these two contracts involves basic studies of the electrical properties of the liquid state of matter. The liquid state of matter has been characterized as "the least understood state of matter" and perhaps this is the reason the knowledge base of the liquid phase which is necessary for technological innovations is so limited compared to the solid and the gaseous phases.

Given the intrinsic difficulties associated with physical studies of liquids (liquids lack the order of the crystal and the large inter-particle distances of the gas) we set out to develop new experimental techniques for and new approaches to the study of the electrical properties of liquids. The stated goals of this research were:

(1) To establish a fundamental understanding of key basic processes and phenomena which determine the electrical properties of fluids, and

(2) To use the new knowledge provided by the basic studies to benefit technological applications, especially in the areas of electrical breakdown of liquids, radiation detectors, pulsed power switches and laser interactions in liquids.

To meet these two goals we emphasized studies in the following areas:

(a) Electron production via ionization and injection in nonpolar liquids and dense gases;
(b) Electron and ion transport in pure liquids and liquid mixtures;
(c) Electron attachment and photodetachment in liquids;
(d) Electron energetics in and mechanisms of the above processes;
(e) Electrical breakdown and partial discharge in pure liquids and mixtures at high electric fields;

(f) Technical aspects of liquids for advanced radiation detectors and pulsed power switches;

(g) Further development of liquid-filled flashlamp-operated pulsed power switch.

Our approach has been comprehensive and relied heavily on our experience and earlier work on electron conduction and interactions in low and high pressure gases [e.g., see 1-11], multiphoton ionization processes in liquids [e.g., see 12-15] and gaseous dielectrics [e.g., see 16-21]. We aimed at bringing together knowledge on photon, electron and ion interactions with molecules in fluids from the low density gas to the liquid in a comprehensive and systematic manner in order to better understand the electrical properties of the liquid state of matter. To this end we focussed on nonpolar hydrocarbon liquids with conduction bands (those with $V_o < 0$ eV; $V_o$ is the energy of the excess electron at the bottom of the liquid conduction band). The excess electrons is such liquids are quasi-free (not localized) and their transport properties and reactions are more likely to relate to gas-phase properties compared, say, to polar liquids. Excess electrons in such liquids are normally characterized by high electron mobilities; such liquids we refer to as fast. As a rule, such liquids are composed of spherically-shaped molecules and usually contain a central atom such as C, Si, Ge, or Sn with four methyl groups attached to it. They include 2,2-dimethylpropane (neopentane) (TMC; $C(CH_3)_4$); tetramethyl silane (TMS; $S_i(CH_3)_4$); tetramethyl-germanium (TMG; $Ge(CH_3)_4$), tetramethyltin (TMT; $Sn(CH_3)_4$) and 2,2,4,4-tetramethylpentane (TMP) $(CH_3)_3\ CCH_2\ C(CH_3)_3$).

The techniques we employed and the new techniques we developed for such studies, as well as the results we obtained and their utilization for applications are briefly summarized in this report. For details the reader is referred to the publications that resulted from these studies which are listed in Table 1 (see also Appendices A through E).

Table 1: PUBLICATIONS*

1. Faidas, H., Christophorou, L. G., McCorkle, D. L., and Carter, J. G., "Electron Drift Velocities and Electron Mobilities in Fast Room-Temperature Dielectric Liquids and Their Corresponding Vapors"
*Nucl. Instr. and Meth.* **A294**, (1990), pp. 575-582

2. Christophorou, L. G., Faidas, H., and McCorkle, D. L.
"Ultrafast and Ultrasensitive Dielectric Liquids/Mixtures: Basic Measurements and Applications"
In *Non-Equilibrium Effects in Ion and Electron Transport* (E. E. Kunhardt, R. Van Brunt, J. Gallagher, and D. Hudson, Eds.) *Plenum Press*, New York (1990), pp. 313-328

3. Faidas, H., Christophorou, L. G., and McCorkle, D. L.
"Electron Transport in Fast Dielectric Liquids at High Applied Electric Fields"
*Proceedings of 10th International Conference on Conduction and Breakdown in Dielectric Liquids*, Grenoble, France, September 10-14, 1990 (P. Atten, R. Tobazeon, Eds.), (1990), pp. 34-38

4. Christophorou, L. G., and Faidas, H.
"Dielectric-Liquid Pulse Power Switch"
*Proceedings of 10th International Conference on Conduction and Breakdown in Dielectric Liquids*, Grenoble, France, September 10-14, 1990 (P. Atten, R. Tobazeon, Eds.) (1990), pp. 454-458

5. Faidas, H., Christophorou, L. G., McCorkle, D. L., and Carter, J. G.
"Electron Drift Velocities in Fast Dielectric Liquids and Their Vapors"
In *"Gaseous Dielectrics VI,"* (L. G. Christophorou and I. Sauers, Eds.), *Plenum Press*, New York, (1991), pp. 179-185

6. Faidas, H., McCorkle, D. L., and Christophorou, L. G.
"Warm Liquids for SSC Calorimetry: Electron Transport and Electrical Properties"
In *"Symposium on Detector Research and Development for the SSC,"* (T. Dombeck, V. Kelly, and G. P. Yost, Eds.), *World Scientific*, New Jersey (1991), pp. 365-367

7. Faidas, H., Christophorou, L. G., and McCorkle, D. L.
"Electron Transport in Fast Dielectric Liquids at High Applied Electric Fields," *IEEE Trans. Electr. Ins.* **26**, (1991), pp. 568-573

8. Christophorou, L. G.
Chasing Electrons in Gases and Liquids
ORNL Review **24**, (No. 3&4), pp. 9-19 (1991)

9. Faidas, H., Christophorou, L. G., and McCorkle, D. L.
"Laser Photodetachment in Liquids: $C_6F_6^-$ in Tetramethylsilane"
*Chem. Phys. Lett.* **193**, (1992), pp. 487-492

10. Faidas, H. and Christophorou, L. G.
"The Low Field Electron Mobility of Tetramethylsilane"
*Nucl. Instr. Meth.* **A320**, (1992), pp. 608-609

11. Christophorou, L. G.
Linking the Gaseous and the Condensed Phases of Matter: The Slow Electron and Its Interactions
In "Linking the Gaseous and the Condensed Phases of Matter," L. G. Christophorou, W. F. Schmidt, and E. Illenberger (Eds.), *Plenum Press*, New York, 1993 (to be published)

12. Faidas, H. and Christophorou, L. G.
Photodetachment in Dense Fluids as a Function of Fluid Density
*J. Chem. Phys.* (to be published)

#Papers published under the partial support of this contract.

## II. ELECTRON AND ION TRANSPORT IN FAST DIELECTRIC LIQUIDS

### A. Background

The measurement of the electron drift velocity, the electron mobility, and the electron diffusion coefficient in nonpolar fast liquids requires the availability of fast electronics and an efficient means of injecting a short pulse of free electrons in the liquid. Based on how and where the electrons are produced in the medium the various techniques for the measurement of electron drift velocity can be divided into the following three categories.

(i) The bulk ionization techniques. In these techniques the electrons are produced by a pulse of x-rays or high-energy electrons which uniformly ionizes the entire volume of the liquid between two electrodes.

(ii) The external photoinjection techniques. In these techniques a light pulse (usually a UV laser) injects a pulse of electrons from a metal photocathode into the liquid.

(iii) The layer ionization techniques. In these methods a thin x-ray pulse or a pulsed laser beam (the latter multiphotonically) ionizes a thin slice of the medium parallel to the electrodes.

We have developed two new electron drift velocity measuring techniques: one using laser photoinjection and another using laser multiphoton (layer) ionization, in order to carry out the measurements conducted under this contract. The photoinjection technique has the advantage that the electron pulse it produces can be very nearly approximated to be a delta function in both space and time. This, in turn, allows accurate measurements in ultrafast liquids (those with very high electron drift velocities) at high electric fields where the electron drift times are very short. Furthermore, the electrons are produced in such a way that recombination and fringe field effects are negligible. Under certain circumstances the layer ionization technique can provide better accuracy at low electric fields.

### B. Experimental Techniques

Laser photoinjection technique. A schematic of the experimental set-up is shown in Fig. 1. The cell containing the sample (liquid or gas) consisted of a six way stainless steel cube with two sapphire windows for the entry and exit of the laser beam, two electrical feedthroughs for the application of high voltage and the extraction of the signal, and liquid and vacuum ports. All cell

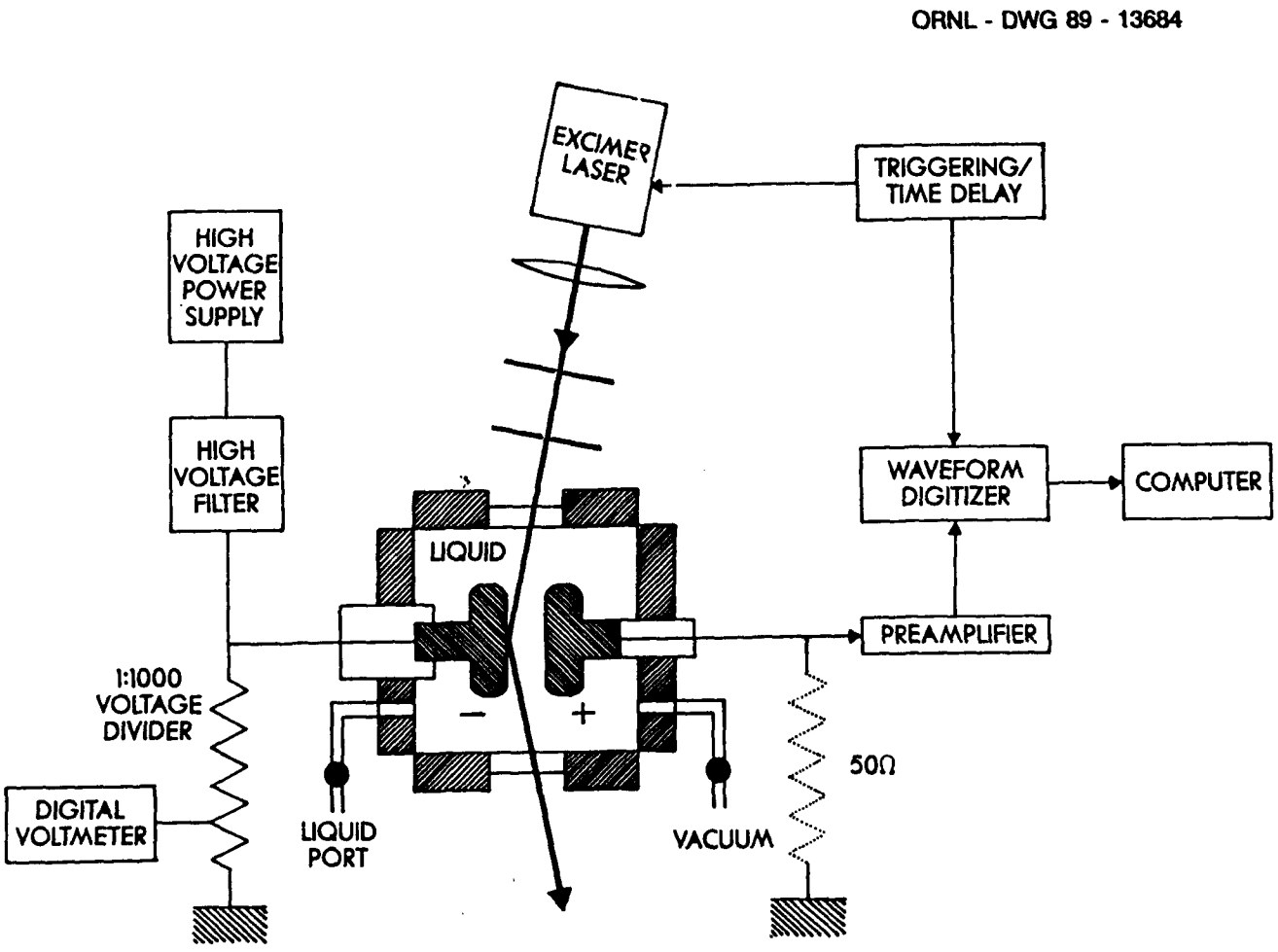


Figure 1: Experimental set-up for the drift velocity measurements. Recently the Excimer laser has been replaced by a Nitrogen laser with 600 ps pulse duration.

components were designed for high temperature (up to 400°C), high voltage (up to 40 kV) and high pressure (up to 150 atm) operation. The electrodes were two stainless steel (or aluminum) circular disks 25 to 30 mm in diameter, parallel to each other at distances, d, ranging from 2 to 7 mm. Negative voltages, V, ranging from 200 V to 40 kV corresponding to electric fields (E = V/d) up to 150 kV/cm were applied to the high voltage electrode. For the photoinjection experiments, an excimer laser ($\lambda$ = 308 nm, pulse duration ~ 15 ns) or a nitrogen laser ($\lambda$ = 337 nm, pulse duration ~ 0.6 ns) beam was striking the center of the negative electrode in a circular area of ~ 5 mm in diameter, (see Fig. 1). The electrons injected into the liquid (or the dense gas) by the laser pulse drifted under the influence of the applied uniform electric field and the signal induced on the anode was measured in two different ways.

(i) In the voltage mode (Fig. 2a) the signal was fed to a fast response (~ 3 ns) charge sensitive preamplifier with a very large input resistance (R = $10^{10}$ $\Omega$). It was then captured, averaged, and stored by a fast transient digitizer (Tektronix 7912 AD or LeCroy 9420). This mode of operation is better suited for low applied electric fields and for weak signals.

(ii) In the current mode (Fig. 2b) the signal was fed directly to the fast digitizer (bandwidth 350 MHz or better, corresponding to a risetime of less than 1 ns) through a 50 $\Omega$ input resistance. This, in effect, corresponds to electronic differentiation of the voltage mode signal and gives the transient current waveform. Typical drift times ranged from 1 $\mu$s to 30 ns. Typical voltages across the 50 $\Omega$ resistor ranged from 5 to 500 mV corresponding to transient currents from 0.1 to 10 mA. This mode of operation is better suited for high applied electric fields and for strong, fast signals.

From these waveforms the electron drift time $\tau$ - defined as the risetime of the voltage waveforms or the full width at half maximum (FWHM) of the current waveforms - was determined at each value of the applied electric field E. Once $\tau$(E) was obtained, the electron drift velocity w(E) and the electron mobility $\mu$(E) were calculated, respectively, from

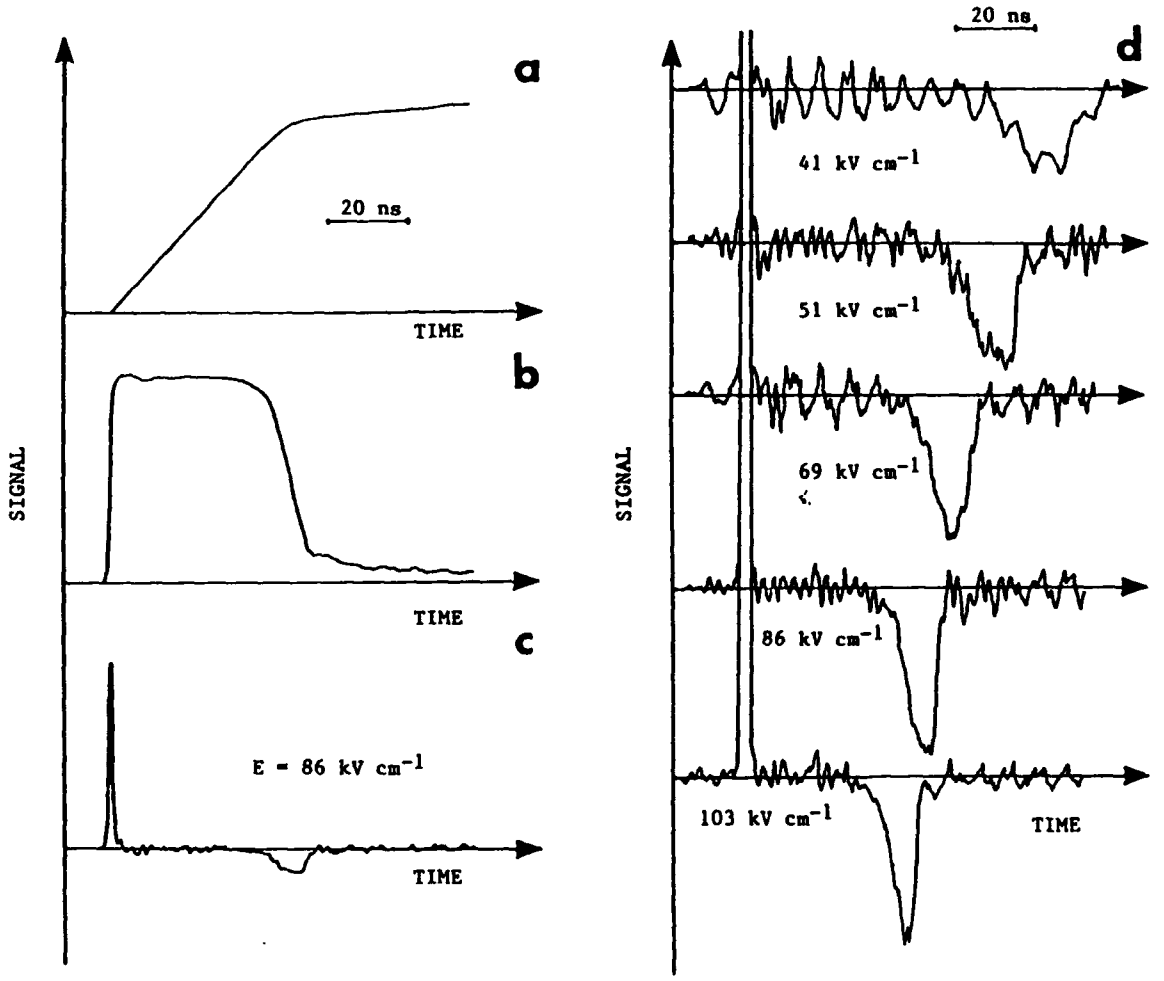


Figure 2: Voltage (a), current (b), and charge injection (c, d), waveforms measured with the Nitrogen laser.

$$w(E) = d/\tau \tag{1}$$

$$\textit{and} \qquad \mu(E) = \frac{w}{E} = \frac{d^2}{\tau V} \tag{2}$$

Numerical differentiation of the current waveforms gives the rate of charge injection at the cathode and charge collection at the anode (see Fig. 2c, d). Besides w, the analysis of the current and charge injection waveforms gave information on the electron transport processes. For example, the dispersion in the electron collection times can give information on the longitudinal electron diffusion coefficient $D_L$.

To check the accuracy of the technique for measuring w and its feasibility for measuring $D_L$ we conducted experiments on gaseous Ar whose w and $D_L$ values are known [1]. The w values we obtained were within 1 to 2 percent of the published data and the $D_L$ values were within the experimental uncertainly of 5 to 20 percent.

Laser Ionization Technique. Under certain circumstances bulk ionization (multiphoton ionization of the medium or impurities in it) might interfere with the drift velocity measurements when using the photoinjection technique (Fig. 3a). For this reason we developed the layer ionization method which gives more accurate results at low electric fields. The principle of this technique is shown in Fig. 3b. Here a short laser pulse ($\lambda$ = 337 nm, duration 0.6 ns) is used to ionize biphotonically the liquid medium. The laser beam passes through a very narrow (0.02 cm) slit and transverses the liquid parallel to the two electrode plates. The electrons drift under the influence of either a positive or a negative applied voltage and the induced signal is measured directly with a digital oscilloscope. The drift time - defined as the time interval from the onset of the signal pulse to the half-height of the signal amplitude at collection - is measured for both positive ($\tau_+$) and negative ($\tau_-$) applied voltages. The total drift time (the electron drift time from one electrode to the other) then is $\tau = \tau_+ + \tau_-$. The electron drift velocity is then calculated using Eq. (1) and the electron mobility using Eq. (2). Figure 4 shows the positive and the negative waveforms and their sum for the particular case where the laser beam passes just off the middle of the interelectrode distance. In this case the peak in the sum waveform corresponds to $\tau/2$.

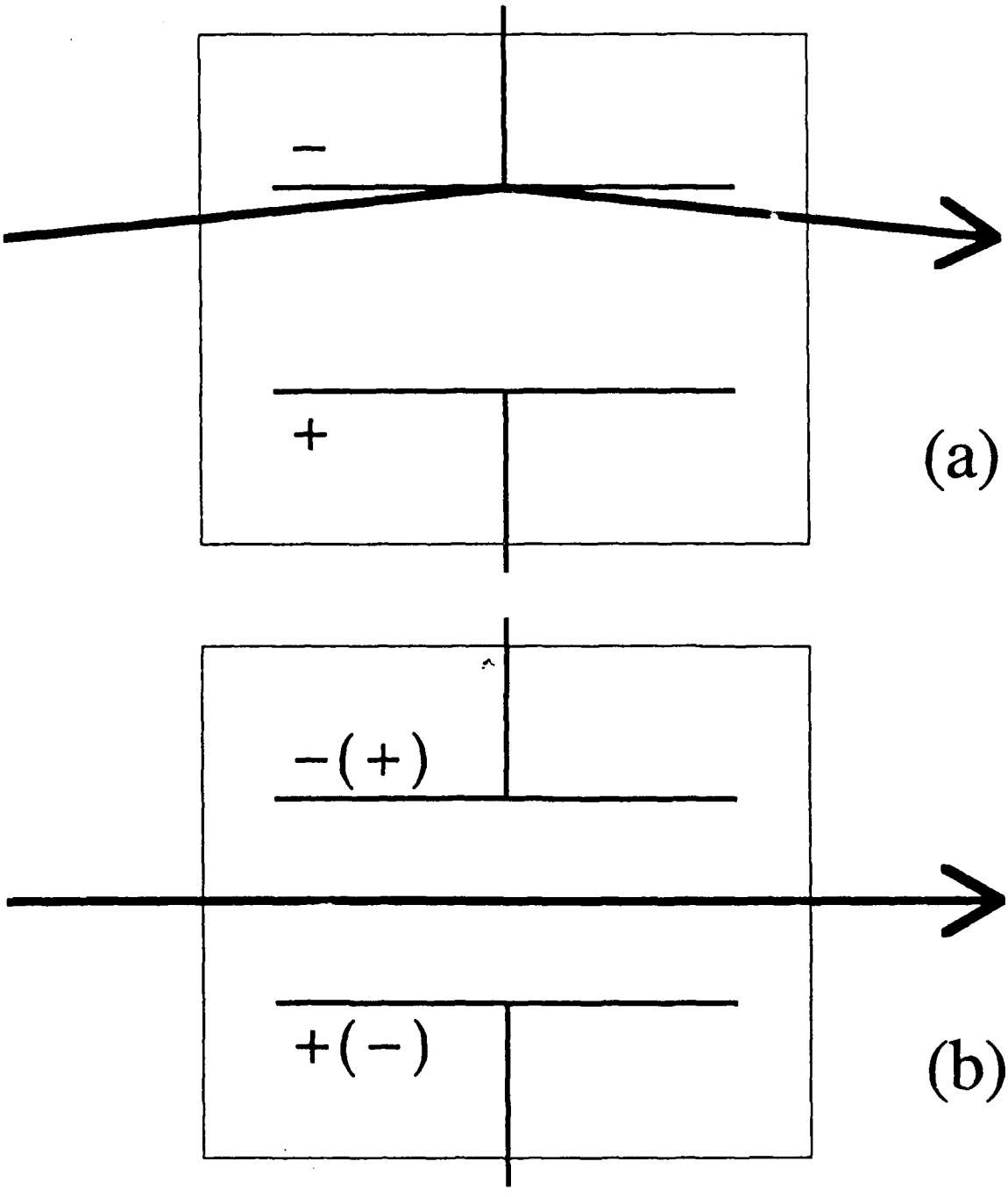


Figure 3: Laser beam path (→) in the laser photoinjection technique (a) and in the laser ionization technique (b).

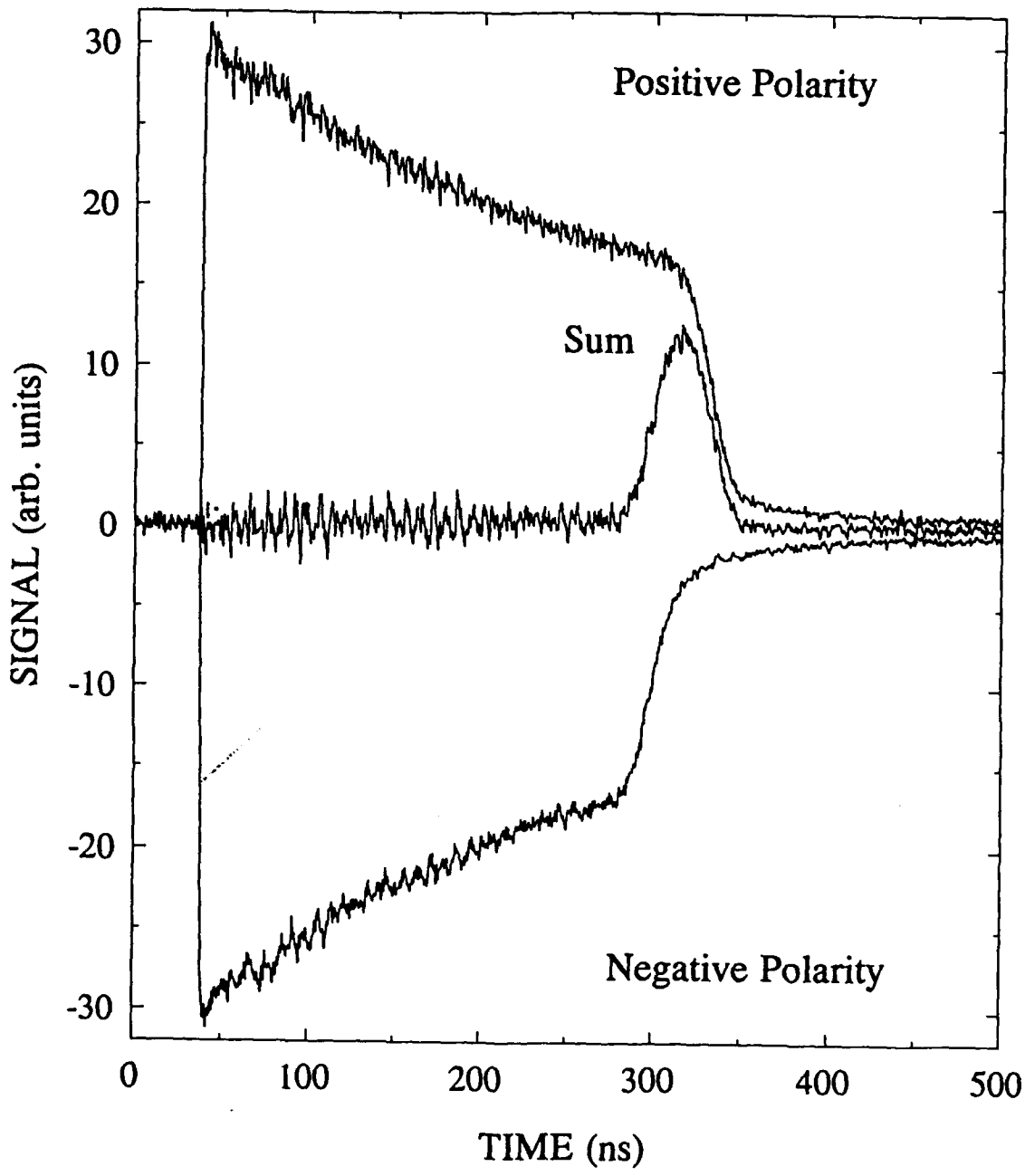


Figure 4: Positive and negative waveforms and their sum due to the drift of electrons generated by a laser beam traversing the cell in the middle of the interelectrode distance (see geometry in Fig. 3b).

Ionic Drift Velocity Measurement. Ions (positive or negative) in liquids or in dense gases are much slower than electrons (by factors of ~ $10^3$). For this reason the difficulty in measuring ionic drift velocities is not in the speed of the electronics, but rather in the sensitivity necessary to detect the weak ionic currents. Our method of measuring ionic drift velocities is essentially similar to the layer ionization technique, using the same liquid cell and electronics, but with an input resistor of 100 kΩ to 1 MΩ depending on the ionic speed. This allows for a fast and sensitive technique to measure ionic drift velocities and offers the capability, by reversing the polarity of the applied voltage, to discriminate between positive and negative ions.

C. Liquid Purification and Cell Cleaning

Thorough purification of the liquids to be studied as well as cleaning of the cell walls to remove electronegative (electron attaching) impurities is necessary to avoid unwanted electron attachment. During these studies we developed and used the following purification and cleaning protocol. The liquids (TMS, TMC, TMP, TMG, and n-pentane) were treated sequentially as follows:

i) Stirring over $H_2SO_4$ to remove olefinic impurities;

ii) Stirring with $BaCO_3$ to neutralize $H_2SO_4$;

iii) Preliminary freeze-pump-thaw cycles to remove dissolved air;

iv) Passage through traps containing NaOH pellets, activated silica gel and activated charcoal to remove $CO_2$ and $H_2O$;

v) Successive distillations under vacuum through traps at liquid $N_2$ temperature while pumping to remove $O_2$ and $N_2$;

vi) Storing and stirring over liquid NaK for over 24h to remove remaining $O_2$ or $H_2O$;

vii) Transfer into the cell through a 0.5 μm filter;

viii) An electrostatic precipitator - built into the cell - further purified the liquid for ~ 24h before and during the measurements.

The above protocol was followed for all liquids except TMT which reacts with $H_2SO_4$ and NaK. For this liquid the corresponding purification steps were omitted.

The cell components (cell body, windows, feedthroughs, valves, and electrodes) were cleaned as follows:

i) Rubbing the cell walls with ethanol or acetone-wetted cotton applicators to remove any deposits from previous experiments;

ii) Cleaning with acetone in an ultrasonic bath for 1 to 2h;

iii) *Drying in an evacuated oven heated at* 150°C;

iv) Following assembly, heating to 200°C and pumping down to ~ 1 x $10^{-7}$ Torr for several days before the liquid was introduced into the cell.

D. Results

Motion of Excess Electrons in Dielectric Liquids. We measured electron drift velocities and electron mobilities in neat neopentane (TMC), tetramethylsilane (TMS), tetramethylgermanium (TMG), tetramethyltin (TMT), tetramethylpentane (TMP), and in mixtures of TMS with n-pentane (molar ratio, M = 102/1, 17/1, and 5.6/1) and TMS with TMP (M = 1.31/1). The w(E) and μ(E) measurements for neat TMC, TMS, TMG, TMT, and TMP are shown in Figs. 5 and 6 and those for the mixtures of TMS with n-pentane and TMP are shown in Figs. 7 and 8.

The salient features of the w(E) data for both the neat liquids and the mixtures are: At low fields and up to a critical field $E_c$, w increases linearly with E and $\mu = w/E = \mu_{th}$ = constant. For $E < E_c$ the electrons are in thermal equilibrium with the molecules of the medium and their mean energy is ~ 1.5 kT. As the field increases beyond $E_c$ the electrons progressively gain energy from the field, their mean kinetic energy becomes > 1.5 kT and the w vs E dependence becomes sublinear. At sufficiently high E values, w(E) tends towards saturation. For all the liquids/mixtures studied, however, saturation was not reached up to the highest fields applied. In Table 2 are summarized the mole ratio M, the critical field $E_c$, the thermal electron mobility $\mu_{th}$, the maximum electric field reached $E_{max}$, and the corresponding maximum drift velocity $w_{max}$ measured for the liquids/mixtures studied. Generally, the maximum field reached in each liquid (except as noted in Table 2) was determined from the voltage where electrical breakdown occurred. For most liquids this was ~ 120 kV/cm, except for TMT where breakdown occurred at 75 kV/cm and the TMS/n-pentane mixtures where fields of ~ 140 kV/cm were reached without electrical breakdown.

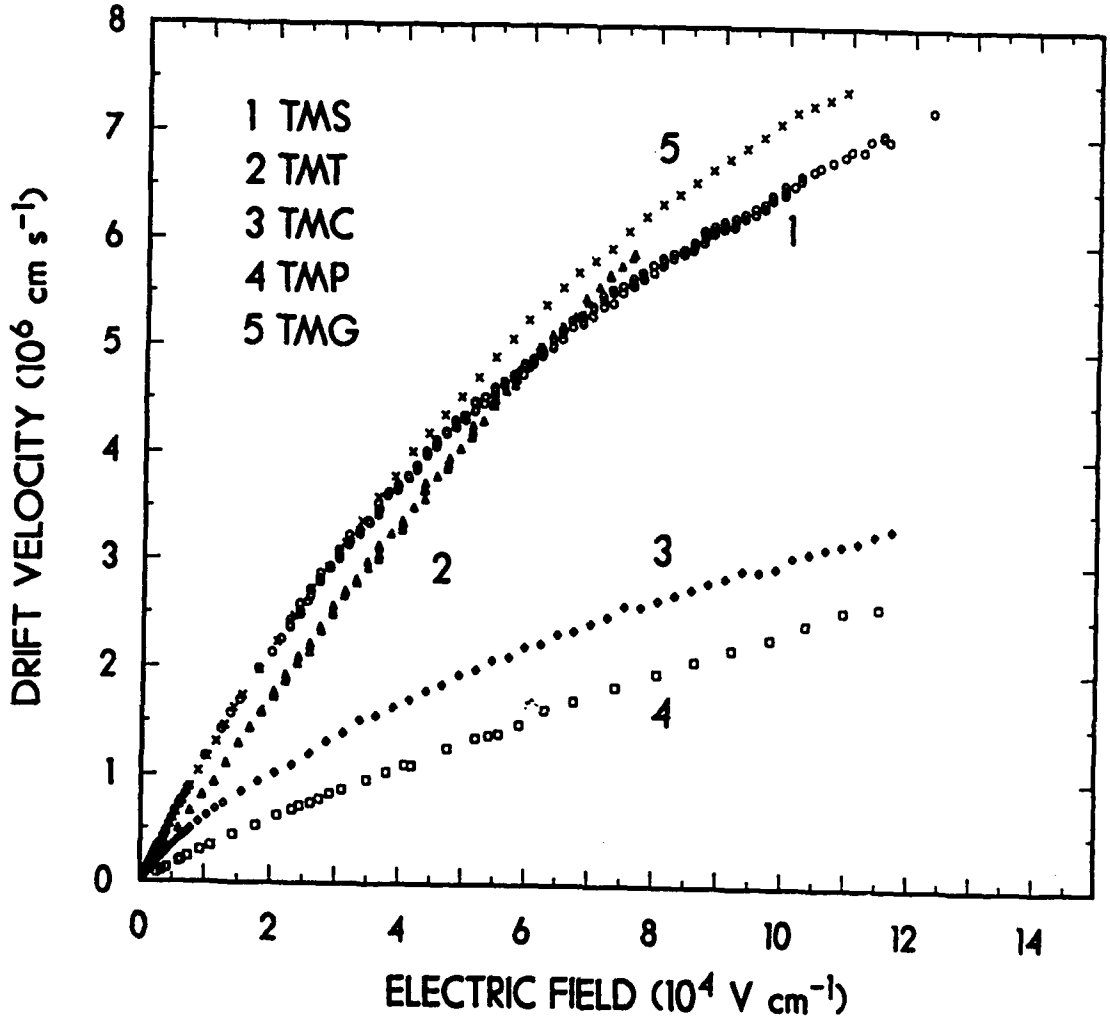


Figure 5: Electron drift velocity as a function of applied electric field for TMS, TMT, TMC, TMP, and TMG.

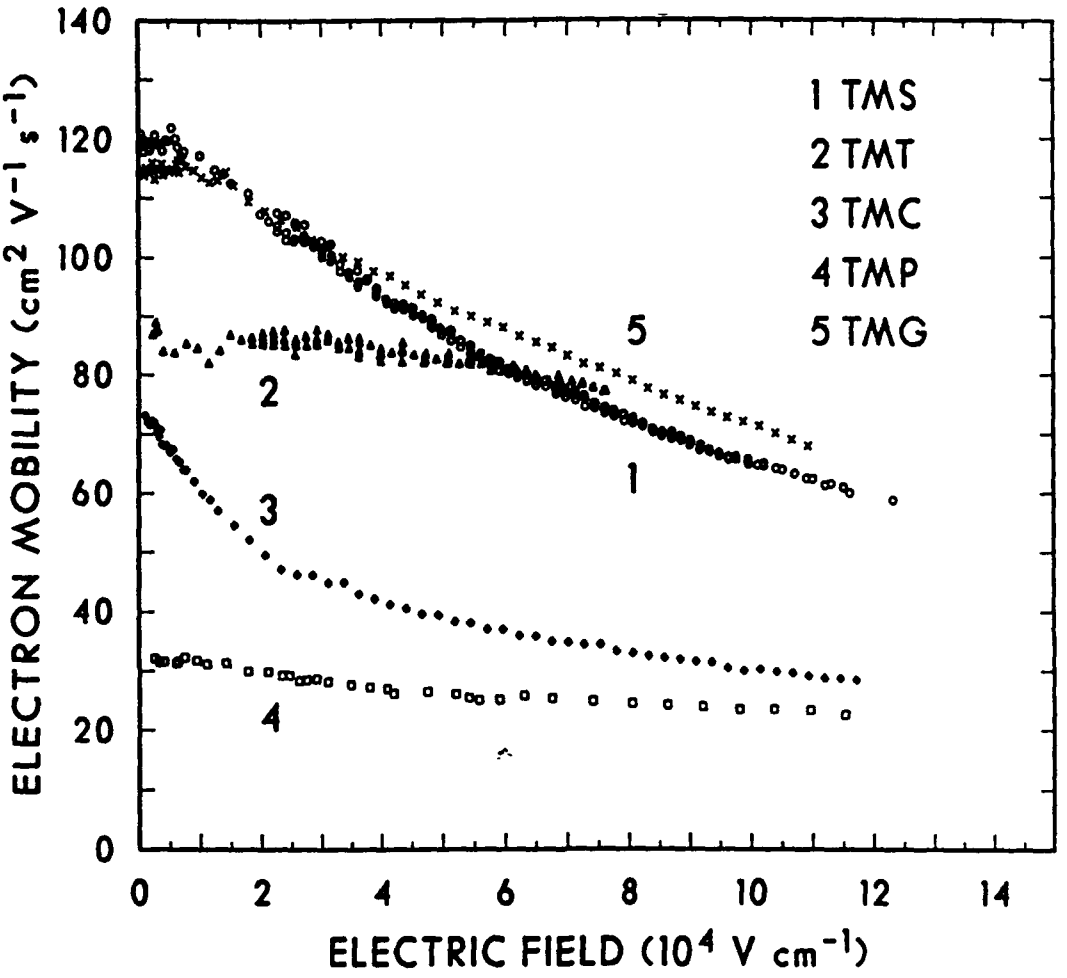


Figure 6: Electron mobility as a function of applied electric field for TMS, TMT, TMC, TMP, and TMG.

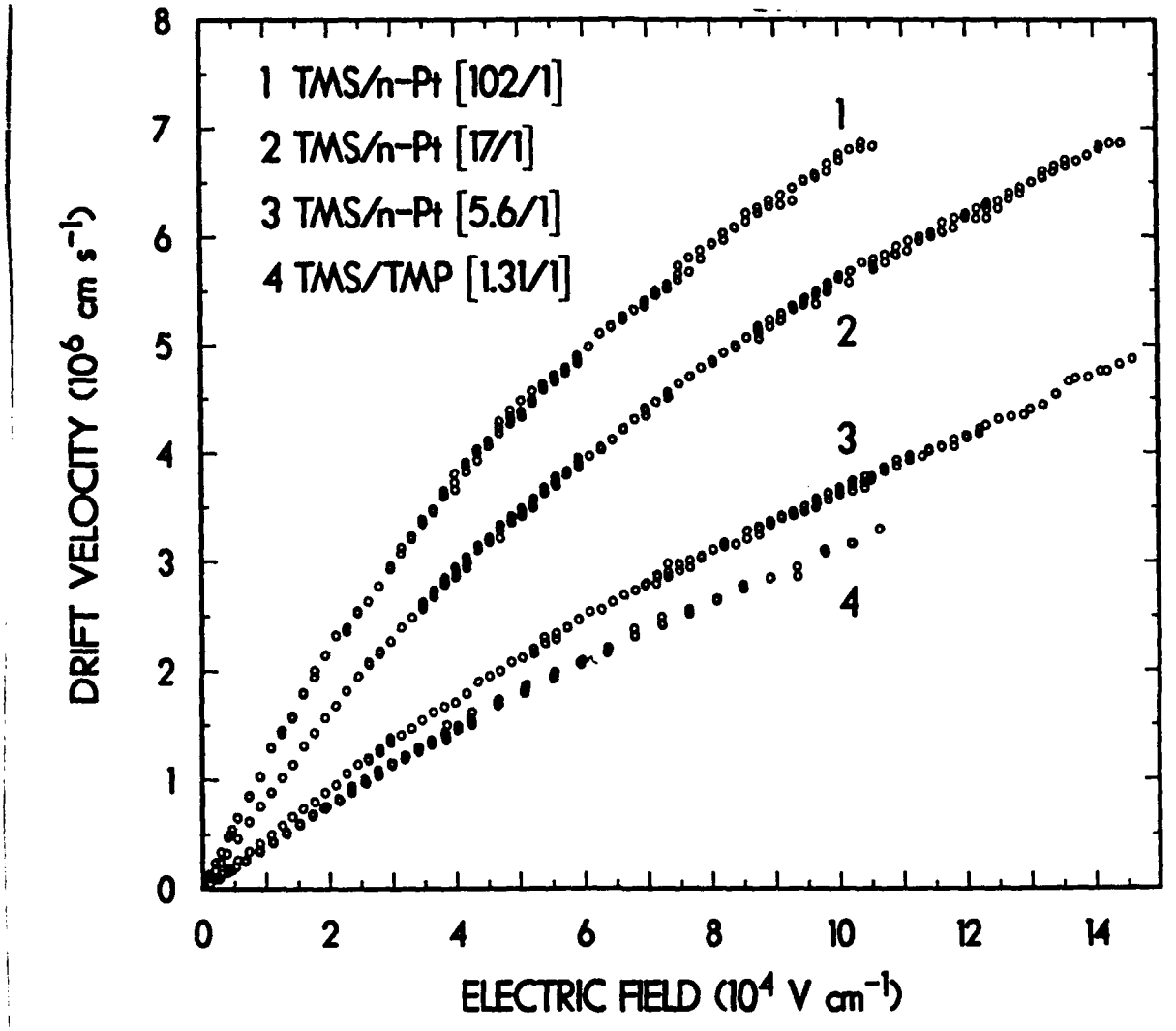


Figure 7: Electron drift velocity as a function of applied electric field for mixtures of TMS with TMP and n-Pt (n-pentane).

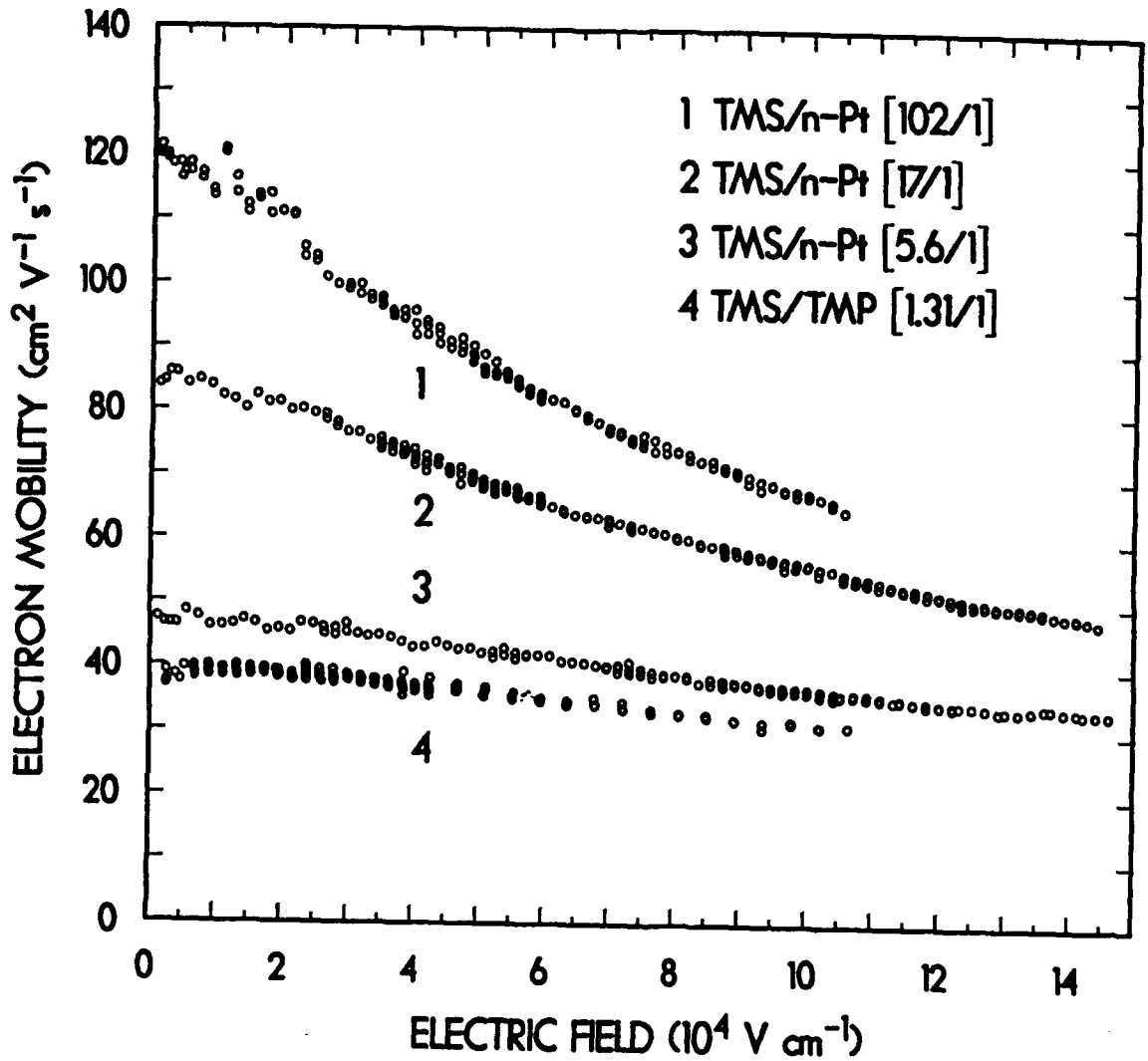


Figure 8: Electron mobility as a function of applied electric field for TMS in TMP and n-Pt (n-pentane).

TABLE 2: Mole Ratio M, Critical Electric Field $E_c$, Thermal Electron Mobility $\mu_{th}$, Maximum Electric Field $E_{max}$, and Maximum Electron Drift Velocity $w_{max}$, for the Fast Neat Liquids and Mixtures Studied

| Liquid/.Mixture | M | $E_c$ (kV $cm^{-1}$) | $\mu_{th}$ ($cm^2$ $s^{-1}$ $V^{-1}$) | $E_{max}$ (kV $cm^{-1}$) | $w_{max}$ ($10^6$ cm $s^{-1}$) |
|---|---|---|---|---|---|
| TMC | Neat | 3.5 | 71.5 | 116[a] | 3.3 |
| TMS | Neat | 7 | 111±4 | 125 | 7.2 |
| TMG | Neat | 15 | 114.7 | 109[b] | 7.4 |
| TMT | Neat | 30 | 85.7 | 75 | 6.0 |
| TMP | Neat | 15 | 31.8 | 115 | 2.6 |
| TMS/TMP | 1.31/1 | 18 | 39.1 | 105 | 3.2 |
| TMS/n-pentane | 102/1 | 7 | 111 | 105[a] | 6.8 |
| TMS/n-pentane | 17/1 | 8 | 85 | 145[a] | 6.8 |
| TMS/n-pentane | 5.6/1 | 15 | 47.6 | 145 | 4.9 |

[a]$E_{max}$ was not limited by electrical breakdown.
[b]Electrical breakdown occurred at 120 kV $cm^{-1}$.

Electron Motion in Dense Vapors/Comparison of Electron Motion in Dense Gases and Liquids. In Fig. 9 are shown the w(E/N) measurements for gaseous and liquid TMS, TMP, and TMC. The measurements were taken at room temperature (~ 295 K) and at vapor pressures of 500 and 680 Torr for TMS, 600 Torr for TMC, and 21.15 Torr for TMP. In Table 3 are listed the gas and the corresponding liquid number densities N, the thermal mobility $\mu_{th}$, the density-normalized electron mobility $\mu_n = \mu_{th} N$ and the ratio of the liquid to the gaseous normalized mobility R.

Clearly the gases have much lower $\mu_n$ values than the corresponding liquids. The ratio $(\mu_n)_L/(\mu_n)_G$ is 62.2, 13.9, and 11.3 for TMS, TMC, and TMP respectively. Also the gases exhibit a supralinear w-E dependence at intermediate E/N values before they reach a saturation w-value of (5 to 8) x $10^6$ cm $s^{-1}$, while the liquids show a sublinear w-E dependence. The larger values of $(\mu_n)_L$ compared to $(\mu_n)_G$ indicate that at thermal and near-thermal energies, the electron scattering cross sections in these liquids are smaller than in the corresponding gases.

Ionic Drift Velocities and Mobilities. Using the layer ionization technique we measured the ionic drift velocity of $C_6F_6^-$ and $TMS^+$ in liquid TMS and of $C_6F_6^-$ in gaseous TMS (600 Torr). For the field values employed, the mobility ($\mu_i = w_i/E$) was 9 x $10^{-4}$ $cm^2$ $s^{-1}$ $V^{-1}$ for $C_6F_6^-$ in liquid TMS and 3.5 x $10^{-1}$ $cm^2$ $s^{-1}$ $V^{-1}$ for gaseous TMS. The mobility of the positive ion was 6 x $10^{-4}$ $cm^2$ $s^{-1}$ $V^{-1}$.

Figure 10 shows the mobility plotted as a function of the applied electric field. The slightly higher mobility values at low fields are due to space charge effects that appear at the lower fields.

In comparing the liquid and gaseous ionic mobilities it should be noted that the number density of liquid TMS is 4.424 x $10^{21}$ molecules $cm^{-3}$ while the density of gaseous TMS (at 600 Torr) is 2.29 x $10^{19}$ molecules $cm^{-3}$.

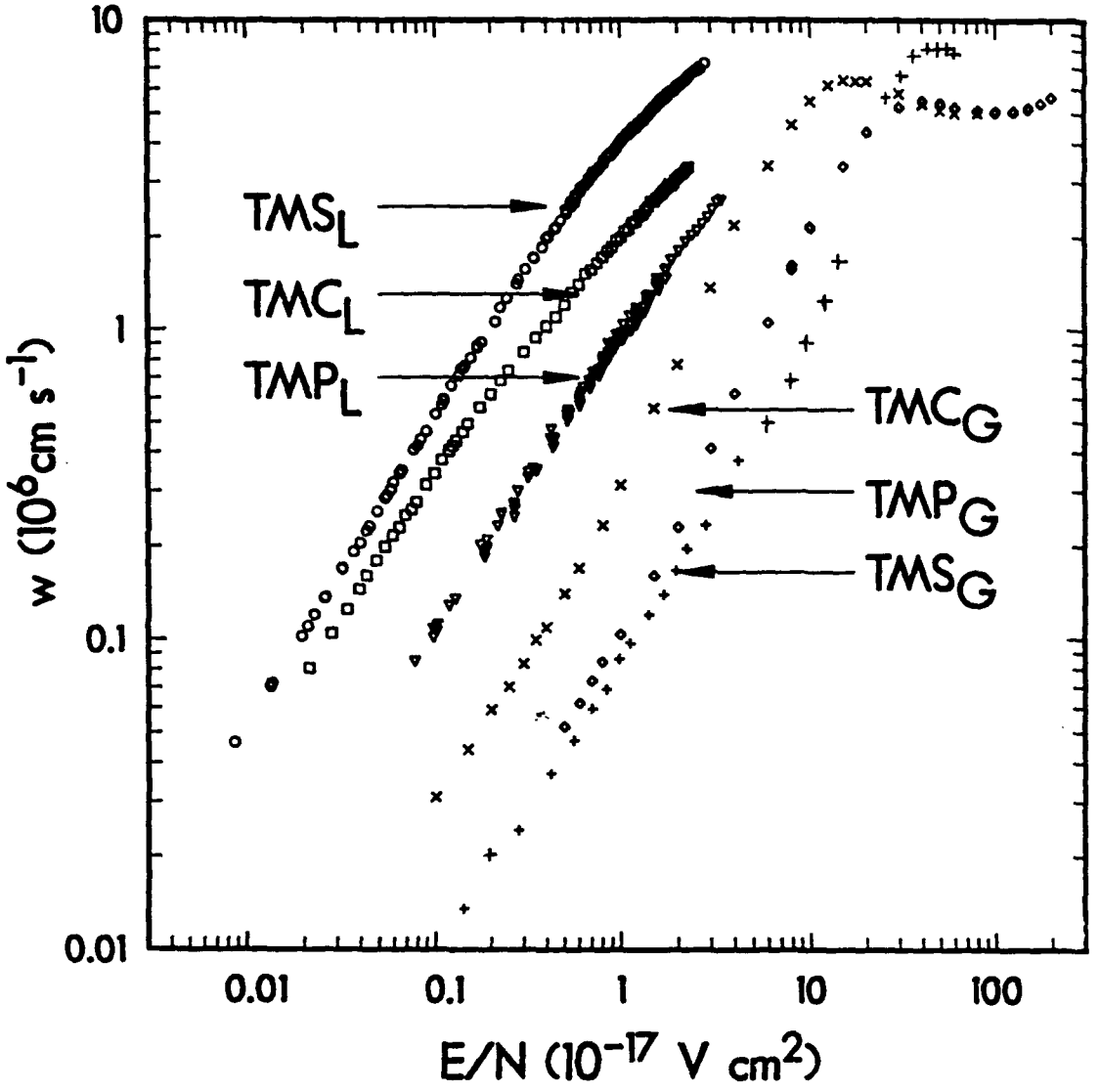


Figure 9: Electron drift velocity as a function of the density-reduced electric field (E/N) for liquid and gaseous TMS, TMC, and TMP.

TABLE 3: Vapor Pressure, Number Density N, Thermal Electron Mobility $\mu_{th}$, Density-Normalized Electron Mobility $\mu_n$, and the Ratio, R, for Liquid and Gaseous TMC, TMS, and TMP

| | TMC | | TMS | | TMP | |
|---|---|---|---|---|---|---|
| | Liquid | Gas | Liquid | Gas | Liquid | Gas |
| Vapor Pressure [Torr] | | 600 | | 680 | | 21.15 |
| N [Molecules $cm^{-3}$] | $5.121x10^{21}$ | $1.963x10^{19}$ | $4.423x10^{21}$ | $2.224x10^{19}$ | $3.378x10^{21}$ | $6.804x10^{17}$ |
| $\mu_{th}$ [$cm^2\ s^{-1}\ V^{-1}$] | 71.5 | 1,338 | 111 | 354.7 | 31.8 | 13,959 |
| $\mu_n$ [$s^{-1}\ V^{-1}\ cm^{-1}$] | $3.66x10^{23}$ | $2.63x10^{22}$ | $4.91x10^{23}$ | $7.89x10^{21}$ | $1.07x10^{23}$ | $9.5x10^{21}$ |
| $R = (\mu_n)_L/(\mu_n)_G$ | 13.9 | | 62.2 | | 11.3 | |

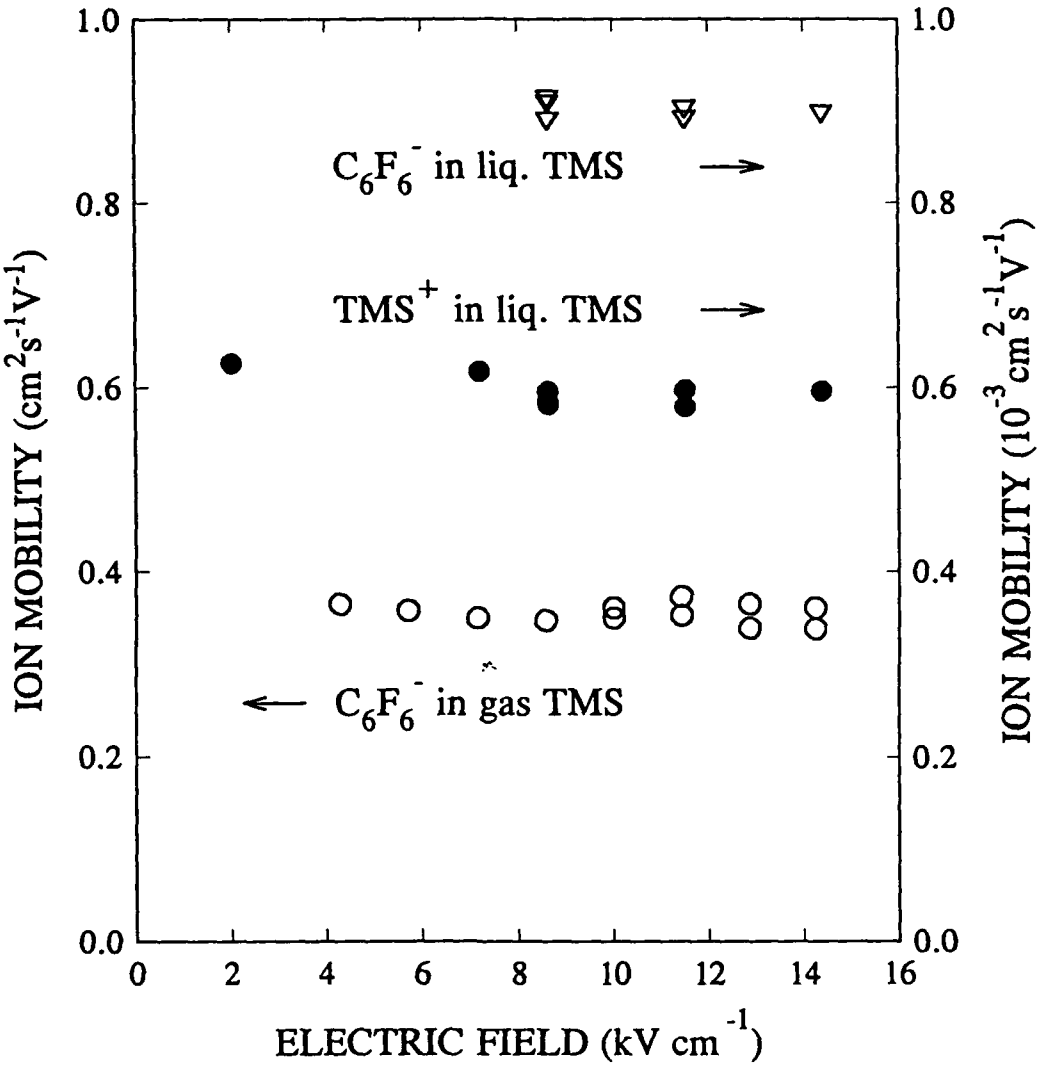


Figure 10: Mobility of $C_6F_6^-$ in liquid TMS (∇) and in gaseous TMS (o) as a function of E. Also given is the mobility of $TMS^+$ in liquid TMS as function of the applied electric field E.

## III. STABILITY OF NEGATIVE IONS IN LIQUIDS: ELECTRON PHOTODETACHMENT

### A. Background

All electrons produced in a liquid or in a gaseous medium ultimately get attached to signle molecules, clusters of molecules or the bulk medium or to electronegative impurities present in the fluid. The free electron half-life, $\tau_{1/2}$, is determined by the concentration and the attachment rate constant of the electron attaching species. It is, therefore, essential in many applications to know the stability of the various negative ions formed and the minimum energy required to photodetach them and the corresponding photodetachment cross section.

The photodetachment of electrons from negative ions in low-pressure gases is well-understood and the relation of the photodetachment threshold $E_{th}$ to the electron affinity, EA, of the electron attaching species is well-established[1,10]. Near threshold, the photodetachment cross section, $\sigma_{pd}$, is predicted to vary as

$$\sigma_{pd}(E) = BE(E-E_{th})^{(2l+1)/2}\alpha k^{2l+1}, \tag{3}$$

where B is a constant, E = hυ is the photon energy, and k and $l$ are the linear and angular momenta of the ejected electron. For atoms, A, the value of the $E_{th}$ for the process

$$A^- + h\nu \rightarrow A + e \tag{4}$$

is equal to the electron affinity EA(A) of A, which in turn, is equal to the "vertical detachment energy" (VDE). For molecules, M, the relation of $E_{th}$ for the process

$$M^- + h\nu \rightarrow M + e \tag{5}$$

to the electron affinity, EA(M), of M and the VDE is complicated by possible differences in the structural parameters of M and $M^-$. If we define the VDE for (5) as the minimum energy required to eject the electron from the negative ion in its ground electronic and molecular state without changing the internuclear separations, then the VDE is related to the EA and $E_{th}$ by

$$E_{th} = VDE = EA + \Delta E, \tag{6}$$

i.e., the VDE for (5) exceeds the EA by ΔE; the magnitude of ΔE depends on the relative positions of the potential energy curves (surfaces) of M and $M^-$.

The photodetachment of electrons from negative ions in dense gases and liquids has been studied for only a limited number of cases. Even more limited seem to be the measurements of the photodetachment cross sections. Establishing the energetics and the cross sections for photodetachment as a function of the nature and density of the medium is significant because it gives a direct measure of the stability of the anion in dense matter and because it provides a basic input for understanding electron transfer mechanisms in dense matter.

In dense gases and liquids the photodetachment process for molecular negative ions is complicated by the effect of the medium on $E_{th}$ and the potential energy curve (surface) of $M^-$. Rewriting reaction (5) for the liquid as

$$M_L^- + h\nu \rightarrow M_L + e_L \tag{7}$$

and assuming that $(EA)_L = (EA)_G + V_o\text{-}P^-$ (Refs. 9,11) we have

$$(E_{th})_L = (VDE)_L = (EA)_L + (\Delta E)_L$$

$$= (EA)_G + V_o - P^- + (\Delta E)_L \tag{8}$$

where $V_o$ and $P^-$ are the polarization energies of the electron and the negative ion in the medium, and $(EA)_L$ and $(EA)_G$ are the values of the electron affinity of M in the liquid and the gas phase. Below we describe a new method developed - in part - under this contract to measure absolute photodetachment cross sections for negative ions in liquids or dense gases and photodetachment thresholds. The method has been successfully applied to the photodetachment of $C_6F_6^-$ is TMS. The results of this study are summarized (see also Appendix B).

B. The Experimental Method

The experimental method we developed for photodetachment studies in liquids utilizes a two-laser photoconductivity technique. A schematic of the experimental arrangement and an outlay of the principle of the technique is shown in Fig. 11. A cell contains the molecule ($C_6F_6$) under study dissolved in the liquid (TMS) at an appropriate concentration. The photodetachment cell was a six way stainless steel cube with two quartz windows and two electrical feedthroughs facing each other. The two parallel electrodes were held at a distance of 4.5 mm and at a potential difference of 9 kV (E = 20 kV/cm). Two counter-propagating coaxial laser beams traverse the interaction volume in the liquid cell with a time delay of ~ 5 μs. The first laser beam from an excimer laser ($\lambda$ = 308 nm; *f*whm = 15 ns) ionizes biphotonically the liquid and produces electrons which give rise to a fast signal (initial drop in Fig. 11b identified by ↓ and the process $nh\upsilon + X \rightarrow X^+ + e$). These electrons quickly (within < 1 ns) attach to $C_6F_6$ forming $C_6F_6^-$ (process $e + M \rightarrow M^-$ in Fig. 11b); the slow falling portion of the signal (indicated by $M^-$ in Fig. 11b) after the initial steep fall is due to these slow-moving anions. At the preset time delay (~ 5 μs), the second laser pulse (tunable dye laser, *f*whm = 0.6 ns) detaches the electron from $C_6F_6^-$ (when $h\upsilon > (E_{th})_L$) and produces a second transient signal (step drop in Fig. 11b identified with ↓ and $h\upsilon + M^- \rightarrow M + e$), followed by a slow drop when the detached electrons attach to $C_6F_6$ again forming slow moving $C_6F_6^-$. Figure 12 shows an actual trace of the photodetachment signal.

The basis for determining the photodetachment cross section $\sigma_{pd}(E)$ as a function of the photon energy E can be seen by referring to Fig. 13. The first (excimer) laser pulse has an essentially flat intensity profile $I_e(r)$ for distances $r < \alpha$ where $\alpha$ is the radius of the cross sectional area of the interaction volume (Fig. 13a). This pulse generates electrons uniformly in the interaction volume with a density distribution $n_{ei}(r) \propto I_e^2(r)$. Under the experimental conditions we employed all these electrons were captured by $C_6F_6$ within 1 ns and the resultant negative ions $C_6F_6^-$ were essentially stationary with an ion density distribution $n_i(r) = n_{ei}(r) \propto I_e^2(r)$ when the second (tunable dye) laser pulse arrived ~ 5 μs later. The intensity profile $I_d(r)$ of the dye laser pulse was Gaussian and lay well within $\alpha$ (Fig. 13c). The density distribution, $n_{ed}(r)$, of the photodetached electrons is

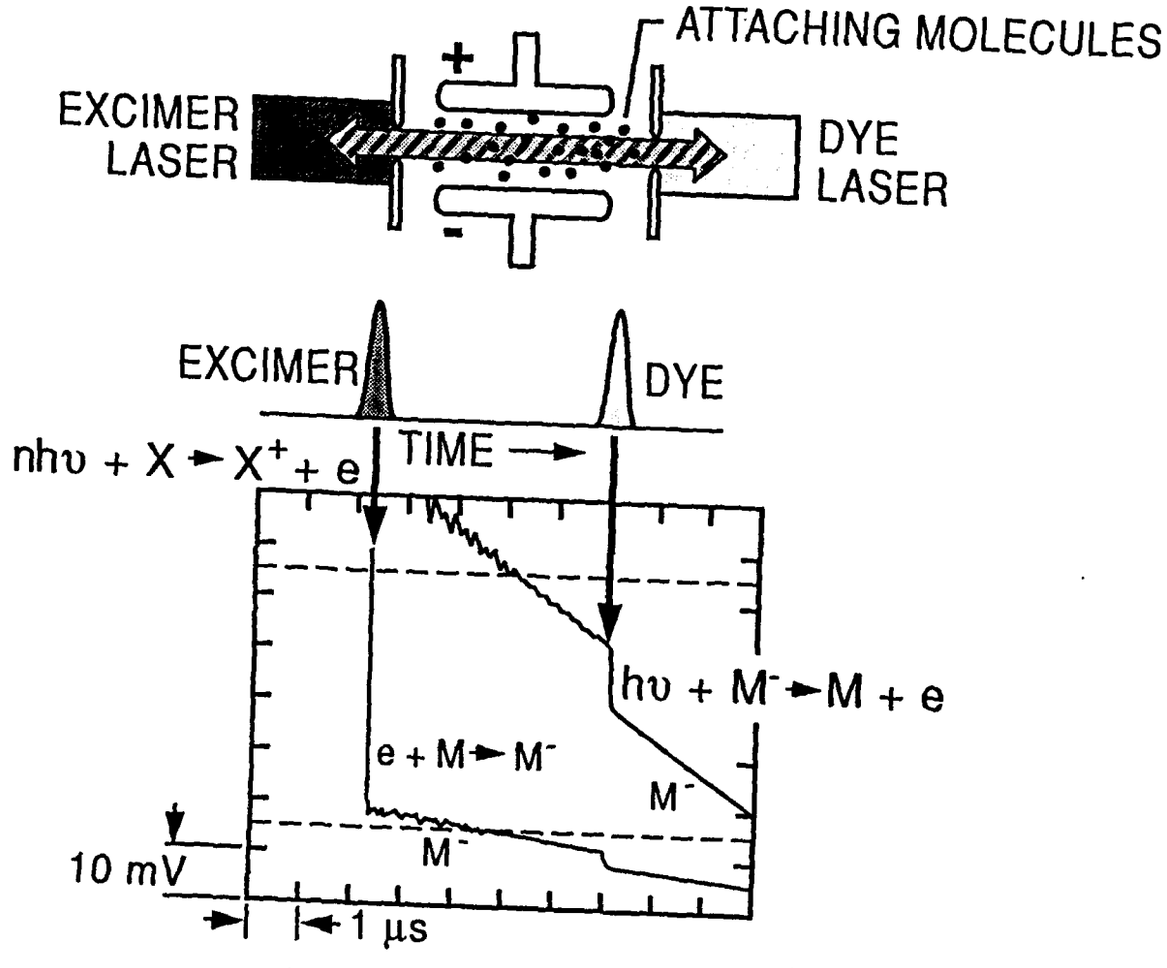


Figure 11: Schematics of two laser photodetachment technique and an oscillogram of the conductivity signal.

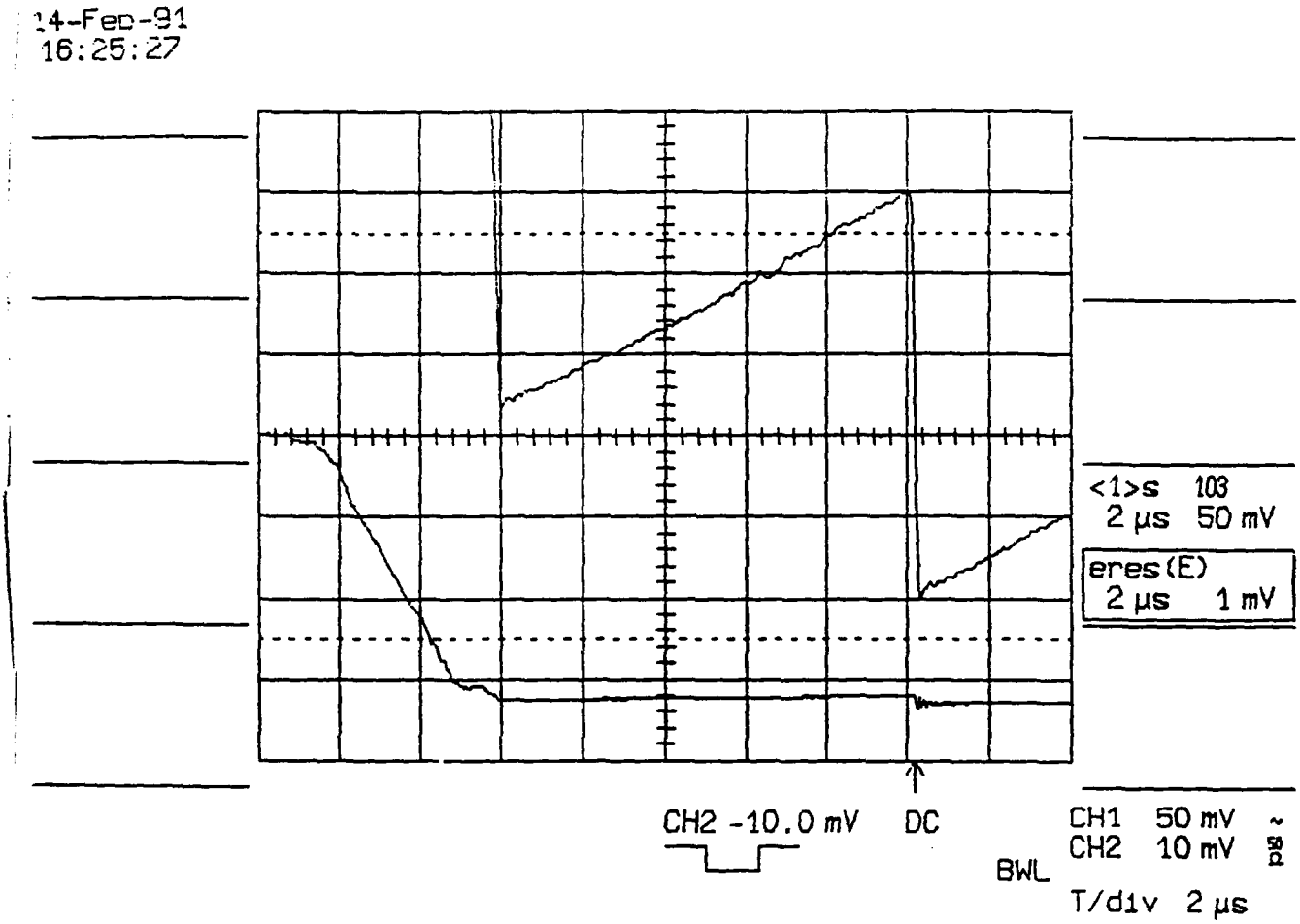


Figure 12: Oscilloscope trace of photodetachment signal. Lower trace is entire signal. Upper trace is the photodetachment signal ($\lambda$ = 500 nm) amplified 50 times.

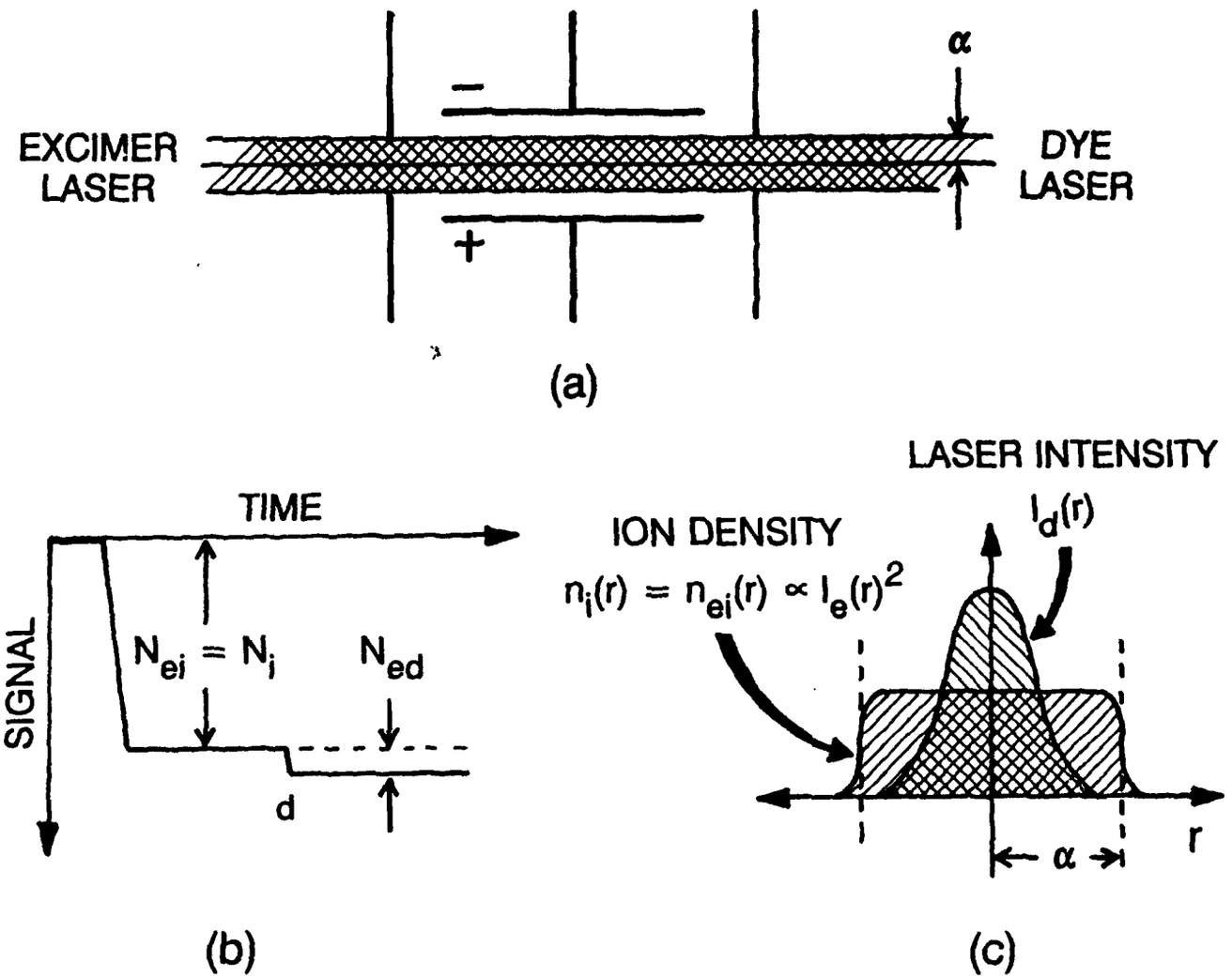


Figure 13: Schematics of the photodetachment technique illustrating: (a) the laser interaction region, (b) the type of signal measured, and (c) the laser intensity and negative ion density profiles.

$$n_{ed}(r) = \sigma_{pd}(E)\, n_i(r)\, I_d(r) \qquad (9)$$

Under the experimental conditions employed, $n_{ed}(r) << n_i(r)$, the $I_e(r)$, $n_i(r)$, and $I_d(r)$ were virtually constant along the axis of the interaction volume, and

$$\sigma_{pd}(E) = \frac{N_{ed}}{N_i}\,\frac{\pi a^2}{I_l} \qquad (10)$$

Thus, $\sigma_{pd}(E)$ can be determined from a measurement of the ratio $N_{ed}/N_i$ of the total number of photodetached electrons, $N_{ed}$, to the total number of negative ions $N_i$, a measurement of the total number of photons in the dye laser pulse $I_t$ and a knowledge of $\alpha$ and the intensity profiles of the two laser beams.

C. Photodetachment Threshold and Photodetachment Cross Section for $C_6F_6^-$ in TMS

The method we developed for studies of photodetachment in liquids has been employed to investigate the photodetachment of $C_6F_6^-$ in TMS. Photodetachment measurements were carried out at dye laser intensities such that $N_{ed}/N_i$ (Eq. (10)) was small ($\leq 0.03$) and consequently $N_{ed}/N_i$ depended linearly on $I_t$ (see Fig. 14). In Fig. 15 is shown $\sigma_{pd}(E)$ for $C_6F_6^-$ in TMS (T = 298 K) for $1.63 \leq E \leq 3.44$ eV corresponding to $360 \leq \lambda \leq 760$ nm. The cross section exhibits well-defined maxima at 2.58 and 3.15 eV; the $\sigma_{pd}$ value of the maxima is about the same and equal to ~ 11 x $10^{-18}$ $cm^2$. To determine the photodetachment threshold $(E_{th})_L$ from the experimental measurements in Fig. 15 we used Eq. (3) which we rewrite as

$$(\sigma_{pd}/E)^{1/n} = B[E-(E_{th})_L] \qquad (11)$$

with $n = 1/2(2l+1)$. The best fit of Eq. (11) to the data was obtained with a 3/2 power law, that is $n = 3/2$ and $l = 1$, for the energy range 1.63 to 1.95 eV. This gave $(E_{th})_L = 1.51$ eV.

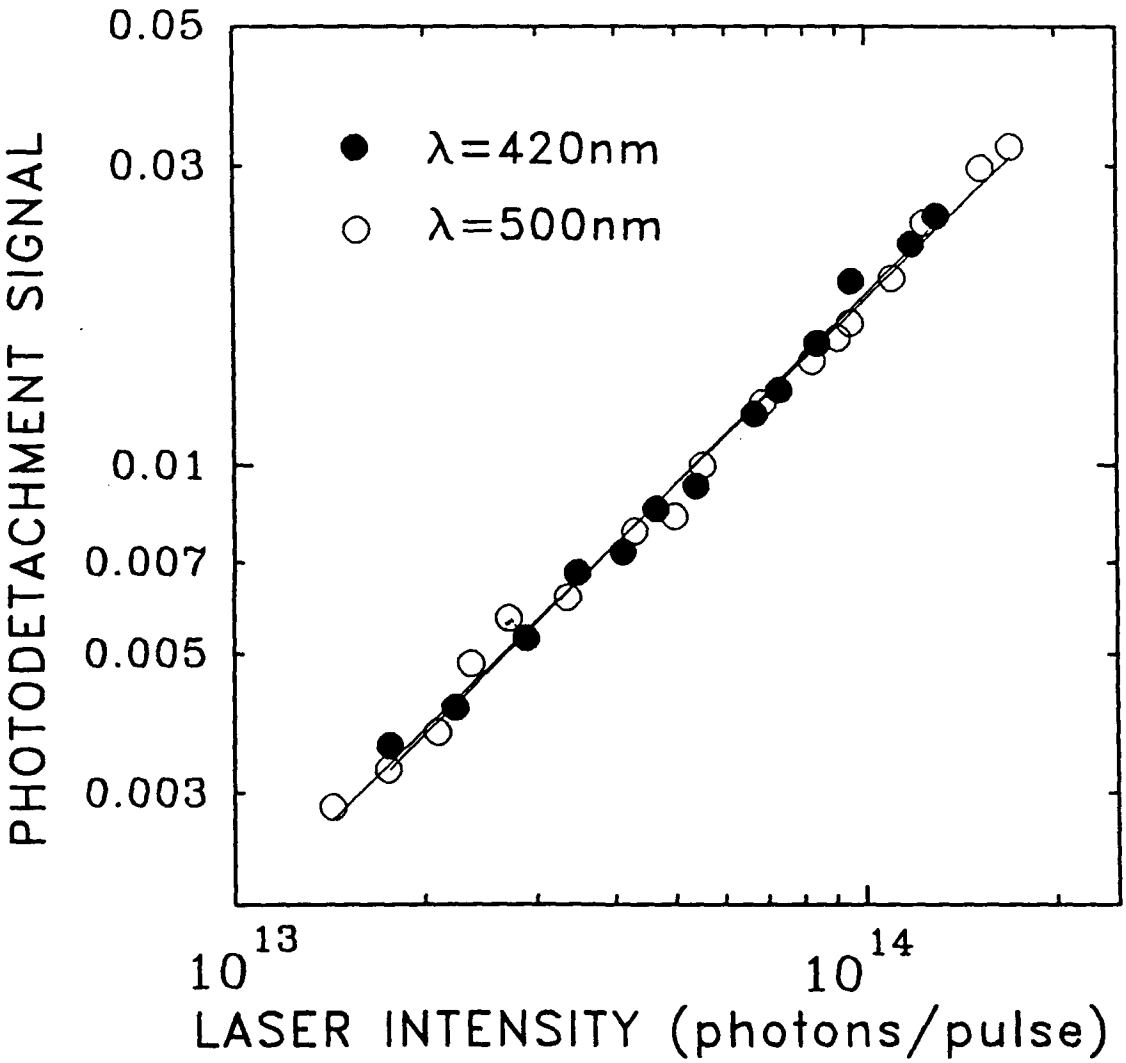


Figure 14: The photodetachment signal ($\propto N_{ed}/N_i$) as a function of the detaching laser intensity (photons/pulse) at $\lambda$ = 420 (●) and 500 (○) nm. The slope of the data at both wavelengths is one indicating a linear dependence.

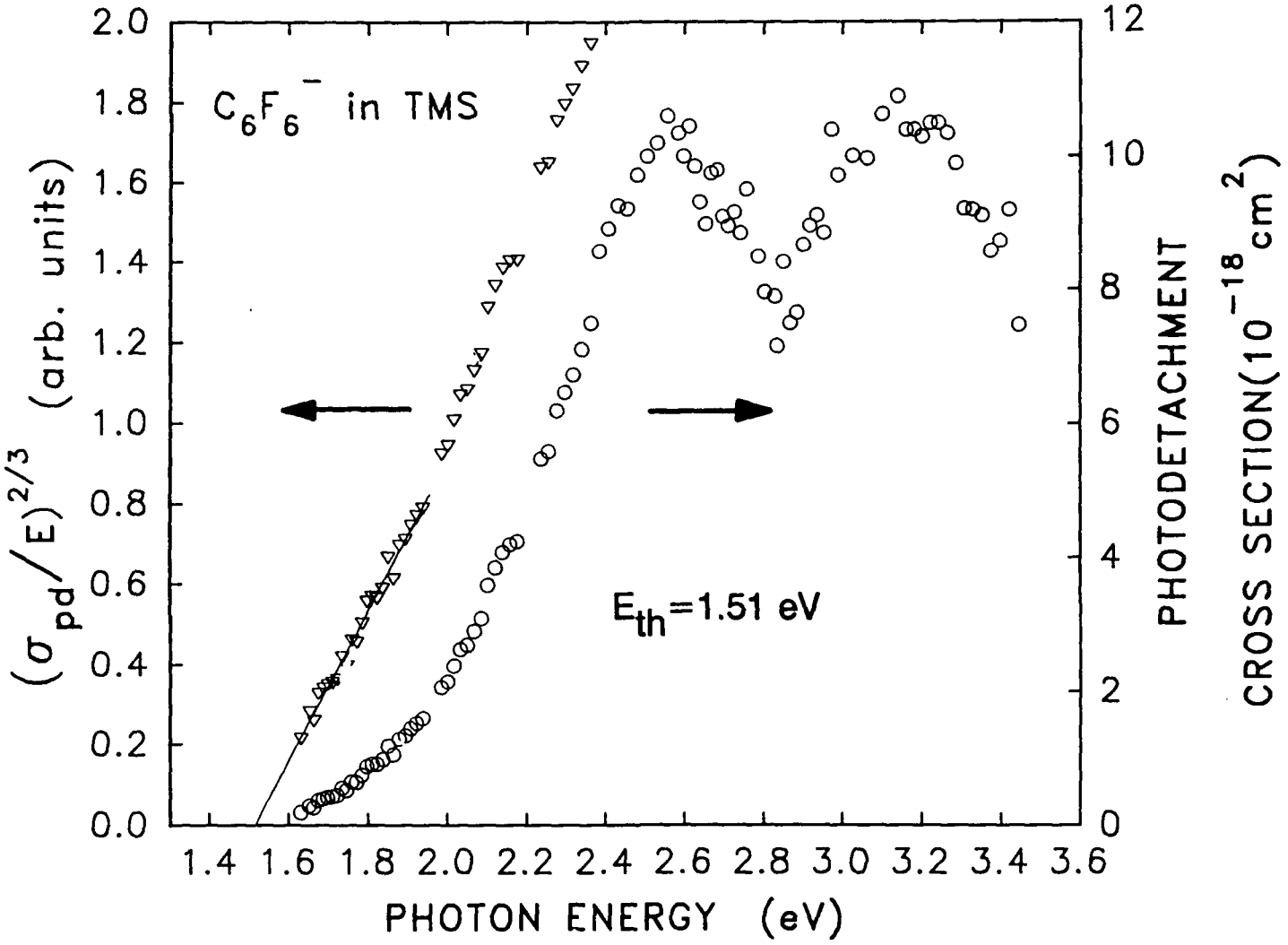


Figure 15: The absolute photodetachment cross section $\sigma_{pd}(E)$ (right-hand side Y axis) of $C_6F_6^-$ in TMS as a function of the photon energy, E, and a linear least squares fit of $(\sigma_{pd}/E)^{2/3}$ (left-hand side Y axis) for E < 1.95 eV. The intercept with the X axis gives a threshold energy $E_{th}$ of 1.51 eV.

There is a considerable uncertainty as to the value of the electron affinity of $C_6F_6$ in the gas, $(EA)_G$. The most reliable values for $(EA)_G$ are 0.86, and 0.52 eV. If we take $(EA)_G = 0.86$ eV, $V_o = -0.51$ eV and $P^- = -0.92$ eV, [see Appendix B], then $(EA)_L = 1.27$ eV which is 0.41 eV larger than $(EA)_G$. From Eq. (8) we have also $(\Delta E)_L = (E_{th})_L - (EA)_L = 0.24$ eV. If we take $(EA)_G = 0.52$ eV, then $(\Delta E)_L = 0.58$ eV. These results demonstrate that an equation of the form of Eq. (8) is necessary to relate the liquid and the gas phase quantities and to account for the changes between the gas and the liquid state.

Currently we are modifying the experimental technique to measure the photodetachment cross section of $C_6F_6^-$ and other negative ions in dense fluids (dense vapors). Figure 16 shows a schematic outlay of the new arrangement.

## IV. TECHNICAL ASPECTS OF FAST DIELECTRIC LIQUIDS

Certain characteristics of fast warm liquids are important for technological applications such as advanced radiation detectors (see also Appendix C) and pulsed power switches (see also Appendix D). These include:

### (i) Purity and Purification Methods

The purification process outlined in IIC is sufficient to allow free electron half lives of at least 1 μs in all liquids and this lifetime should be sufficient for most applications. Liquid TMS was the easiest to purify. The purification of TMP was very slow because of its low vapor pressure. For large scale calorimeters where continuous circulation and purification might be necessary the ease of purification of TMS will be an obvious advantage. Alternatively electrostatic precipitators or other means of passive purification such as alkali traps can be used.

We operated a TMS-filled stainless steel cell with an electrostatic precipitator without any significant reduction in the electron lifetime.

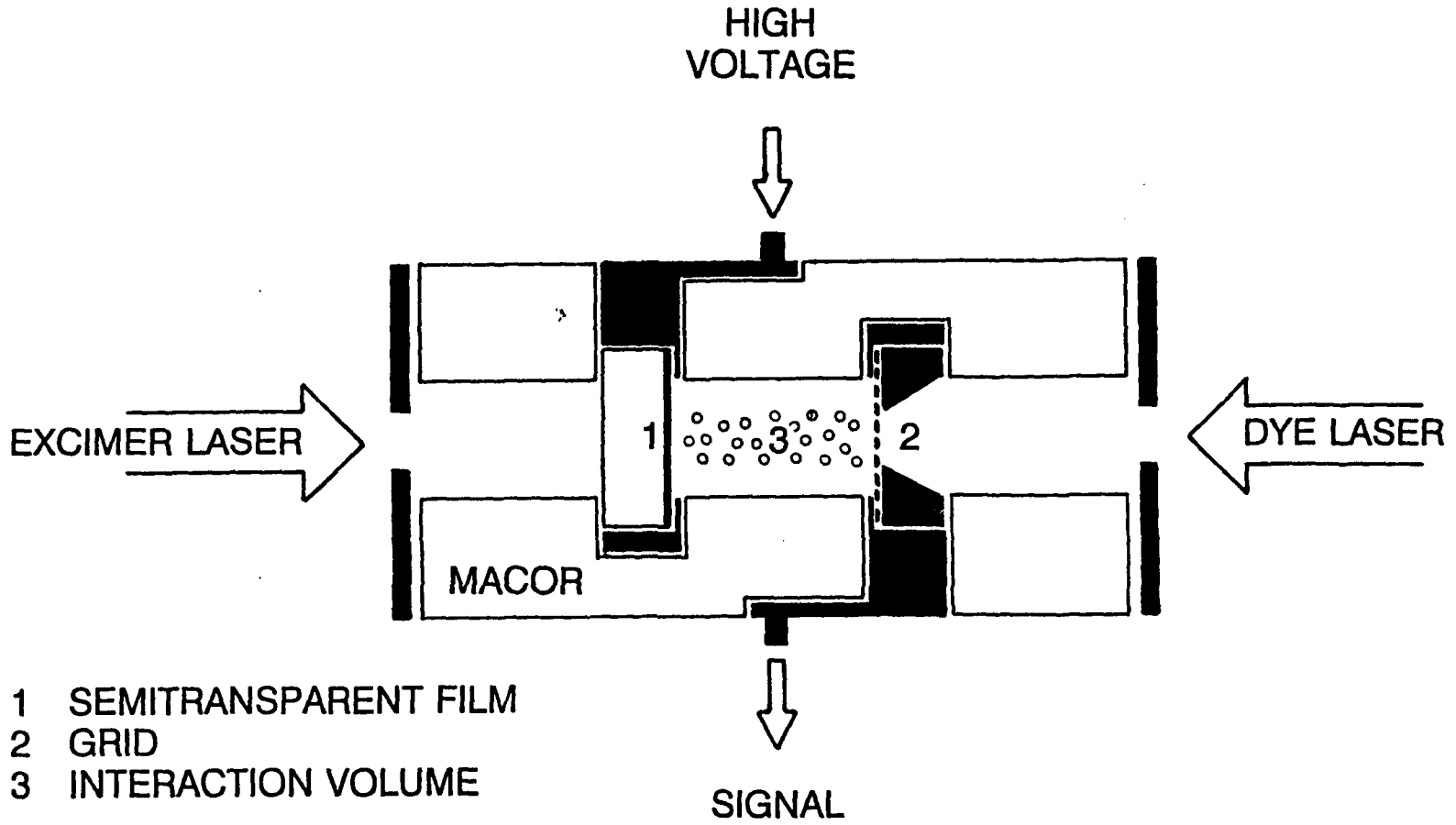


Figure 16: New arrangement for photodetachment studies in dense fluids.

Besides electronegative impurities, microparticles can be a potential problem especially in high voltage applications since they lower the dielectric strength of the liquid (or gas). Consequently, filtering of the liquid and effective ways of cleaning the device surfaces from microparticles are necessary to maintain high dielectric strength.

(ii) Dielectric Strength, Electrical Breakdown, and Byproducts Produced

In Table 2 we gave the maximum field $E_{max}$ reached in each liquid/mixture before an electrical breakdown (EB) occurred. In all liquids except TMT, EB occurred above $10^5$ V $cm^{-1}$. It should be noted, however, that the values in Table 2 are rough estimates of the "dielectric strength" of these liquids. The actual $E_{max}$ in any given device will depend on the purity of the liquid, the cleanliness of the cells, the presence, size, shape, and type of microparticles in the liquid, and the electrode shape and surface condition. The EB in TMS and its mixtures, TMG and TMT was strong, explosive, damaged the electronics and damaged the fine polish of the electrodes.

In TMS and in the TMS/n-pentane mixtures no apparent deterioration of the liquid was observed following an EB. However, in TMT and TMG EB led to significant chemical decomposition which rendered the system unusable. A heavy tin or germanium layer (as shown by an ESCA analysis of the coating on the cell surfaces) covered the inside surfaces of the cell, and large amounts of gases (possibly $H_2$ and $CH_4$) raised the pressure in the cell to several atmospheres. Figure 17 shows the electrode surface before and after an EB in TMT. In TMP and in the TMS/TMP mixture no major decomposition was apparent, but an electron-attaching impurity was produced. The concentration of this impurity increased with the number of EBs and reduced the electron lifetime to less than ~100 ns after 4 or 5 EBs. This seriously affected the electron signal. A gas chromatographic analysis identified this impurity with a negative ion of mass 126 amu.

Table 4 summarizes the comparative technical properties of the liquids TMC, TMS, TMG, TMT, and TMP.

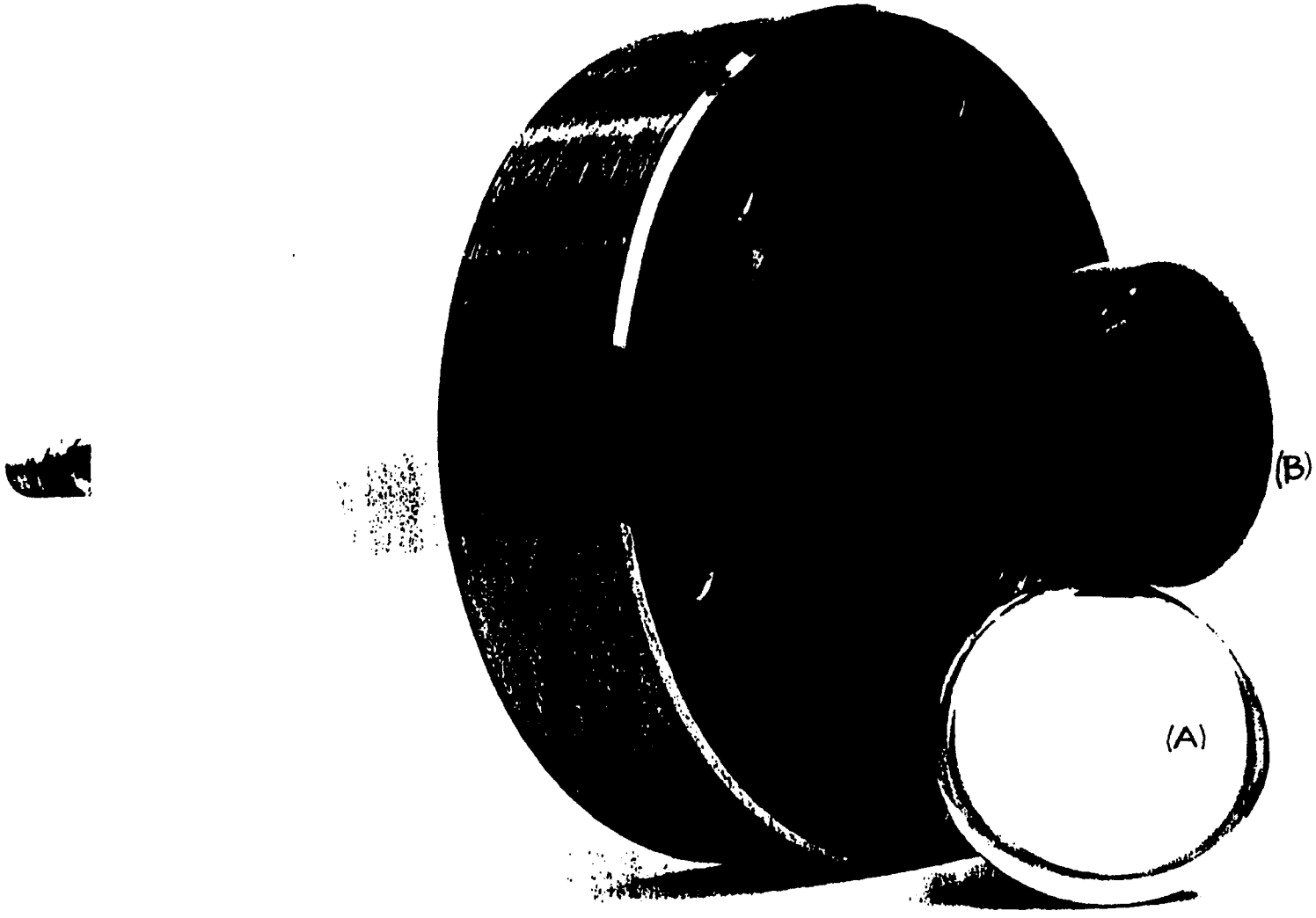


Figure 17: Electrode surfaces before (A) and after (B) an electrical breakdown in liquid TMT.

Table 4: Comparative "Practical" Properties of TMC, TMS, TMG, TMT, and TMP

| Liquid | Purification | Drift Velocity | Dielectric Strength | Effects of Electrical Breakdown |
|---|---|---|---|---|
| TMC | Easy/Quick | Inter-mediate | High | |
| TMS | Easy/Quick | Fast | High | No apparent liquid deterioration. Damage to electronics/pitting of electrodes. |
| TMG | Easy/Quick | Fast | High | Extensive liquid decomposition rendered system unusable. Electro-negative impurity(ies) formed. Damage to electronics/pitting of electrodes. |
| TMT | Difficult; reacts with $H_2SO_4$ and NaK | Fast | Low | Same as TMG. |
| TMP | Slow | Slow | High | Electronegative impurity(ies) formed. |

## V. LIQUID-FILLED PULSED POWER SWITCH

Fast dielectric liquids such as TMS, TMC, and TMG have the unique capacity of being excellent insulators - their dielectric strength exceeds $10^5$ V $cm^{-1}$ - and also very good conductors when excess electrons are injected into them. This makes them very good candidates for switching media in pulsed power applications. Recently we patented a flashlamp powered, dielectric-liquid-filled pulsed power switch, and designed and built a prototype model. Currently a private company (Tetra Corporation) is working to commercialize the switch. Figure 18 shows a schematic diagram of the switch. A prototype actual switch has been constructed (see Fig. 19) and preliminary results were encouraging. The switch is composed of two coaxial cylinders, the inside of quartz, the outside of metal. The inner tube, equipped with two electrodes and filled with Xe (or another gas), is a flashlamp. The space between the cylinders is filled with liquid, a semitransparent conducting film on the outside of the inner cylinder is the cathode and the outer cylinder is the anode. A potential is applied across the anode and the cathode so that when the flashlamp fires a current flows through the liquid. When the flashlamp is off, the liquid is an insulator withstanding fields of up to $10^5$ V $cm^{-1}$.

Our prototype switch passed significant (kA) current levels during the ON phase, before a deterioration in the metallic film contacts reduced its efficiency. The switch constructed by Tetra Corporation appears to operate close to its theoretical efficiency.

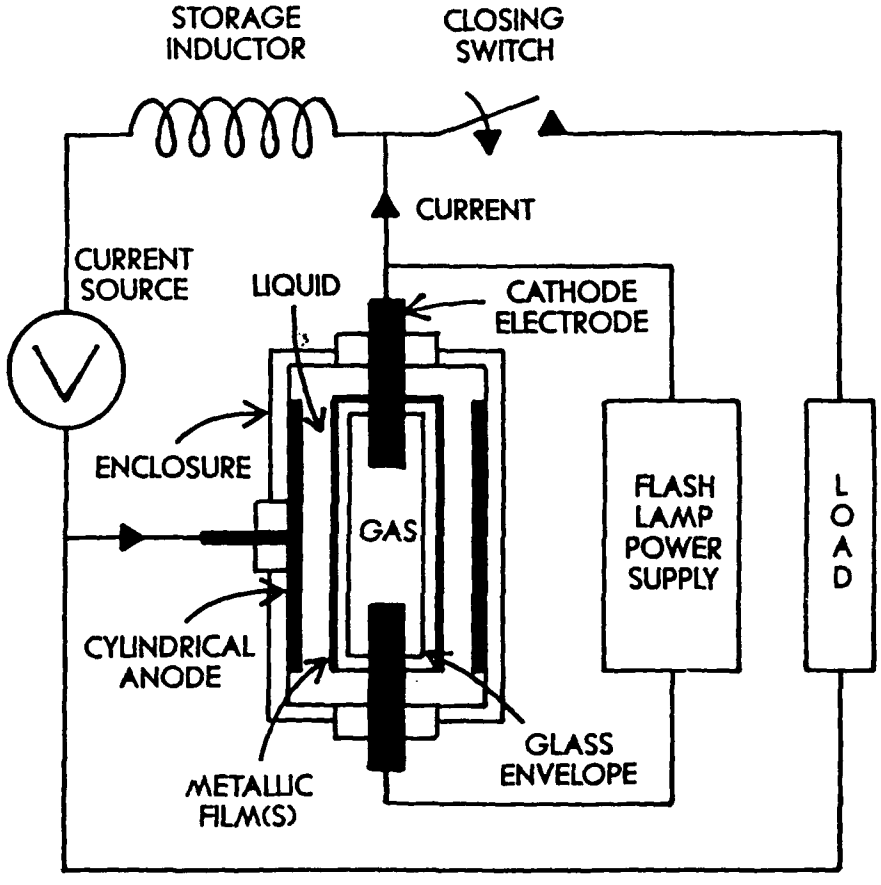


Figure 18: Schematic diagram of the dielectric liquid pulsed power switch employing a pulsed flashlamp.

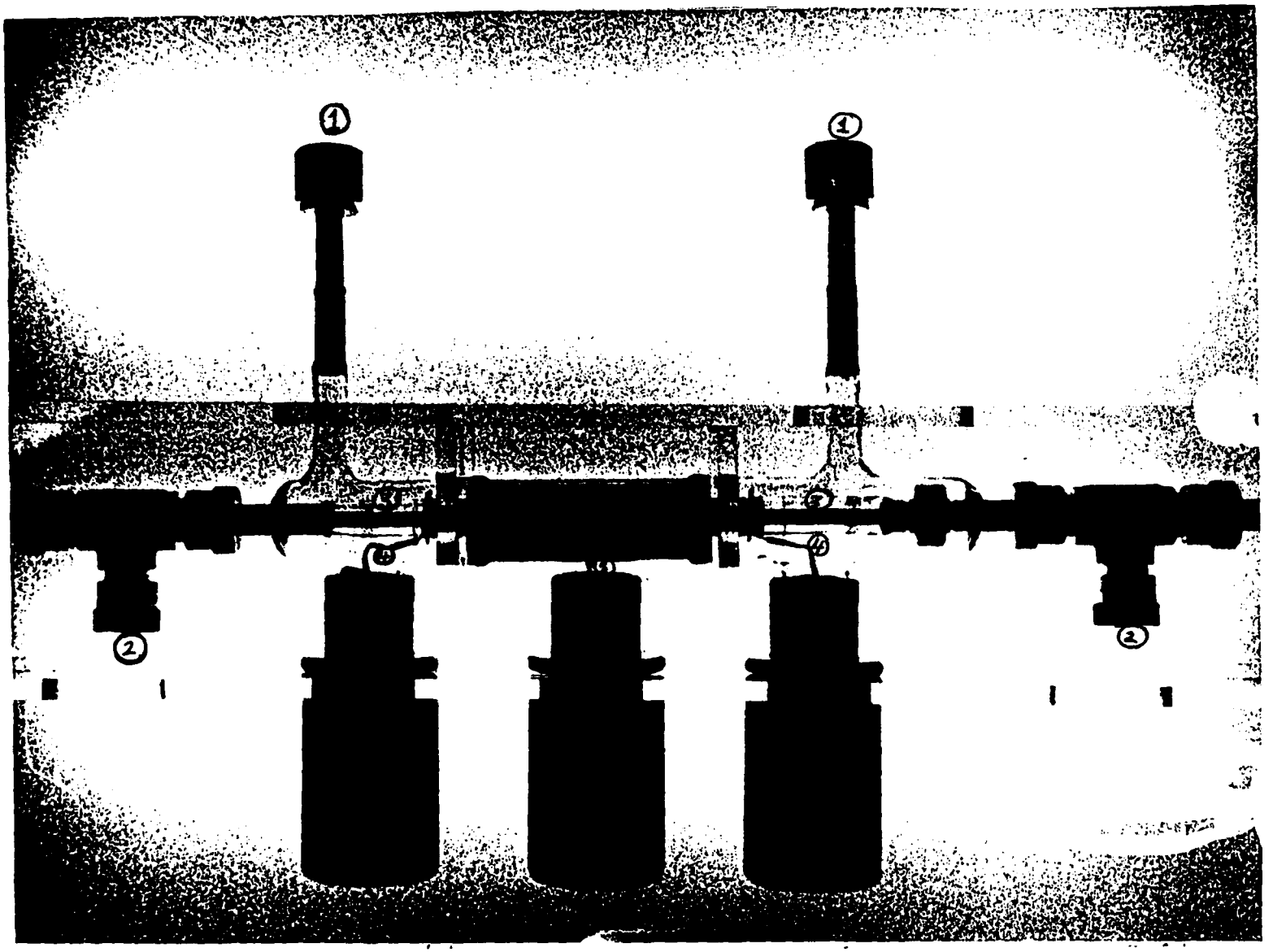


Figure 19: Prototype fast-liquid-filled pulsed power switch: (1) liquid ports; (2) Xe ports, (3) flashlamp electrodes, (4) cathode connections, and (5) anode connections.

## VI. REFERENCES


1. L. G. Christophorou
   Atomic and Molecular Radiation Physics
   Wiley-Interscience, New York, 1971

2. L. G. Christophorou (Editor)
   Electron-Molecule Interactions and Their Applications, Volume 1, Academic Press, New York, 1984

3. L. G. Christophorou (Editor)
   Electron-Molecule Interactions and Their Applications, Volume 2, Academic Press, New York, 1984

4. L. G. Christophorou (Editor)
   Electron and Ion Swarms (Proceedings of the Second International Swarm Seminar, Oak Ridge, Tennessee, July 22-23, 1981)
   Pergamon Press, New York, 1981

5. L. G. Christophorou
   The Lifetimes of Metastable Negative Ions
   In Advances in Electronics and Electron Physics (L. Marton, Ed.), Vol. 46, Academic Press, New York, 1978, pp. 55-129

6. L. G. Christophorou
   Negative Ion States of Polyatomic Molecules
   In Photon, Electron, and Ion Probes of Polymer Structure and Properties
   (D. W. Dwight, T. J. Fabish, and H. R. Thomas, Eds.), ACS Symposium Series 162, American Chemical Society, Washington, D.C., 1981, pp. 11-34

7. L. G. Christophorou, D. L. McCorkle, and A. A. Christodoulides
   Electron Attachment Processes
   In Electron-Molecule Interactions and Their Applications
   (L. G. Christophorou, Ed.), Vol. 1, Chapt. 6, Academic Press, New York, 1984, pp. 477-617

8. S. R. Hunter and L. G. Christophorou
   Electron Motion in Low- and High-Pressure Gases
   In Electron-Molecule Interactions and Their Applications (L. G. Christophorou, Ed.), Vol. 2, Chapt. 3, Academic Press, New York, 1984, pp. 89-219

9. L. G. Christophorou and K. Siomos
   Interphase Physics: Linking Knowledge on Electron-Molecule Interactions in Gases with That in Condensed Matter
   In Electron-Molecule Interactions and Their Applications (L. G. Christophorou, Ed.), Vol. 2, Chapt. 4, Academic Press, New York, 1984, pp. 221-316

10. L. G. Christophorou
Electron Attachment and Detachment Processes in Electronegative Gases
Plasma Physics 27, 1-46 (1987)

11. L. G. Christophorou
Gas/Liquid Transition: Interphase Physics
NATO ASI Series, E. Kunhardt, L. G. Christophorou, and L. H. Luessen (Eds.), Plenum Press, New York, 1988, pp. 283-316

12. K. Siomos and L. G. Christophorou
Laser Two-Photon Ionization Spectroscopy of Molecules in Liquids
Chem. Phys. Lett. **72**, 43-48 (1980)

13. H. Faidas and L. G. Christophorou
Multiphoton Ionization of Fluoranthene in Tetramethylsilane
*J. Chem. Phys.* **86**, 2505-2509 (1987)

14. H. Faidas and L. G. Christophorou
Determination of the Ionization Threshold of Azulene in Hydrocarbon Liquids by Multiphoton Ionization
*J. Chem. Phys.* **88**, 8010-8011 (1988)

15. H. Faidas and L. G. Christophorou
Laser Multiphoton Ionization of Aromatic Molecules in Nonpolar Liquids
*Intern. J. Radiat. Phys. Chem.* **32**, 433-438 (1988)

16. L. G. Christophorou (Ed.), Gaseous Dielectrics I, II, III, and IV, Pergamon Press, New York, respectively 1978, 1980, 1982, and 1984

17. L. G. Christophorou et al., "Recent Advances in Gaseous Dielectrics at ORNL," *IEEE Trans. Electr. Insul.* **EI-19**, 550 (1984)

18. L. G. Christophorou, "Breakdown Potential," in Encyclopedia of Science and Technology, McGraw-Hill Publishing Company, Vol. 3, p. 40

19. L. G. Christophorou and S. J. Dale, "Dielectric Gases," in Encyclopedia of Physical Science and Technology (R. A. Meyers, Ed.), *Academic Press*, Orlando, Florida, Vol. 4, pp. 246-262

20. L. G. Christophorou et al., High Voltage Research (Breakdown Strengths of Gaseous and Liquid Insulators) and Environmental Effects of Dielectric Gases, ORNL Report ORNL/TM-7862 (1981)

21. D. H. Smith, D. W. Bouldin, and L. G. Christophorou, "DC Dielectric Strengths of Fluorinated Benzenes and the Stored Energy Theory," Proceedings of the 7th International Conference on Conduction and Breakdown in Dielectric Liquids, W. F. Schmidt (Ed.), Berlin, 1981, pp. 246-250

APPENDIX A

Nuclear Instruments and Methods in Physics Research A294 (1990) 575–582
North-Holland



# ELECTRON DRIFT VELOCITIES AND ELECTRON MOBILITIES IN FAST ROOM-TEMPERATURE DIELECTRIC LIQUIDS AND THEIR CORRESPONDING VAPORS *

H. FAIDAS **, L.G. CHRISTOPHOROU **, D.L. McCORKLE **, and J.G. CARTER

*Atomic, Molecular, and High Voltage Physics Group, Health and Safety Research Division, Oak Ridge National Laboratory, Oak Ridge, TN 37831, USA*

Received 19 March 1990

The drift velocity, $w$, of excess electrons as a function of the applied uniform electric field, $E$, in liquid tetramethylsilane (TMS), 2,2,4,4-tetramethylpentane (TMP), tetramethyltin (TMT), and in mixtures of TMS with TMP (molar ratio, $M = 1.31/1$) and n-pentane ($M = 102/1$; 17/1; 5.6/1) has been measured up to $E$-values of $\sim 10^5$ V cm$^{-1}$ or density($N$)-reduced electric field $E/N$-values of $\sim 3\times10^{-17}$ V cm$^2$. The maximum $w$ attained for these liquids, and the corresponding values of $E$ are: $7.2\times10^6$ cm s$^{-1}$ at 125 kV cm$^{-1}$ for TMS, $6.0\times10^6$ cm s$^{-1}$ at 75 kV cm$^{-1}$ for TMT, $2.6\times10^6$ cm s$^{-1}$ at 115 kV cm$^{-1}$ for TMP, $3.2\times10^6$ cm s$^{-1}$ at 105 kV cm$^{-1}$ for TMS/TMP ($M = 1.31/1$), $6.8\times10^6$ cm s$^{-1}$ at 105 kV cm$^{-1}$ for TMS/n-pentane ($M = 102/1$), $6.8\times10^6$ cm s$^{-1}$ at 145 kV cm$^{-1}$ for TMS/n-pentane ($M = 17/1$), and $4.9\times10^6$ cm s$^{-1}$ at 145 kV cm$^{-1}$ for TMS/n-pentane ($M = 5.6/1$). The thermal-electron mobilities in the above liquid media are respectively 119.3, 85.7, 31.8, 39.1, 118, 85, and 47.6 cm$^2$ s$^{-1}$ V$^{-1}$. Also, $w$ was measured as a function of $E/N$ for TMS, TMP, and neopentane vapors at room temperature and is compared with that in the corresponding liquids. Properties of these media which make them desirable for radiation detectors are discussed.

## 1. Introduction

Hydrocarbon liquids and gases (and their mixtures with rare gases) are increasingly used as detector media in high-energy-physics radiation detectors (e.g. calorimeters and muon chambers). Room-temperature liquids, suitable for calorimeter detectors [1–4] (especially those for the superconducting super collider, SSC), should be fast (have short electron collection times) and sensitive (have good energy resolution and particle identification properties) [5,6], while the hydrocarbon/rare-gas mixtures used in gas-filled drift chambers [7] should have electron transport parameters (electron drift velocity, $w$, and longitudinal, $D_L$, and transverse, $D_T$, electron diffusion coefficients) which optimize the operating characteristics of the detector [8–10]. In order for the response of the detector to be fast, the excess electrons in these detector media must be either free, as in gases, or quasifree, as in dense gases and liquids for which the electron ground-state energy $V_0 < 0$ eV, and they should attain high drift velocities ($\sim 10^6$–$10^7$ cm s$^{-1}$) at practical values of the applied electric field ($\sim 10^4$–$10^5$ V cm$^{-1}$). In most types of detectors, knowledge of the dependence of $w$ on $E$ is essential for the design and operation of the detector. For example, in liquid calorimeters [1] $w(E)$ determines the electron drift time $\tau = d/w$ ($d$ = drift distance) at any particular operating field $E$, and in wire chambers $w(E)$ must be accurately known in order to reconstruct the particle tracks [8,9]. In spite of the fact that the magnitude of $w$ and its $E$-dependence is crucial for most detector designs, accurate values of $w(E)$ – especially at high $E$ – for many detector liquids are lacking. Also, for most fast liquids (say those with $w \geq 1\times10^6$ cm s$^{-1}$ at $E = 5\times10^4$ V cm$^{-1}$) the thermal-electron mobilities, $\mu_{th} = w/E$ for $E \to 0$, that have been reported in the literature vary considerably.

In table 1 are listed thermal-mobility, $\mu_{th}$, values for some fast liquids (tetramethylsilane (TMS), neopentane (TMC), 2,2,4,4-tetramethylpentane (TMP), tetramethyltin (TMT), and tetramethylgermanium (TMG)), which were determined using time-of-flight (TOF) or Hall-mobility methods [11–14]. All measurements relied on techniques utilizing bulk ionization of the medium to generate excess electrons, except for our previous [18] and present work where a photoinjection technique is used. The $E$-dependence of $w$ up to $E \gtrsim 10^5$ V cm$^{-1}$ has been measured for TMS [27,18], TMC [20], and

* Research sponsored by the Office of Naval Research and the U.S. Department of Energy under, respectively, Contracts no. N00014-89-J-1990 and DE-AS05-76ER03956 with the University of Tennessee, and by the Office of Health and Environmental Research, U.S. Department of Energy, under Contract no. DE-AC05-840R21400 with Martin Marietta Energy Systems, Inc.

** Also, Dept. of Physics, University of Tennessee, Knoxville, TN 37996, USA.

0168-9002/90/$03.50 

Table 1
Thermal-electron time-of-flight (TOF) and Hall mobilities in TMS, TMC, TMP, TMT, and TMG

| | TOF mobility [a] | | Hall mobility | |
|---|---|---|---|---|
| | [$cm^2 s^{-1} V^{-1}$] | ref. | [$cm^2 s^{-1} V^{-1}$] | ref. |
| TMS | $90 \pm 5$ | [15] | 124 | [22] |
| | ~98 | [16] | $101 \pm 7$ | [23] |
| | 98 | [17] | | |
| | 125 | [18] [b] | | |
| | 119.3 | present [b] | | |
| TMC | $55 \pm 5$ | [15] | 85 | [24,25] |
| | 50 | [19] | 59 | [14] |
| | $70 \pm 10$ | [20] | | |
| TMP | 24 | [19] | 32 | [26] |
| | 29 | [21] | | |
| | 30 | [1] | | |
| | 31 | [18] [b] | | |
| | 31.8 | present [b] | | |
| TMT | 70 | [11] | | |
| | 85.7 | present [b] | | |
| TMG | 90 | [11] | | |

[a] Except otherwise noted, bulk ionization techniques were used.
[b] A photoinjection technique was used.

TMP [18]. Because of the uncertainty of the $\mu_{th}$ and $w(E)$ data and the current interest in practical uses of fast room-temperature dielectric liquids, we undertook a systematic study of electron transport in some of the fastest hydrocarbon liquids (TMS, TMP, and TMT), their mixtures (TMS/TMP, $M = 1.31/1$ and TMS/n-pentane, $M = 102/1$, 17/1 and 5.6/1) and their vapors (TMS, TMP, and TMC). The results of these studies are reported here. We also report our observations and findings on the purification and purity requirements, dielectric strength and electrical-breakdown decomposition byproducts of these liquids; these findings and observations are important in assessing the suitability of warm liquids as detector materials.

## 2. Experimental technique

In the present studies a laser photoionization technique was used to inject excess electrons into the dielectric liquids [18] and vapors [28]. A somewhat similar laser photoinjection technique was used in the past to measure $w$ in cryogenic liquids [29]. Fig. 1 shows schematically the experimental setup for the liquid measurements. The cell consisted of a six-way stainless-steel cube with two windows for the entry and exit of the laser beam, a high-voltage feedthrough, a low-voltage feedthrough for the signal, and vacuum and liquid ports. A pair of parallel-plate stainless-steel electrodes immersed in the liquid under study were kept at a distance $d$ (2 to 4 mm) and a potential difference $V$ (0 to 50 kV). An excimer laser pulse (XeCl, $\lambda = 308$ nm, full width at half maximum FWHM $\simeq$ 15 ns) struck the center of the cathode and generated a pulse of electrons that drifted to the anode. The anode signal due to these photoinjected electrons was measured and recorded in two different ways:

(i) In the voltage mode (fig. 2a) (which was generally used at relatively low $E$-values, and therefore longer electron drift times, $\tau$) the signal was fed to a fast-response (~ 3 ns) charge-sensitive preamplifier and was captured, averaged (16 to 64 pulses) and stored by a transient digitizer as a voltage waveform. The drift time,

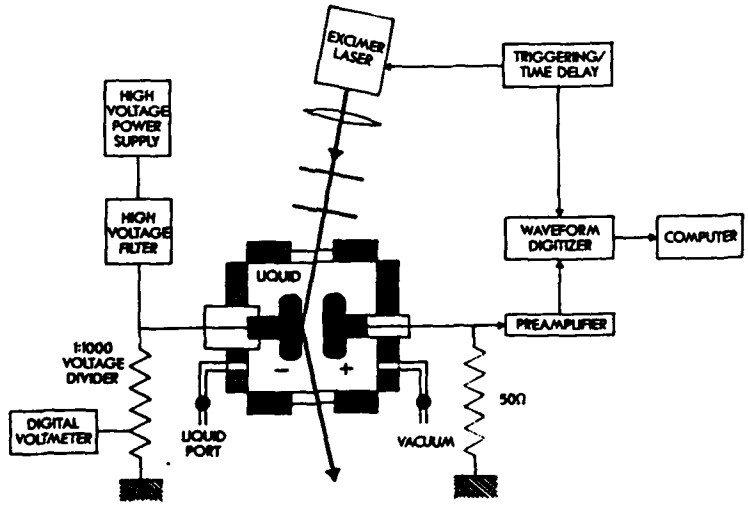


Fig. 1. Setup of laser-induced photoinjection apparatus in liquids.

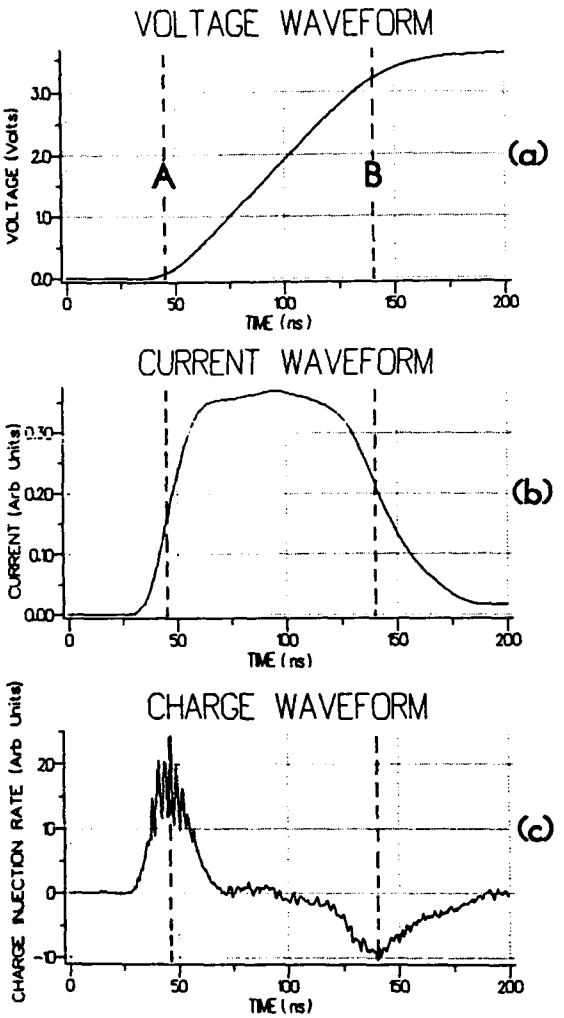


Fig. 2. Voltage (a), current (b), and charge-injection rate (c) waveforms in TMP.

$\tau$, was determined numerically from the waveform rise time (the distance between points A and B in fig. 2a).

(ii) In the current mode (fig. 2b) (which was generally used at relatively high fields; and short $\tau$) the signal output was grounded through a 50 Ω resistor, and the signal passed either directly to the transient digitizer or (in order to protect the digitizer from possible electrical-breakdown transients at high fields) through the preamplifier. The drift time was obtained from the FWHM of the current pulse determined numerically. By numerically differentiating the current-mode signal, a waveform corresponding to the rate of charge injection from the cathode (positive pulse in fig. 2c) and collection at the anode (negative pulse in fig. 2c) was obtained. Then $\tau$ is the time between the maximum and the minimum of the two pulses.

The agreement between the values of $\tau$ obtained via the voltage, current, and charge-injection waveforms was good ($\tau$ was always longer than the laser pulse duration). The electron drift velocity and the electron mobility, $\mu$, were calculated from:

$$w = \frac{d}{\tau} \quad \text{and} \quad \mu = \frac{d^2}{\tau V}.$$

All measurements were made at room temperature ($T =$ 295 K) and the accuracy of the data is estimated to be within ~ 2 to 3%.

The advantages of the laser photoinjection technique for measuring $w$ and $\mu$ over traditional radiation pulse techniques [11,15,16,27] are: (i) the electrons are injected into the liquid or the gas medium from a metal surface instead of being produced by bulk ionization of the medium. Thus there are no positive ions produced in the medium itself and, therefore, no recombination and/or space-charge effects, (ii) the electrons drift in a constant electric field region so that fringe field effects are minimized, and (iii) the drift time is determined directly and accurately without resorting to deconvolution or fitting to simulated waveforms; thus, very short drift times and high drift velocities can be measured accurately, provided the laser pulse duration is much shorter than $\tau$.

## 3. Purification of the liquids and cleaning of the cell

### 3.1. Liquid/vapor purification

The liquids (TMS, 99.9% +; TMP, 99.99%; TMT, 99%; n-pentane, 99.99%) were purified further to remove electronegative and/or polar impurities according to the following protocol:
(i) Stirring over $H_2SO_4$ to remove olefinic impurities. (ii) Stirring with $BaCO_3$ to neutralize $H_2SO_4$. (iii) Preliminary freeze–pump–thaw cycles to remove dissolved air. (iv) Passage through traps containing NaOH pellets, activated silica gel and activated charcoal to remove $CO_2$ and $H_2O$. (v) Successive distillations through traps at liquid-$N_2$ temperature while pumping to remove $O_2$ and $N_2$. (vi) Storing and stirring over liquid NaK for over 24 h to remove remaining $O_2$ or $H_2O$. (vii) Transfer into the cell through a 0.5 μm filter. (viii) An electrostatic precipitator – built into the liquid cell – further purified the liquid for ~ 24 h before and during the measurements.

The above protocol was followed for all liquids studied except TMT which reacts with $H_2SO_4$ and NaK. For TMT the corresponding purification steps were omitted. Similar purification procedures and techniques to monitor the liquid purity, specifically adapted to calorimeter applications, were described elsewhere [30–32].

For the measurements in vapors, the purification consisted of only the freeze–pump–thaw cycles.

### 3.2. Cell cleaning

The cell components (cell body, windows, feedthroughs, valves and electrodes) were cleaned as follows: (i) Rubbing the cell walls with ethanol- or acetone-wetted cotton applicators to remove any deposits from previous experiments. (ii) Cleaning with acetone in an ultrasonic bath for 1 to 2 h. (iii) Drying in an evacuated oven held at 150 °C. (iv) Following assembly, heating to 200 °C and pumping down to $\sim 1 \times 10^{-7}$ Torr for several days before the liquid was introduced into the cell.

## 4. Results and discussion

### 4.1. Liquids

The $w(E)$ and $\mu(E)$ data in neat TMS, TMT, and TMP are shown in figs. 3 and 4, while the data in the mixtures of TMS with TMP and n-pentane are shown in figs. 5 and 6, respectively. The salient features of the $w(E)$ data for both the neat liquids and the mixtures are: At low fields and up to a critical electric field $E_c$, $w$ increases linearly with $E$ and $\mu = w/E = \mu_{th} =$ constant [33]. For $E < E_c$, the electrons are in thermal equilibrium with the molecules of the medium (liquid or gas) and their mean kinetic energy is $\sim 1.5kT$. As the field is increased beyond $E_c$ the electrons progressively gain energy from the field, their mean kinetic energy becomes greater than $1.5kT$, and the $E$-dependence of their $w$ becomes sublinear. At sufficiently high $E$-values (see figs. 3 and 5), $w(E)$ tends toward saturation. For all the liquids we studied, however, electrical breakdown occurred before saturation was reached, unlike in some of the vapors (see fig. 7 and section 4.2).

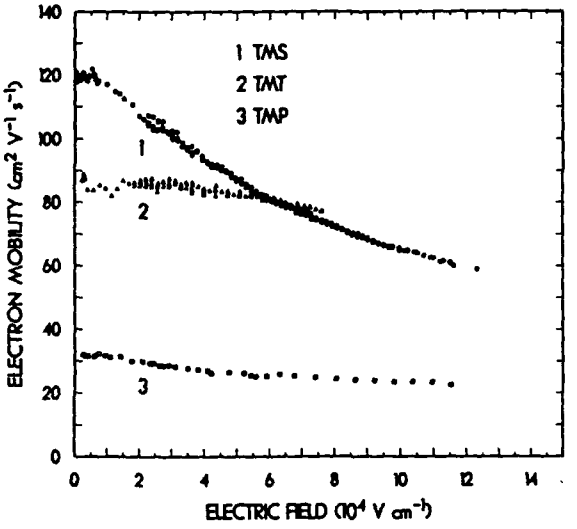


Fig. 4. Electron mobility, $\mu = w/E$ as a function of applied electric field in neat TMS, TMT, and TMP.

In table 2 are summarized the mole ratio of the liquids/mixtures studied, and for each liquid medium the values of $E_c$, $\mu_{th}$, the maximum ($E_{max}$) $E$-field reached, and the (maximum) drift velocity $w_{max}$ corresponding to $E_{max}$. For comparison we have included the data of ref. [20] on liquid TMC.

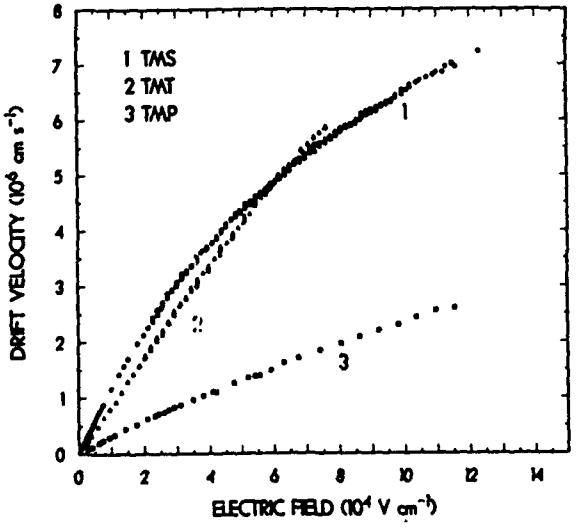


Fig. 3. Electron drift velocity as a function of applied electric field in neat TMS, TMT, and TMP.

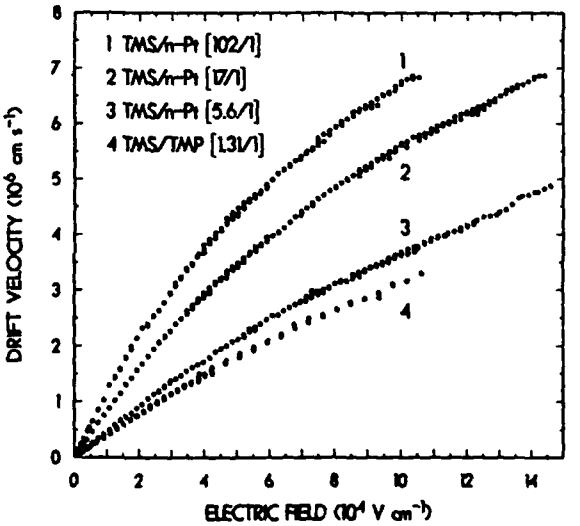


Fig. 5. Electron drift velocity as a function of applied electric field in TMS/TMP and the TMS/n-pentane mixtures.

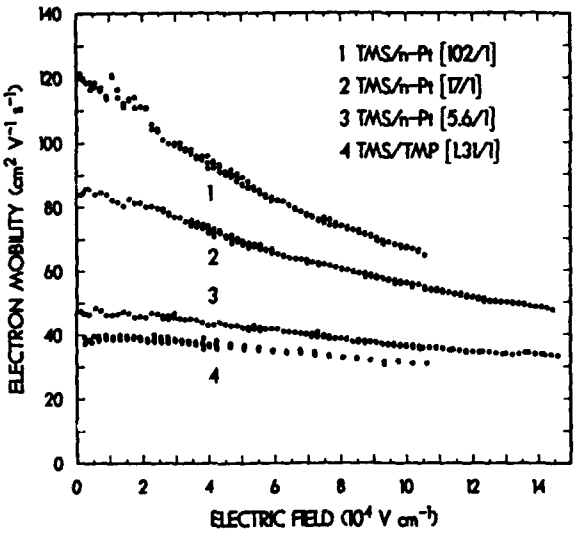


Fig. 6. Electron mobility $\mu = w/E$ as a function of applied electric field in TMS/TMP and the TMS/n-pentane mixtures.

Our present and previous [18] measurements of $\mu_{th}$ for TMS, TMP, and TMT are compared with literature data in table 1. It is clear that TOF electron mobilities differ greatly among themselves and with the Hall mobilities. Our values are significantly higher than other TOF values, but are close to some Hall-mobility measurements (i.e. to those of ref. [22] for TMS and ref. [26] for TMP). Similarly, our $w(E)$ data for TMS are 10 to 20% higher than those of ref. [27]. It is possible that these differences can be traced to the uncertainties inherent in the bulk ionization methods.

### 4.2. Vapors

In fig. 7 are shown our $w(E/N)$ measurements for gaseous TMS, TMP, and TMC, together with the corresponding liquid-phase data for comparison. The measurements were taken at room temperature ($\sim$ 295 K) and at vapor pressures of 500 and 680 Torr for TMS, 600 Torr for TMC, and 21.15 Torr for TMP. In table 3 are listed the gas pressures at which measurements were made, the gas and corresponding liquid number densities $N$, $\mu_{th}$, and the density-normalized electron mobility $\mu_n = \mu_{th}N$ for TMS, TMC, and TMP.

The gases have a much lower $\mu_n$ value than the corresponding liquids. The ratio $(\mu_n)_L/(\mu_n)_G$ is 66.8, 13.7, and 11 for TMS, TMC, and TMP respectively. Also, the gases exhibit a supralinear $w$–$E$ dependence at intermediate $E/N$-values before they reach a saturation value for $w$ at $\sim(5\text{–}6)\times10^6$ cm s$^{-1}$, while the liquids

Table 2
Mole ratio $M$, critical electric field $E_c$, thermal-electron mobility $\mu_{th}$, maximum electric field $E_{max}$, and maximum electron drift velocity $w_{max}$, for the fast neat liquids and mixtures studied

| Liquid/mixture | $M$ | $E_c$ [$10^3$ V cm$^{-1}$] | $\mu_{th}$ [cm$^2$ s$^{-1}$ V$^{-1}$] | $E_{max}$ [$10^3$ V cm$^{-1}$] | $w_{max}$ [$10^6$ cm s$^{-1}$] |
|---|---|---|---|---|---|
| TMS | neat | 7 | 119.3 | 125 | 7.2 |
| TMT | neat | 30 | 85.7 | 75 | 6.0 |
| TMC [a] | neat | ~3 | 70 | 116 | 2.8 |
| TMP | neat | 15 | 31.8 | 115 | 2.6 |
| TMS/TMP | 1.31/1 | 18 | 39.1 | 105 | 3.2 |
| TMS/n-pentane | 102/1 | 7 | 118 | 105 [b] | 6.8 |
| TMS/n-pentane | 17/1 | 8 | 85 | 145 [b] | 6.8 |
| TMS/n-pentane | 5.6/1 | 15 | 47.6 | 145 | 4.9 |

[a] Data from ref. [20].
[b] $E_{max}$ was not limited by electrical breakdown.

Table 3
Vapor pressure, number density $N$, thermal-electron mobility $\mu_{th}$, density-normalized electron mobility $\mu_n$, and the $\mu_n$ ratio $R$, for liquid and gaseous TMS, TMC, and TMP

| | TMS | | TMC | | TMP | |
|---|---|---|---|---|---|---|
| | Liquid | Gas | Liquid | Gas | Liquid | Gas |
| Vapor Pressure [Torr] | | 680 | | 600 | | 21.15 |
| $N$ [Molecules cm$^{-3}$] | $4.423\times10^{21}$ | $2.224\times10^{19}$ | $5.121\times10^{21}$ | $1.963\times10^{19}$ | $3.378\times10^{21}$ | $6.804\times10^{17}$ |
| $\mu_{th}$ [cm$^2$ s$^{-1}$ V$^{-1}$] | 119.3 | 354.7 | 70 | 1,338 | 31.8 | 13,959 |
| $\mu_n$ [s$^{-1}$ V$^{-1}$ cm$^{-1}$] | $5.27\times10^{23}$ | $7.89\times10^{21}$ | $3.6\times10^{23}$ | $2.63\times10^{22}$ | $1.05\times10^{23}$ | $0.95\times10^{22}$ |
| $R = (\mu_n)_L/(\mu_n)_G$ | 66.8 | | 13.7 | | 11.0 | |

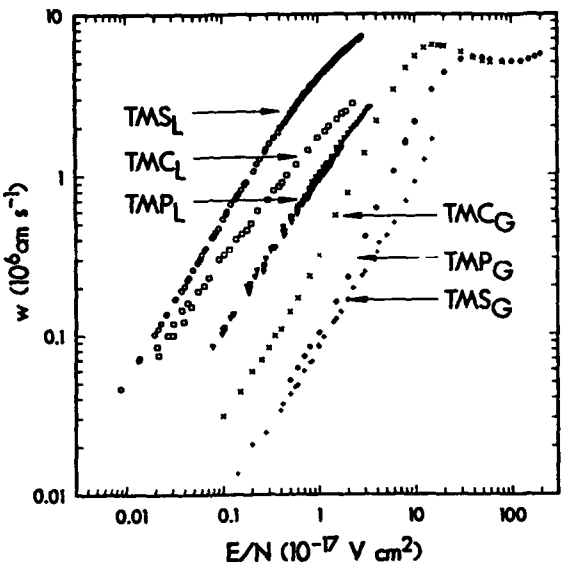


Fig. 7. Electron drift velocity as a function of $E/N$ for liquid and gaseous TMS, TMC, and TMP. The data for liquid TMC are from ref. [20].

show a sublinear $w$–$E$ dependence. The larger values of $(\mu_n)_L$ compared to $(\mu_n)_G$ would indicate that at thermal and near-thermal energies, the electron scattering cross sections in these liquids are smaller than in the corresponding gas. Such changes are known to occur especially for molecules whose electron scattering cross sections in the gas phase exhibit at low energies ($\lesssim 0.5$ eV) a Ramsauer–Townsend minimum [34,35].

## 5. Observations relevant to fast-detector applications

### 5.1. Purification

The purification process outlined in section 3.1 was sufficient to allow, in all liquids and gases studied, free-electron lifetimes in excess of 20 μs which is adequate for most detector applications. Tetramethylsilane was the easiest liquid to purify. The purification process for TMP was slow because of its low vapor pressure. For a large-scale calorimeter where continuous circulation and purification might be necessary in order to maintain the liquid purity over long periods of time, the low viscosity of TMS and its ease of purification are obvious advantages. Alternatively, electrostatic precipitators or other means of passive purification (e.g. alkali traps) can be incorporated into the calorimeter design. We operated a TMS-filled stainless-steel cell with an electrostatic precipitator for two months without any significant electron lifetime reduction. Besides electronegative impurities, microparticles in the liquid (or the gas) are a potential problem, since they lower the dielectric strength of both the gas [36] and the liquid [37]. Consequently, filtering of the liquid and effective ways of cleaning the detector surfaces from microparticles are necessary to maintain high dielectric strengths.

### 5.2. Dielectric strength and electrical breakdown

In table 2 we give the maximum field, $E_{max}$, reached in each liquid/mixture before an electrical breakdown (EB) occurred. Occasionally EB occurred at slightly lower fields, but in all liquids (except TMT) breakdown occurred above $10^5$ V cm$^{-1}$. It should be noted that the $E_{max}$ values in table 2 can serve only as rough estimates of the "dielectric strength" of these liquids. The value of $E_{max}$ depends on many factors, such as the purity of the liquid and the cleanliness of the cell walls, the presence, size, shape and type of microparticles in the liquid (or the gas), and electrode shape and electrode-surface condition [36,37].

The EB in TMS and its mixtures and in TMT was strong, damaging to the preamplifiers, and damaging to the fine polish of the electrodes. Damage to the electrode surface caused a lowering of $E_{max}$.

### 5.3. Electrical-breakdown byproducts

In TMS and in the TMS/n-pentane mixtures, no apparent deterioration of the liquid following a breakdown was observed. However, in TMT EB led to significant chemical decomposition of the liquid. A heavy tin layer (as shown by an ESCA analysis of the metallic coating on the cell surfaces) covered the inside surfaces of the cell, and large amounts of gases (possibly $H_2$ and $CH_4$) were produced, which raised the pressure in the cell to several atmospheres. Fig. 8 shows the effect an EB in TMT had on the cell surfaces; A is the electrode before and B is the electrode after the breakdown. In TMP and in the TMS/TMP mixture no major decomposition was apparent, but an electron-attaching impurity was produced. The concentration of this impurity increased with the number of EBs and reduced the electron lifetime to less than ~ 100 ns after 4 or 5 EBs, and thus seriously affected the electron signal. A gas chromatographic analysis identified this impurity with a negative ion of mass 126 amu.

It is emphasized that a study and an evaluation of the effects of EB and partial discharges (corona) is required to properly assess the suitability of a detector liquid, since such events – especially corona – are likely to occur in actual situations. In this respect, the present preliminary findings indicate that of the liquids we studied TMS appears to be the most suitable for radiation detectors.

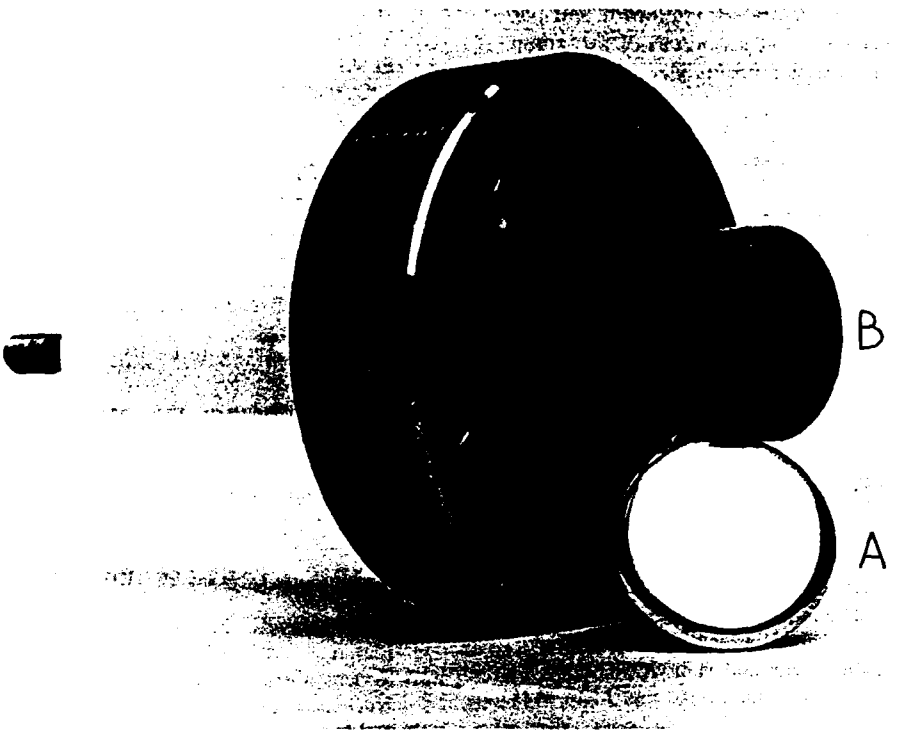


Fig. 8. Electrode surfaces before (A) and after (B) an electrical breakdown in liquid TMT.

*5.4. Properties of liquid mixtures*

The present limited studies on liquid mixtures indicate that small (~ 1 to 2%) amounts of nonelectronegative impurities (e.g. TMS/n-pentane, $M = 102/1$) do not seriously affect $w$ or $\mu$, and they might actually improve the dielectric strength of the liquid (see fig. 5 and table 2).

*5.5. Conclusions*

In table 4 are listed some of the properties of TMS, TMT, and TMP that are relevant to liquid-detector calorimetry. From this work, we conclude that of the liquids studies TMS is the most promising for warm-liquid calorimetry. In this regard, the following should be noted: (i) Removal of electronegative impurities is essential to achieve long electron lifetimes; this is especially significant for TMP because of its slow $w$, and for any liquid at low applied electric fields. At higher $E$-values, where $\tau$ is short purity requirements can be relaxed. (ii) Removal of microparticles from the system is important to maintain a high dielectric strength. (iii) Nonpolar impurities are not harmful up to ~ 1 to 2% as long as they are not electron-attaching; they may even increase the dielectric strength of the pure liquid. (iv)

Table 4
Comparative properties of TMS, TMT, and TMP

| | Purification | Drift velocity | Dielectric strength | Effects of electrical breakdown |
|---|---|---|---|---|
| TMS | Easy and quick | fast | high | damage to electronics/electrodes; no apparent liquid deterioration |
| TMT | difficult (reacts with $H_2SO_4$ and NaK) | fast | low | damage to electronics/electrodes; extensive decomposition rendered system unusable. |
| TMP | slow | slow | high | electronegative impurity(-ies) formed |

Studies of the effects of electrical breakdown and partial discharges on the electrical properties of fast room-temperature detector liquids are indicated.

## References


[1] M.G. Albrow et al., Nucl. Instr. and Meth. A265 (1988) 303.
[2] J. Engler and H. Keim, Nucl. Instr. and Meth. 223 (1984) 47.
[3] J. Engler, H. Keim and C. Müller, Nucl. Instr. and Meth. A254 (1987) 311.
[4] D.F. Anderson, Nucl. Instr. and Meth. A273 (1988) 657.
[5] L.G. Christophorou, H. Faidas and D.L. McCorkle, in: Nonequilibrium Effects in Ion and Electron Transport, eds. E.E. Kunhardt, R. Van Brunt, J. Gallagher and D. Hudson (Plenum Press, New York) in press.
[6] R.A. Holroyd and D.F. Anderson, Nucl. Instr. and Meth. A236 (1985) 294;
J. Feltesse, Nucl. Instr. and Meth. A283 (1989) 375.
[7] J. Va'vra, Nucl. Instr. and Meth. A244 (1986) 391.
[8] J. Konijn and F. Hartjes, Nucl. Instr. and Meth. A276 (1989) 582.
[9] J.R. Carter et al., Nucl. Instr. and Meth. A278 (1989) 725.
[10] B. Schmidt and S. Polenz, Nucl. Instr. and Meth. A273 (1988) 488.
[11] W.F. Schmidt, Can. J. Chem. 55 (1977) 2197.
[12] A.O. Allen, NSRDS Nat. Bur. Stand. 58 (1976) 1.
[13] W.F. Schmidt, IEEE Trans. Electr. Insul. EI-19 (1984) 389.
[14] R.C. Muñoz, Rad. Phys. Chem. 32 (1988) 169.
[15] W.F. Schmidt and A.O. Allen, J. Chem. Phys. 52 (1970) 4788.
[16] N.E. Cipollini and A.O. Allen, J. Chem. Phys. 67 (1977) 131.
[17] R.C. Muñoz, R.A. Holroyd and M. Nishikawa, J. Phys. Chem. 89 (1985) 2969.
[18] H. Faidas, L.G. Christophorou and D.L. McCorkle, Chem. Phys. Lett. 163 (1989) 495.
[19] J. Dodelet and G.R. Freeman, Can. J. Chem. 50 (1972) 2667.
[20] G. Bakale and W.F. Schmidt, Chem. Phys. Lett. 22 (1973) 164.
[21] T.G. Ryan and G.R. Freeman, J. Chem. Phys. 68 (1978) 5144.
[22] R.C. Muñoz and G. Ascarelli, Chem. Phys. Lett. 94 (1983) 235.
[23] R.C. Muñoz and R.A. Holroyd, Chem. Phys. Lett. 137 (1987) 250.
[24] R.C. Muñoz and G. Ascarelli, Phys. Rev. Lett. 51 (1983) 215.
[25] R.C. Muñoz and G. Ascarelli, J. Phys. Chem. 88 (1984) 3712.
[26] K. Itoh, R.C. Muñoz and R.A. Holroyd, J. Chem. Phys. 90 (1989) 1128.
[27] W. Doldissen and W.F. Schmidt, Chem. Phys. Lett. 68 (1979) 527.
[28] L.G. Christophorou, D.L. McCorkle, D.V. Maxey and J.G. Carter, Nucl. Instr. and Meth. 163 (1979) 141;
S.R. Hunter and L.G. Christophorou, in: Electron–Molecule Interactions and Their Applications, ed. L.G. Christophorou (Academic Press, New York, 1984) vol. 2, chap. 3.
[29] Y. Sakai, H. Bottcher and W.F. Schmidt, J. Electrost. 12 (1982) 89.
[30] W.F. Schmidt, 22nd Symp. on Electrical Insulating Materials, 1989, Tokyo, Japan, pp. 13–24.
[31] S. Ochsenbein, D. Schinzel, A. Gonidec and W.F. Schmidt, Nucl. Instr. and Meth. A273 (1988) 654.
[32] F. Moreau and E. Barrelet, Nucl. Instr. and Meth. A278 (1989) 417.
[33] W.F. Schmidt, in: The Liquid State and Its Electrical Properties, eds. E.E. Kunhardt, L.G. Christophorou and L.H. Luessen (Plenum, New York, 1988) pp. 273–282.
[34] D.L. McCorkle, L.G. Christophorou, D.V. Maxey and J.G. Carter, J. Phys. B11 (1978) 3067.
[35] L.G. Christophorou, in ref. [33], pp. 283–316.
[36] L.G. Christophorou and S.J. Dale, Encyclopedia of Physical Science and Technology (Academic Press, 19[illegible] vol. 4, pp. 246–262;
A.H. Cookson and O. Farish, IEEE Trans. Power Appl. Syst. PAS-92 (1973) 871.
[37] A.H. Sharbaugh, J.C. Devins and S.J. Rzad, IEEE Trans. Electr. Insul. EI-13 (1978) 249.

APPENDIX B



# Laser photodetachment in liquids: $C_6F_6^-$ in tetramethylsilane ☆

H. Faidas, L.G. Christophorou and D.L. McCorkle

*Atomic, Molecular, and High Voltage Physics Group, Health and Safety Research Division, Oak Ridge National Laboratory, Oak Ridge, TN 37831-6122, USA*

*and Department of Physics, The University of Tennessee, Knoxville, TN 37996-1200, USA*

Received 25 February 1992; in final form 7 April 1992

The photodetachment cross section of $C_6F_6^-$ in liquid tetramethylsilane was measured as a function of the photon energy, using a new two laser photoconductivity technique. The photodetachment threshold was found to be 1.51 eV using a 3/2 power threshold law. Two maxima were observed in the photodetachment cross section at photon energies of 2.58 and 3.15 eV; the cross section value at these two maxima is $\approx 11 \times 10^{-18}$ cm$^2$.

## 1. Introduction

The photodetachment of electrons from negative ions in low-pressure gases has been well-studied and is well-understood [1–6]. Similarly the relation of the photodetachment threshold $E_{th}$ to the electron affinity, EA, of the electron attaching species has been well-established [1–6]. In the photodetachment process, the electron is photoejected preferentially into the lowest angular momentum state which is allowed by conservation of angular momentum and parity. Near threshold, the photodetachment cross section, $\sigma_{pd}$, is predicted [7,8] to vary as

$$\sigma_{pd}(E) = BE(E - E_{th})^{(2l+1)/2} \propto k^{2l+1}, \qquad (1)$$

where $B$ is a constant, $E = h\nu$ is the photon energy, $E_{th}$ is the threshold energy for photodetachment, and $k$ and $l$ are the linear and angular momenta of the ejected electron. Thus, the threshold behavior of $\sigma_{pd}(E)$ depends on the type of orbital the electron occupied prior to its detachment: for example, detachment of a p electron (as in $O^-$) leads to $\sigma_{pd} \propto k$ and detachment of an s electron (as in $H^-$) to $\sigma_{pd} \propto k^{3/2}$ near threshold. For atoms, A, the value of the $E_{th}$ for the process

$$A^- + h\nu \rightarrow A + e \qquad (2)$$

is equal to the EA(A), which in turn, is equal to the "vertical detachment energy" (VDE). For molecules, M, the relation of $E_{th}$ for the process

$$M^- + h\nu \rightarrow M + e \qquad (3)$$

to the EA(M) and the VDE is complicated by possible differences in the structural parameters of M and $M^-$ and, also, by the existence of other processes (e.g., dissociation) that can follow photoabsorption by $M^-$. Defining the VDE for reaction (3) as the minimum energy required to eject the electron from the negative ion in its ground electronic and molecular state without changing internuclear separation, then (see fig. 1a) VDE is related to EA and $E_{th}$ by

$$E_{th} = \mathrm{VDE} = \mathrm{EA} + \Delta E, \qquad (4)$$

i.e. the VDE for (3) exceeds the EA by $\Delta E$; the magnitude ($\geq$ eV) of $\Delta E$ depends on the relative position of the potential energy curves (surfaces) of M and $M^-$.

In dense gases and in liquids the photodetachment process for molecules is not yet well studied or

*Correspondence to:* H. Faidas, Atomic, Molecular, and High Voltage Physics Group, Health and Safety Research Division, Oak Ridge National Laboratory, Oak Ridge, TN 37831-6122, USA.

☆ Research sponsored by the Office of Naval Research under contract N00014-89-J-1990 with the University of Tennessee and by the Office of Health and Environmental Research, US Department of Energy, under contract DE-AC05-84OR21400 with Martin Marietta Energy Systems, Inc.

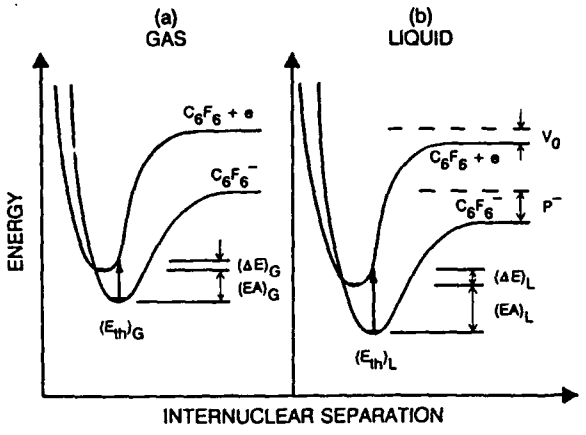


Fig. 1. Schematic potential energy curves for the $C_6F_6$ neutral molecule and the $C_6F_6^-$ negative ion in the gas phase and in a nonpolar liquid such as TMS which has neither permanent dipole moment nor polarization anisotropy. The vertical detachment energy (VDE $= E_{th}$) is indicated by an upward arrow. (The other symbols are explained in the text.)

understood [#1]. It is complicated by the effect of the medium on $E_{th}$ and the potential energy curve (surface) of $M^-$. Rewriting reaction (3) for the liquid as

$$M_L^- + h\nu \rightarrow M_L + e_L \qquad (5)$$

and assuming that $(EA)_L = (EA)_G + V_0 - P^-$ [9,10] we have

$$(E_{th})_L = (VDE)_L = (EA)_L + (\Delta E)_L$$
$$= (EA)_G + V_0 - P^- + (\Delta E)_L , \qquad (6)$$

where $V_0$ and $P^-$ are the polarization energies of the electron and the negative ion in the medium, and $(EA)_L$ and $(EA)_G$ are the values of the electron affinity of M in the liquid and the gas phase (see fig. 1).

There have been only a few earlier studies of photodetachment in nonpolar liquids, namely on $O_2^-$ and $(anthracene)^-$ anions in liquid tetramethylsilane (TMS) and iso-octane [11,12] and on $C_6F_6^-$ [13], $O_2^-$ [14] and a number of aromatic anions [15] in nonpolar solvents. In these studies an X-ray pulse or a gas discharge lamp was used to produce initially the electrons in the liquid and a flashlamp or a tunable dye laser was used to detach the electrons after they were captured by the electronegative molecule under study. A 3/2 power threshold low was employed [11–16] to determine $(E_{th})_L$ from above threshold measurements of $(\sigma_{pd})_L(E)$ and the so determined $(E_{th})_L$ was discussed via eq. (6) assuming $(\Delta E)_L = 0$ eV.

In this Letter, we report a new two-laser photoconductivity technique for photodetachment studies in dense fluids (liquids or high pressure gases) and present measurements of the absolute photodetachment cross section $(\sigma_{pd})_L(E)$ $(1.63 \leqslant E \leqslant 3.44$ eV) and the photodetachment threshold $(E_{th})_L$ for $C_6F_6^-$ in TMS. We, also, discuss the relation of $(E_{th})_L$ to $(EA)_L$ and $(EA)_G$ for this system.

## 2. Experimental

In fig. 2 is shown a schematic of the experimental arrangement we employed. The cell consisted of a six-way stainless-steel cube with two quartz windows and two electrical feedthroughs facing each other. The two parallel electrodes were held at a distance of 4.5 mm and at a potential difference of 9 kV ($E = 20$ kV $cm^{-1}$). Two counter-propagating coaxial laser beams passing through two circular apertures (2.4 mm in

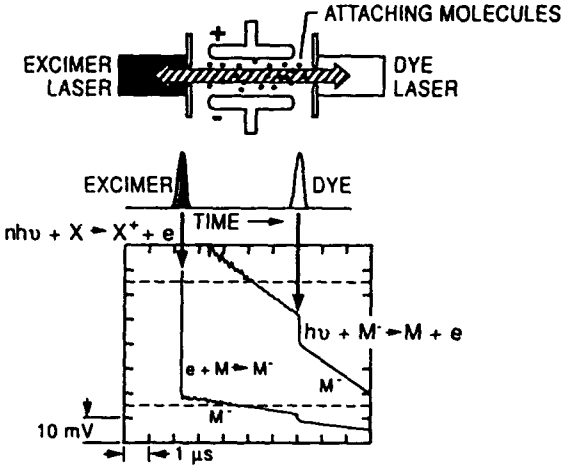


Fig. 2. Schematics of the two laser photodetachment technique, and an oscillogram of the conductivity signal indicating the ionization ($2h\nu + X \rightarrow X^* + e$), attachment ($e + M \rightarrow M^-$) and detachment ($h\nu + M^- \rightarrow M + e$) processes taking place.

[#1] This situation is unlike that for the photoionization process (e.g., see refs. [9,10]).

diameter) on each side of the cell transversed the interaction volume with a time delay of $\approx 5$ μs. The first beam from an excimer laser ($\lambda = 308$ mm; fwhm = 15 ns) ionized biphotonically TMS (or possibly impurities in it) and produced electrons which gave rise to a fast signal (initial drop in fig. 3b). These electrons were quickly (in < 1 ns) attached to $C_6F_6$ (present in TMS at a concentration of $1.73 \times 10^{-5}$ M) forming $C_6F_6^-$. The slowly dropping portion of the signal (figs. 2 and 3b), following the initial steep fall is due to these slow moving anions. The mobility of the negative ions ($C_6F_6^-$) was measured to be $9 \times 10^{-4}$ cm$^2$ s$^{-1}$ V$^{-1}$. At the preset time delay ($\approx 5$ μs), the second laser pulse (from a tunable dye laser; fwhm = 0.6 ns) detached the electrons from $C_6F_6^-$ (when $h\nu > (E_{th})_L$) and produced a second transient electronic signal (step drop in fig. 3b, designated by the letter d), followed by a slow drop when the detached electrons were again captured by $C_6F_6$ forming, slow moving $C_6F_6^-$ ions.

The experimental conditions and the procedure we employed to determine $\sigma_{pd}(E)$ can be discussed with the aid of fig. 3. The first (excimer) laser pulse was picked from the central portion of the excimer laser

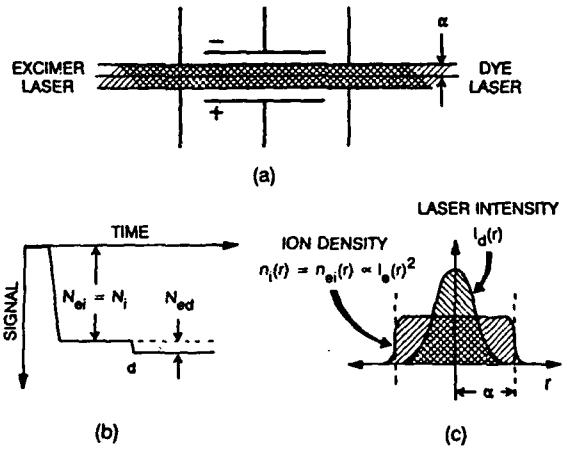


Fig. 3. Schematics of the photodetachment technique illustrating: (a) the laser interaction region, (b) the type of signal measured, and (c) the laser intensity and negative ion density profiles (see the text). $\alpha$ is the radius of the interaction volume; $I_d(r)$ and $I_e(r)$ represent the intensities of the dye and excimer laser beams respectively (in photons cm$^{-2}$); $n_{ei}(r)$ and $n_i(r)$ represent the densities of the initially produced electrons and anions and $N_{ei}$, $N_i$, and $N_{ed}$ represent the total number of initially produced electrons, anions, and detached electrons.

beam and had an essentially flat intensity profile $I_e(r)$ (in photons cm$^{-2}$) for distances $r < \alpha$ where $\alpha$ (= 1.2 mm) is the radius of the cross sectional area of the interaction volume (see fig. 3a). This beam produced the initial pulse of electrons via two-photon ionization. These electrons were uniformly distributed in the interaction volume with a density distribution $n_{ei}(r) \propto I_e(r)^2$. Under our experimental conditions all electrons are captured by $C_6F_6^-$ within 1 ns. Since, at the electric field applied (20 kV cm$^{-1}$), the initial electrons drift $\approx 20$ μm per ns and the $C_6F_6^-$ $\approx 0.18$ μm per μs we can assume that the negative ion density distribution when the tunable laser pulse arrives $\approx 5$ μs later is $n_i(r) = n_{ei}(r) \propto I_e(r)^2$. The tunable dye laser intensity profile $I_d(r)$ was Gaussian (lying well within $\alpha$; see fig. 3c). Under these conditions the density distribution of the photodetached electrons is

$$n_{ed}(r) = \sigma_{pd}(E)\, n_i(r)\, I_d(r) \qquad (7)$$

provided that $n_{ed}(r) \ll n_i(r)$. Furthermore, since neither laser beam was significantly attenuated by the medium, $I_e(r)$, $n_i(r)$, and $I_d(r)$ were virtually constant along the axis of the interaction volume. Under these conditions we find [#2]

$$\sigma_{pd}(E) = \frac{N_{ed}}{N_i} \frac{\pi\alpha^2}{I_t}, \qquad (8)$$

where $N_{ed}$ is the total number of detached electrons, $N_i$ is the total number of negative ions and $I_t = 2\pi \int_0^\alpha I_d(r) r\, dr$ is the total number of photons in the dye laser pulse. The present technique, therefore, can be used to calculate $\sigma_{pd}$ by measuring the ratio $N_{ed}/N_i$ (fig. 3b) and $I_t$ and by knowing the intensity and profile of the two laser beams.

The photodetachment signal was kept small ($N_{ed}/N_i \lesssim 0.03$) so that no volume saturation occurred. The ratio $N_{ed}/N_i$ depended linearly on $I_t$ (see fig. 4). We estimate that the overall error in determining $\sigma_{pd}$ is of the order of 5% to 10%. This error is both systematic (mostly due to errors in determining the size and shape of $I_e(r)$ and $n_i(r)$ and the value of $\alpha$) and random (mostly in measuring $I_t$).

The liquid TMS was purified so that the free electron lifetime in neat TMS was $\gtrsim 1$ μs; $C_6F_6$ (99%

[#2] If both $I_d(r)$ and $n_i(r)$ have Gaussian profiles with halfwidths at $1/e$ of $\beta$ and $\gamma$, eq. (8) becomes $\sigma_{pd}(E) = N_{ed}\pi(\beta^2 + \gamma^2)/N_i I_t$.

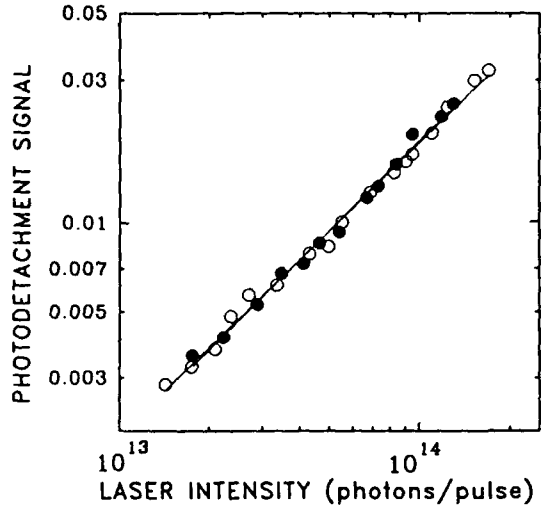


Fig. 4. The photodetachment signal ($\propto N_{ed}/N_i$) as a function of the detaching laser intensity (photons/pulse) at $\lambda=420$ (●) and 500 (○) nm. The slope of the data at both wavelengths is 1 indicating a linear dependence.

pure) was only degassed before it was used. All experiments were performed at room temperature ($T=298$ K).

## 3. Results and discussion

### *3.1. Photodetachment cross section as a function of photon energy*

In fig. 5 is shown the photodetachment cross section $\sigma_{pd}(E)$ of $C_6F_6^-$ in TMS ($T\approx298$ K) for photon energies between 1.63 and 3.44 eV ($360\leqslant\lambda\leqslant760$ nm). The cross section exhibits well-defined maxima at 2.58 and 3.15 eV; the cross section value at these maxima is about the same and equal to $\approx11\times10^{-18}$ cm$^2$. The positions of the two maxima correspond well to those reported [13] in the absorption spectrum of $C_6F_6^-$. The present $\sigma_{pd}(E)$ for $C_6F_6^-$ in TMS is also in good agreement with earlier data [13] taken over a somewhat smaller energy range ($\approx1.75$ to 3 eV).

### *3.2. Photodetachment threshold*

To determine the photodetachment threshold $(E_{th})_L$ from the experimental measurements in fig.

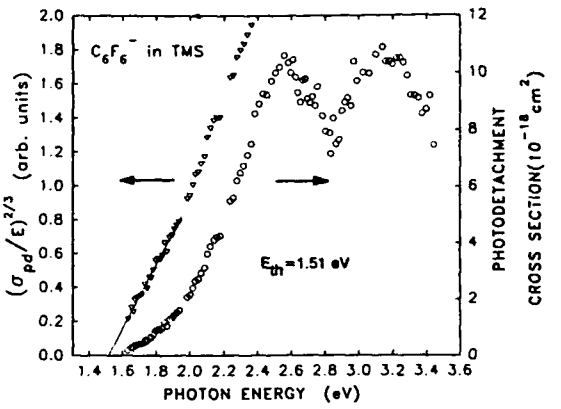


Fig. 5. The absolute photodetachment cross section $\sigma_{pd}(E)$ (right-hand side $Y$ axis) of $C_6F_6^-$ in tetramethylsilane as a function of the photon energy, $E$, and a linear least squares fit of $(\sigma_{pd}/E)^{2/3}$ (left-hand side $Y$ axis) for $E<1.95$ eV. The intercept with the $X$ axis gives a threshold energy $E_{th}$ of 1.51 eV.

5 we made us of (1) which we rewrite as

$$(\sigma_{pd}/E)^{1/n}=B[E-(E_{th})_L]\,, \qquad (9)$$

with $n=\frac{1}{2}(2l+1)$. There are two generic problems in fitting the experimental data to eq. (9): (i) lack of knowledge of the exact value of $n$ (i.e. $l$), and (ii) lack of knowledge of the energy range above $(E_{th})_L$ over which eq. (9) is applicable. We, thus, determined $(E_{th})_L$ and $n$ by fitting eq. (9) to the experimental data over three different energy regions as shown in table 1. Columns 2 and 3 give respectively, the values of $(E_{th})_L$ and the correlation coefficients (CC) when only the data points in the lowest energy range (1.63 to 1.95 eV) are used. The best least squares fit to these data is for $n\approx1.5$ (i.e. $l=1$) and gives a value for $(E_{th})_L=1.51$ eV. In columns 4 and 5 are listed the values of $(E_{th})_L$ and the CC values obtained by a least squares fit to all the data points between 1.63 and 2.37 eV. This procedure indicates a lower $(E_{th})_L=1.41$ eV and a value for $n=2.2$ ($\approx2.5$) consistent with an $l=2$. We take the values of $l=1$ and $(E_{th})_L=1.51$ eV to be the better estimates since (i) we were unable to observe any photodetachment signal at $E=1.48$ eV ($\lambda=840$ nm) and (ii) these values were obtained from experimental data which were energetically closer to the photodetachment threshold. The excellent fit to the data with these values is shown in fig. 5 by the straight line through the measurements which have been

Table 1
Photodetachment threshold $(E_{th})_L$ and corresponding correlation coefficient, CC, for three energy ranges and values of $n$ between 0.5 and 2.5 (see text)

| $n$ | Energy range 1.63–1.95 eV | | Energy range 1.63–2.37 eV | | Energy range 1.75–2.15 eV | |
|---|---|---|---|---|---|---|
| | $(E_{th})_L$(eV) | CC | $(E_{th})_L$(eV) | CC | $(E_{th})_L$(eV) | CC |
| 0.5 | 1.67 | 0.90870 | 1.77 | 0.81817 | | |
| 1.5 | 1.51 | 0.98559 | 1.57 | 0.99050 | 1.59 | 0.98516 |
| 1.6 | 1.50 | 0.98576 | 1.55 | 0.99274 | | |
| 2.2 | 1.40 | 0.98433 | 1.41 | 0.99725 | | |
| 2.5 | 1.35 | 0.98310 | 1.35 | 0.99694 | | |

plotted as $(\sigma_{pd}/E)^{2/3}$ versus $E$. Finally in column 6 of table 1 is listed the value 1.59 eV we obtained for the $(E_{th})_L$ by fitting to eq. (9) the data between 1.75 and 2.15 eV and using $n=1.5$. This energy range and this value for $n$ were used in an earlier study [13] which gave $(E_{th})_L=1.61$ eV for $C_6F_6^-$ in TMS at 296 K.

### 3.3. Possible effects due to impurity anions

If an impurity negative ion $X^-$ is present in the interaction volume in addition to $C_6F_6^-$, then the measured, apparent photodetachment cross section will be

$$\sigma'_{pd}=(N_i\sigma_{pd}+N_{ix}\sigma_{pdx})/(N_i+N_{ix})\,, \qquad (10)$$

where $N_{ix}$ and $\sigma_{pdx}$ are respectively the number of $X^-$ ions in the interaction volume and the photodetachment cross section of $X^-$. The possibility that photodetachment from impurity ions was affecting the measurements (especially the determination of $(E_{th})_L$) was ruled out by performing photodetachment experiments in neat TMS. In these experiments the same purity TMS was used as with the TMS/$C_6F_6$ mixtures, but a lower electric field ($<100$ V cm$^{-1}$) was applied to ensure that the electrons do not escape from the interaction volume. For $E=1.77$ eV ($\lambda=700$ nm) we observed no measurable photodetachment in neat TMS. For $E=2.48$ eV ($\lambda=500$ nm) we observed some photodetachment due to impurity anions and estimated a photodetachment cross section of $1\times10^{-18}$ to $2\times10^{-18}$ cm$^2$, i.e. about a factor of 10 lower than that of $C_6F_6^-$ at this photon energy. We, also, measured the free electron lifetime in neat TMS and in the TMS/$C_6F_6$ mixture we investigated and found it to be $>1$ μs and $<1$ ns respectively. These two measurements indicate that the contribution of any impurity anions present in TMS to the photodetachment signal measured in the TMS/$C_6F_6$ mixture is $<0.01\%$ at $\lambda=500$ nm. Similarly we concluded that possible impurities in $C_6F_6$ itself would not have significantly affected the photodetachment signal for the TMS/$C_6F_6$ mixture.

### 3.4. Relation of $(E_{th})_L$ to $(EA)_L$ and $(EA)_G$

There is a considerable spread in the values of $(EA)_G$ for $C_6F_6$ [17]. Two recent determinations of the $(EA)_G$ of $C_6F_6$ gave a value of 0.86 eV [18,19] and 0.52 eV [20]. The latter value is probably too low and may correspond to an excited state of $C_6F_6^-$. If we take $(EA)_G=0.86$ eV and the values of $-0.51$ eV for $V_0$ [13] and $-0.92$ eV for $P^-$ [14] then from eq. (6) we find $(EA)_L=1.27$ eV which is 0.41 eV larger than $(EA)_G$. From eq. (6), also, we have $(\Delta E)_L=(E_{th})_L-(EA)_L=0.24$ eV. The value of $(\Delta E)_L$ is as expected positive and larger than any possible error. The value of $(\Delta E)_L$ would be 0.58 eV if we used $(EA)_G=0.52$ eV.

## 4. Conclusion

A two laser photoconductivity technique has been developed for the measurement of photodetachment cross sections from negative ions and the determination of the photodetachment thresholds in dense fluids. Using this technique we measured the photodetachment cross section of $C_6F_6^-$ in liquid TMS. The cross section had two maxima at $E=2.58$ and

3.15 eV with a $(\sigma_{pd})_L$ value of $\approx 11 \times 10^{-18}$ cm$^2$. Using a 3/2 power threshold law, the photodetachment threshold was determined to be $(E_{th})_L = 1.51$ eV. An equation of the form

$$(E_{th})_L = (EA)_G + V_0 - P^- + (\Delta E)_L \qquad (11)$$

is necessary to relate the measured photodetachment threshold to the gas phase electron affinity.

## References


[1] L.G. Christophorou, Atomic and molecular radiation physics (Wiley–Interscience, New York, 1971).
[2] T.M. Miller, Advan. Electr. Electron Phys. 55 (1981) 119.
[3] P.S. Drzaic, J. Marks and J.I. Brauman in: Gas phase ion chemistry: ions and light, Vol. 3, ed. M.T. Bowers (Academic Press, New York, 1984) p. 167.
[4] R.D. Mead, A.E. Stevens and W.C. Lineberger, in: Gas phase ion chemistry: ions and light, Vol. 3, ed. M.T. Bowers (Academic Press, New York, 1984), p. 213.
[5] H. Hotop and W.C. Lineberger, J. Phys. Chem. Ref. Data 4 (1975) 539; 14 (1985) 731.
[6] L.G. Christophorou, Contrib. Plasma Phys. 27 (1987) 237.
[7] S. Geltman, Phys. Rev. 112 (1958) 176.
[8] D.S. Burch, S.J. Smith and L.M. Branscomb, Phys. Rev. 112 (1958) 171.
[9] H. Faidas and L.G. Christophorou, Radiation Phys. Chem. 32 (1988) 933.
[10] L.G. Christophorou and K. Siomos in: Electron molecule interactions and their applications, Vol. 2, ed. L.G. Christophorou (Academic Press, New York, 1984) p. 301.
[11] L.V. Lukin and B.S. Yakovlev, Chem. Phys. Letters 92 (1976) 307.
[12] L.V. Lukin, A.A. Balakin and B.S. Yakovlev, Opti. Spectroskopiya 47 (1979) 498.
[13] U. Sowada and R.A. Holroyd, J. Phys. Chem. 84 (1980) 1150.
[14] U. Sowada and R.A. Holroyd, J. Phys. Chem. 70 (1979) 3586.
[15] U. Sowada and R.A. Holroyd, J. Phys. Chem. 85 (1981) 541.
[16] J.K. Baird and T.P. Schuman, Radiation Phys. Chem. 32 (1988) 493.
[17] A.A. Christodoulides, D.L. McCorkle and L.G. Christophorou, in: Electron–molecule interactions and their applications, Vol. 2, ed. L.G. Christophorou (Academic Press, New York, 1984) p. 423.
[18] E.C.M. Chen and W.E. Wentworth, Mol. Cryst. Liquid Cryst. 171 (1989) 271.
[19] W.E. Wentworth, T. Limero and E.C.M. Chen, J. Phys. Chem. 91 (1987) 241.
[20] S. Chowdhury, E.P. Grimsrud, T. Heinis and P. Kebarle, J. Am. Chem. Soc. 108 (1986) 3630.

APPENDIX C

# ULTRAFAST AND ULTRASENSITIVE DIELECTRIC LIQUIDS/MIXTURES: BASIC MEASUREMENTS AND APPLICATIONS

L. G. Christophorou, H. Faidas, and D. L. McCorkle

Atomic, Molecular, and High Voltage Physics Group
Health and Safety Research Division
Oak Ridge National Laboratory
Oak Ridge, Tennessee 37831

The Department of Physics
University of Tennessee
Knoxville, Tennessee 37996

Basic properties of cryogenic and room temperature dielectric liquids/mixtures with high electron yields (under irradiation by ionizing particles) and high excess electron drift velocities are discussed. A number of ultrafast and ultrasensitive liquid media--appropriate for possible use in liquid-filled radiation detectors and other applications--are identified.

## INTRODUCTION

Contrary to low-pressure gases where electrons are "free," in liquids electrons are quasifree or localized; e.g., see Christophorou and Siomos (1984), Christophorou (1988), Schmidt (1984), Freeman (1987), Kunhardt et al. (1988). Excess electrons are quasifree in liquids for which the electron ground-state energy, $V_0$, is negative (< 0 eV). Such liquids can be cryogenic or "warm" (room temperature). Examples are given in Table 1. It is in such liquids (and their mixtures with appropriate additives) that the search for ultrafast and ultrasensitive liquid media is being focused.

## ELECTRON DRIFT VELOCITIES, ELECTRON ENERGIES, AND ELECTRON ATTACHMENT TO MOLECULES IN DIELECTRIC LIQUIDS WITH $V_0$ < 0 eV

In liquids/mixtures with $V_0$ < 0 eV (such as those in Table 1), quasifree electrons drift fast, have energies in excess of thermal at high applied electric fields E, and attach to molecules as in gases (but with notable changes in the energy position, cross section, and lifetime of the negative ion state(s) involved); e.g., see Christophorou and

*Nonequilibrium Effects in Ion and Electron Transport*
Edited by J. W. Gallagher *et al.*, Plenum Press, New York, 1990

Table 1. Examples of Liquids with Negative $V_o$

| | Liquid | $V_o$(eV)[a] |
|---|---|---|
| - | Cryogenic | |
| | Ar(87 K) | -0.20 |
| | Xe(165 K) | -0.61 |
| - | Room Temperature | |
| | Neopentane [$C(CH_3)_4$] | -0.43 |
| | Tetramethylsilane [$Si(CH_3)_4$] | -0.57 |
| | Tetramethylgermanium [$Ge(CH_3)_4$] | -0.64 |
| | Tetramethyltin [$Sn(CH_3)_4$] | -0.75 |
| | 2,2,4,4-Tetramethylpentane [$(CH_3)_3CCH_2C(CH_3)_3$] | -0.36 |

[a] See Christophorou and Siomos (1984), Christophorou (1988), Schmidt (1984), Freeman (1987), Kunhardt et al. (1988), Allen (1976) for original sources of $V_o$ data.

Siomos (1984), Christophorou (1988), Schmidt (1984), Freeman (1987), Kunhardt et al. (1988), Allen (1976), Christophorou (1985), Christophorou et al. (1989). Figs. 1 through 6 exemplify these properties for cryogenic liquids

In Fig. 1 the electron drift velocity (w) as a function of the density-reduced electric field E/N is shown for gaseous Ar (Christohphorou, 1971; Robertson, 1977) and Xe (Christophorou, 1971; Hunter et al., 1988) and for liquid Ar and Xe (Miller et al., 1968). ($w_L$ and $w_G$ refer to the w in the liquid and the gas, respectively.) At any value of E/N, the $w_L$ in the liquid far exceeds the $w_G$ in the low-pressure gas, especially for Xe at low E/N, reflecting the profound changes in the momentum transfer cross section $\sigma_m(\varepsilon)$ between the gas, $(\sigma_m)_G(\varepsilon)$, and liquid, $(\sigma_m)_L(\varepsilon)$ (Christophorou, 1988; Christophorou et al., 1989).

In Fig. 2 the characteristic energy $\left(\frac{3}{2} e \frac{D_T}{\mu}\right)_L$ versus E/N (where $D_T$ is the transverse electron diffusion coefficient and $\mu$ is the electron mobility) is shown for liquid Ar (Shibamura et al., 1979) (T = 87 K) and liquid Xe (Kubota et al., 1982) (T = 165 K). For comparison, the calculated (Christophorou et al., 1989; Hunter et al., 1988) $\left(\frac{3}{2} e \frac{D_T}{\mu}\right)_G$ versus E/N for gaseous Ar and gaseous Xe at room temperature (T = 300 K) and at T = 165 K for Xe and at T = 87 K for Ar are also shown in the

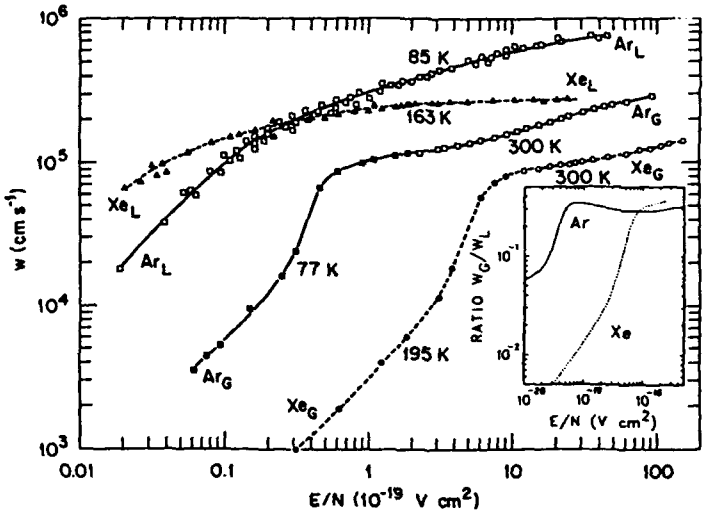


Fig. 1. w versus E/N in gaseous Ar [■,□ ; see Christophorou (1971), Robertson (1977)] and Xe [●, ○; see Christophorou (1971), Hunter et al. (1988)] and liquid Ar [□; see Miller et al. (1968)] and Xe [▲, see Miller et al. (1968)]. Inset: Ratio $w_G/w_L$ versus E/N for Ar and Xe.

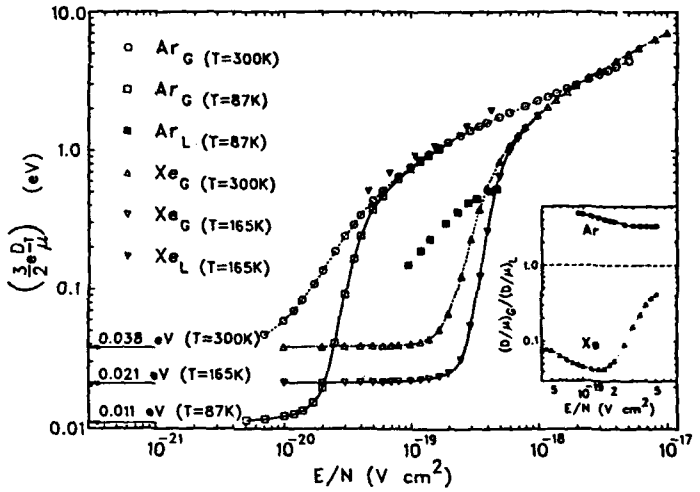


Fig. 2. Calculated (Christophorou et al., 1989; Hunter et al., 1988) $\left(\frac{3}{2} e \frac{D_T}{\mu}\right)_G$ versus E/N for gaseous Ar at T = 300 K (o) and T = 87 K (□) and gaseous Xe at T = 300 K (Δ) and 165 K (∇). The experimental $\left(\frac{3}{2} e \frac{D_T}{\mu}\right)_L$ versus E/N for liquid Ar [■: see Shibamura et al. (1979)] and for liquid Xe [▼: see Kubota et al. (1982)] respectively at 87 and 165 K. Inset: Ratio $\left(\frac{D_T}{\mu}\right)_G \Big/ \left(\frac{D_T}{\mu}\right)_L$ versus E/N for Ar (●) and Xe (Δ).

figure. While the $\left(\frac{3}{2} e \frac{D_T}{\mu}\right)_L$ for liquid Ar are lower than the corresponding gaseous values, the opposite behavior is observed for Xe. In the E/N range over which $D_T/\mu$ measurements were made in the liquid phase (Fig. 2), the characteristic energies are larger in liquid Xe than in liquid Ar.

In Fig. 3 are shown (Christophorou et al., 1989) the various estimates of the mean electron energy $\langle\varepsilon\rangle_L$ versus E/N in liquid Ar. For comparison, the gaseous $\langle\varepsilon\rangle_G$ versus E/N is shown in the figure for T = 300 K and 87 K. Over the entire E/N range investigated, all estimates give—for a fixed E/N—$\langle\varepsilon\rangle_L$ less than $\langle\varepsilon\rangle_G$. Similarly, in Fig. 4 are shown the $\langle\varepsilon\rangle_L$ versus E/N estimates (Christophorou et al., 1989) for liquid Xe. Contrary to the case of Ar, $\langle\varepsilon\rangle_L$ is greater than $\langle\varepsilon\rangle_G$ for Xe at all E/N values (see Fig. 4). The fact that for Xe $\langle\varepsilon\rangle_L > \langle\varepsilon\rangle_G$ at all values of E/N in Fig. 2 is consistent with the result $w_L > w_G$ (Fig. 1) and indicates $(\sigma_m)_L << (\sigma_m)_G$ for $\varepsilon < 1$ eV.

In Fig. 5 is plotted the rate constant $(k_a)_L$ for electron attachment to $SF_6$, $N_2O$, and $O_2$ in liquid Ar (Bakale et al., 1976) as a function of $\langle\varepsilon\rangle_L$ (Christophorou et al., 1989; see Fig. 3). While the $\langle\varepsilon\rangle_L$ dependence of $(k_a)_L$ for the three solutes is similar to the respective $(k_a)_G$ ($\langle\varepsilon\rangle$) in gases (Christophorou et al., 1989; Christophorou, 1971; Christophorou et al., 1984), the $(k_a)_L$ ($\langle\varepsilon\rangle$) functions are normally shifted to lower energies and are larger in magnitude than those $(k_a)_G$ ($\langle\varepsilon\rangle$) in gases (e.g., see Fig. 6 and Christophorou, 1988; 1985).

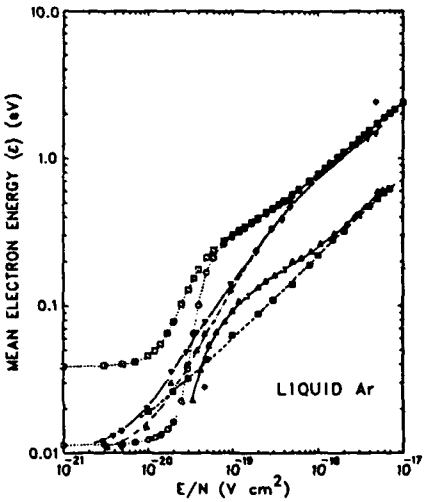


Fig. 3. Calculated $\langle\varepsilon\rangle_L$ versus E/N for liquid Ar, ▼: Nakamura et al. (1986); ■: Christophorou (1985); ▲: Gushchin et al. (1982); ◆: Lekner (1967) in comparison with the calculated values of Christophorou et al. (1989) in liquid Ar at T = 87 K (Δ) and gaseous Ar at T = 87 K (o) and 300 K (□).

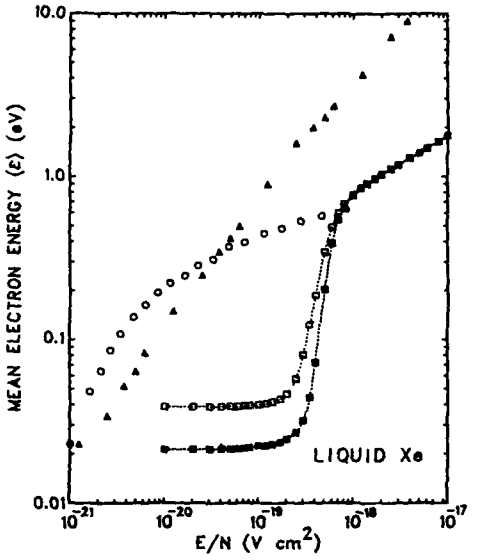


Fig. 4. Calculated $\langle\varepsilon\rangle_L$ versus E/N for liquid Xe, ▲: Gushchin et al. (1982) in comparison with the calculated values of Christophorou et al. (1989) in liquid Xe at T = 165 K (o) and gaseous Xe at T = 165 K (■) and 300 K (□).

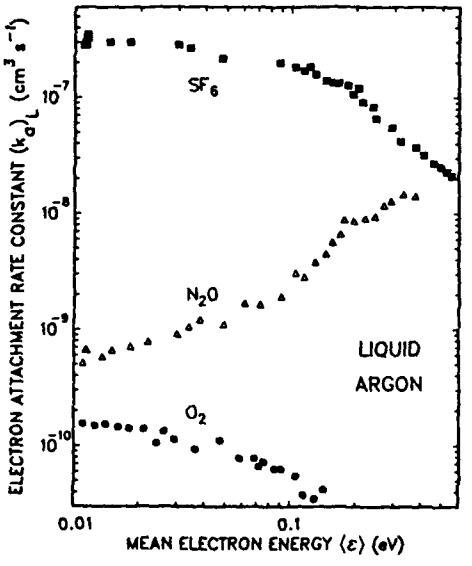


Fig. 5. Rate constant, $(k_a)_L$, for electron attachment to $SF_6$, $N_2O$ and $O_2$ measured in liquid Ar [Bakale et al. (1976)], plotted versus $\langle\varepsilon\rangle_L$ [using the $\langle\varepsilon\rangle_L$ versus E/N estimates of Christophorou et al. (1989)].

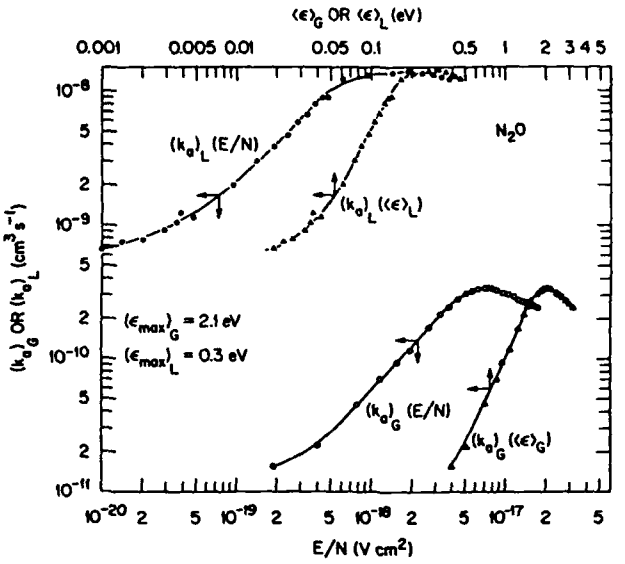


Fig. 6. Electron attachment rate constant for $N_2O$ in gaseous, $(k_a)_G$, and liquid, $(k_a)_L$, argon plotted versus E/N and $\langle\varepsilon\rangle_G$ or $\langle\varepsilon\rangle_L$, see Christophorou (1985). The attachment is due to the reaction $e + N_2O \longrightarrow N_2O^{-*} \longrightarrow O^- + N_2$. Note the shift of the resonance to lower energies— and the increase in the rate constant—in liquid.

For room-temperature dielectric liquids, w(E) has been measured by many authors especially at low E [see Christophorou and Siomos (1984), Christophorou (1988), Schmidt (1984), Freeman (1987), Kunhardt et al. (1988), Allen (1976), Christophorou et al. (1989), Döldissen and Schmidt (1979), Faidas et al. (1989a)]. In Fig. 7 are shown our (Faidas et al., 1989a) recent measurements of w(E) in tetramethylsilane (TMS) and 2,2,4,4-tetramethylpentane (TMP). These measurements extend to $E \gtrsim 1.2 \times 10^5$ V $cm^{-1}$ and were made using a new technique (see below). For both TMS and TMP, the mobility $\mu$ (=w/E) decreases with E (Fig. 8) indicating that the $\langle\varepsilon\rangle_L$ exceeds 1.5 kT, see Bakale and Beck (1986).

The technique employed for the w(E) measurements in Fig. 7 is especially suitable for accurate measurements of w(E) in fast dielectric liquids; it is being developed (through the use of a subnanosecond laser pulse) to also measure longitudinal electron diffusion coefficients in dielectric liquids. The principle of the technique is shown in Fig. 9. After extensive purification (Faidas and Christophorou, 1987), the liquid under study was contained in a cell which consisted of a six-way stainless steel cube with two windows for the entry and exit of the laser beam

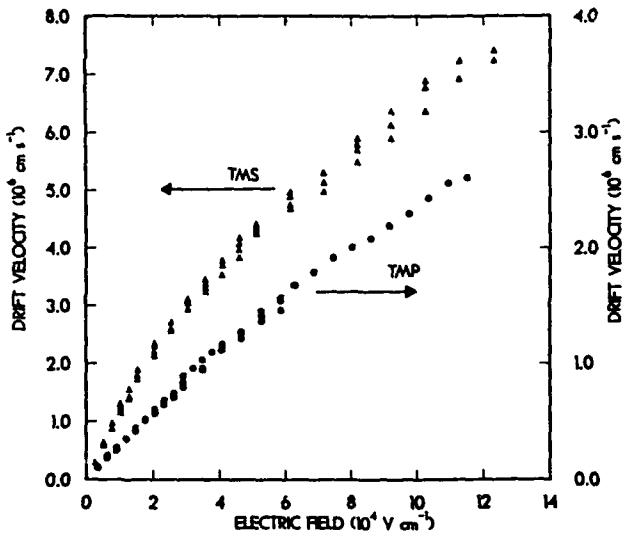


Fig. 7. w versus E for TMS (▲) and TMP (●), Faidas et al. (1989a). The w(E) values of Faidas et al. (1989a) for TMS are ~ 20 percent higher than those of Döldissen and Schmidt (1979). See discussion in Faidas et al. (1989a).

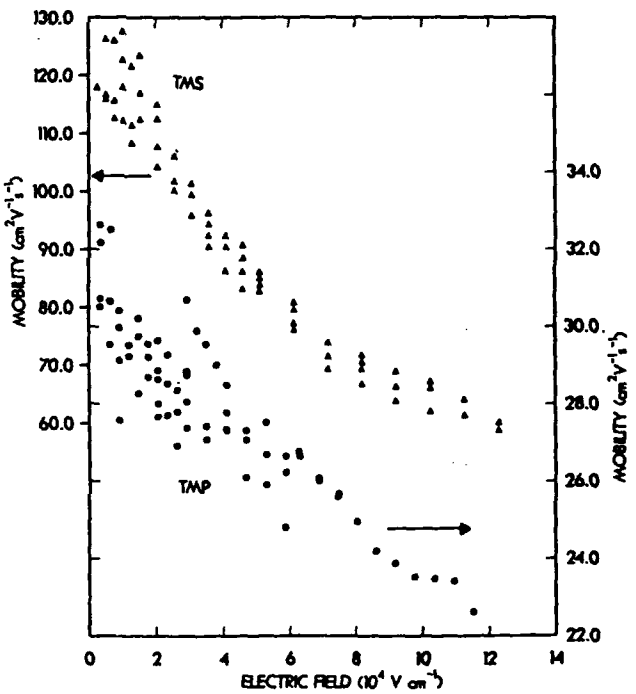


Fig. 8. Mobility of excess electrons versus applied electric field in TMS (▲) and TMP (●), Faidas et al. (1989a).

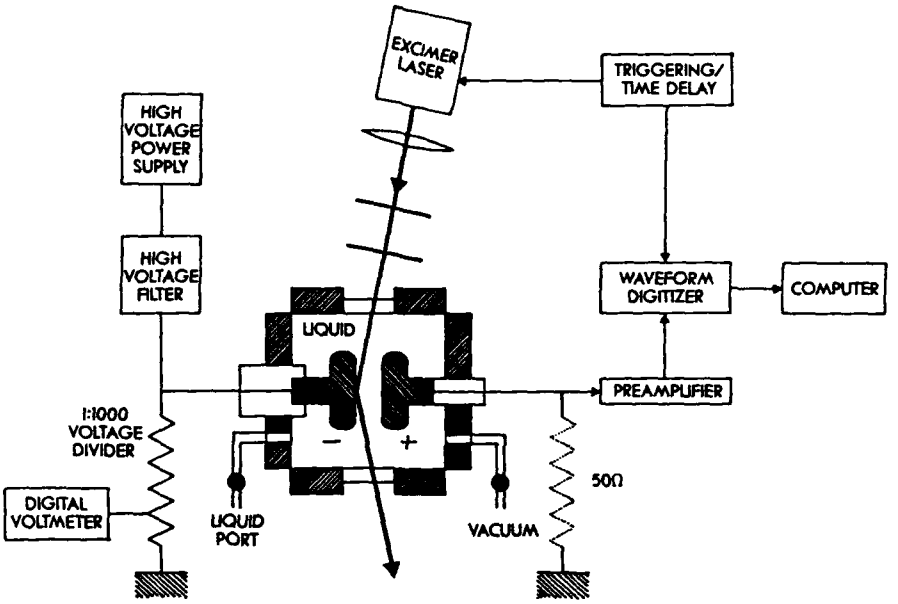


Fig. 9. Schematic of the experimental set up for the measurement of w(E) in fast liquids, Faidas et al. (1989a).

and two electrical feedthroughs (one for the high voltage and the other for the signal) to which the electrodes (two stainless steel parallel-plate circular disks of 1" in diameter and at a distance of a few mm apart) were attached. The beam of an excimer laser ($\lambda$ = 308 nm, pulse duration ~ 17 ns) was focused at the center of the negative high voltage electrode in a circular area of ~ 5 mm in diameter. Voltages in excess of 40 kV could be applied to the high voltage electrode.

The signal due to the drifting pulse of electrons--generated by the laser pulse at the cathode--was measured and recorded in two different ways: (i) In the voltage mode (Fig. 10a) the signal was fed directly to a fast (response time ~ 3 ns) charge-sensitive preamplifier and was captured, averaged and stored, by a transient digitizer as a voltage waveform. (ii) In the current mode (Fig. 10b) the input of the preamplifier was grounded through a 50 Ω resistor. This, in effect, corresponds to electronic differentiation of the voltage-mode signal and gives the transient current waveform.

By numerically differentiating the current-mode signal (Fig. 10c), a waveform corresponding to the rate of charge injection from the cathode and collection at the anode is obtained. The drift time was measured by determining points A and B on any of the three types of waveforms (voltage, current or charge).

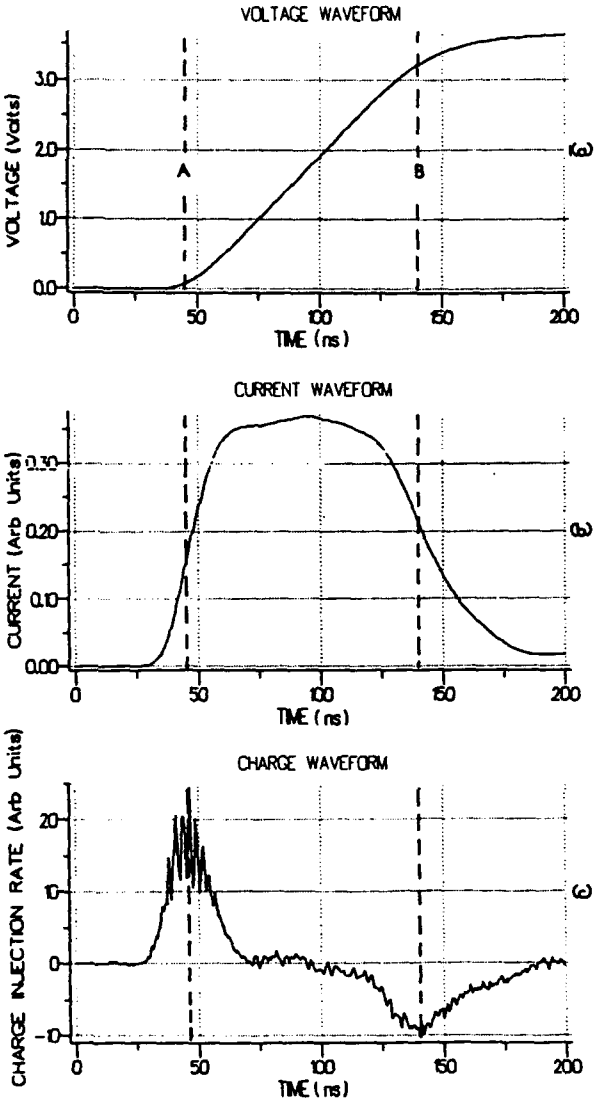


Fig. 10. Voltage (a), current (b), and charge (c) waveforms in TMP. Drift distance = 2.04 mm, applied voltage = 17,574 V, drift time = 97.8 ns, see Faidas et al. (1989a).

## ULTRAFAST AND ULTRASENSITIVE DIELECTRIC LIQUIDS/MIXTURES

### Ultrafast Dielectric Liquids/Mixtures

The fast electron motion in such (cryogenic or room temperature) media finds application in a number of areas such as radiation detectors, see Brassard (1979), Doke (1981), Holroyd and Anderson (1985) and pulsed power switches (Christophorou and Faidas, 1989). In connection with

radiation detectors, liquid Ar and liquid Xe are excellent detector media. It can be seen from Fig. 1, for example, that the w in liquid Ar—and especially liquid Xe—is larger than in the corresponding gas over a large range of E/N. This is highly desirable since the magnitude of w determines the time response of radiation detectors and since a large w reduces electron-ion recombination and thus increases the gain of the detector. The saturation of the w versus E/N curve for liquid Xe at comparatively low E/N values (see Fig. 1) and the much higher density of liquid Xe (allowing improved detector spatial resolution) are additional advantages for using Xe as a detector fluid.

The magnitude of w can be considerably increased over a wide E/N range—as in gases (Christophorou et al., 1979)—by the addition of suitable molecular additives to liquid Ar and Xe. Such additives must be nonelectron-attaching, have appropriate cross sections at low energies, and adequate vapor pressure so that additive concentrations of a few percent are possible. Besides enhancing w, such additives would reduce the size and affect the E/N dependence of the electron diffusion coefficient and mean electron energy, which crucially affect the particle detector's spatial resolution and gain and the influence of electronegative impurities. By analogy to gases, small amounts (< few percent) of molecular additives (e.g., $CH_4$, $C_2H_6$) were added to liquid Ar and Xe and remarkable increases in w were observed (see Fig. 11 and Yoshino et al., 1976; Shibamura et al., 1975).

Similarly, the large w values for a number of room temperature liquids [Fig. 7; Table 2; Christophorou and Siomos (1984), Christophorou (1988), Schmidt (1984), Freeman (1987), Kunhardt et al. (1988), Holroyd

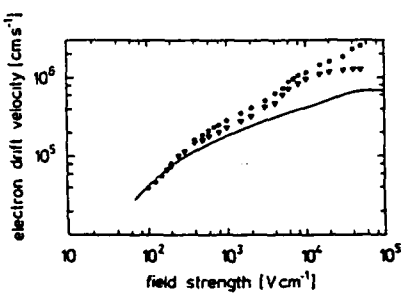


Fig. 11. w versus E in liquid Ar (——) and liquid Ar/$CH_4$ mixtures; ▼ ($N_{CH_4}$ = 2.6 x $10^{20}$ molecules $cm^{-3}$), ●($N_{CH_4}$ = 6.5 x $10^{20}$ molecules $cm^{-3}$). T(Ar) = 87 K, see Yoshino et al. (1976); see this reference for data on other liquid Ar and liquid Xe mixtures).

Table 2. $V_o$, $I_L$, and w for Four Fast Room Temperature Liquids

| Liquid | $V_o$(eV) | $I_L$(eV)[a] | w (cm $s^{-1}$)[b] |
|---|---|---|---|
| 2,2,4,4-Tetramethylpentane | -0.36 | 8.2 | $2.4 \times 10^6$ |
| Neopentane | -0.40 | 8.85 | $\sim 2.5 \times 10^6$ |
| Tetramethylsilane | -0.57 | 8.1 | $6.5 \times 10^6$ |
| Tetramethyltin | -0.75 | 6.9 | - |

[a] Schmidt (1984), Böttcher and Schmidt (1984) and Buschick and Schmidt (1989).

[b] For $E = 10^5$ V $cm^{-1}$.

and Anderson (1985)] make such media good candidates for liquid-filled radiation detectors. It is seen from Fig. 7 that the w approaches $10^7$ cm $s^{-1}$ at E values of $\sim 10^5$ V $cm^{-1}$. While the w(E) of such room temperature liquids may be further increased by appropriate additives, such w(E) enhancements are not expected to be significant.

Ultrasensitive Dielectric Liquids/Mixtures

In attempting to identify the key physical quantities which determine free electron production (by ionizing particles) and allow the selection and development of "ultrasensitive" liquids, let us refer to the following three simple expressions:

$$G_{fe}^{o} = p_{esc}\, G_{te} \tag{1}$$

$$G_{fe}^{E} = G_{fe}^{o} + AE \tag{2}$$

$$I_L = I_G + V_o + P^+ \tag{3}$$

In Eq. (1), $G_{fe}^{o}$ is the yield of free electrons generated in the liquid by the deposition of 100 eV energy by a particular type (e.g., $\alpha$, $\beta$, $\gamma$) of ionizing radiation in the absence of an applied electric field (i.e., E = 0); $G_{te}$ is the total electron yield [$G_{te}$ = 100 eV/W, where W is the average energy (in eV) required to produce an electron-ion pair]; and $p_{esc}$ is the escape probability (i.e., the probability that the initial electron-ion pair will separate and not recombine). While $p_{esc}$ = 1 for low-pressure gases (i.e., geminate recombination is unimportant), in liquids normally $p_{esc} \ll 1$ (i.e., most geminate electron-ion pairs recombine with a resultant strong reduction in $G_{fe}^{o}$). In Eq. (2), (Freeman, 1987; Onsager, 1938) $G_{fe}^{E}$ is the free electron yield when an electric field E is applied across the volume in which the electrons are generated; $G_{fe}^{E}$ exceeds $G_{fe}^{o}$ by an amount AE where A is a constant that depends on the liquid. In Eq. (3) (see Christophorou and Siomos, 1984;

Christophorou, 1988; Schmidt, 1984; Freeman, 1987; Kunhardt et al., 1988; Faidas et al., 1989b; Faidas and Christophorou, 1988), $I_L$ and $I_G$ are the ionization threshold energies for a species embedded in the liquid and in the low pressure gas, respectively, and $P^+$ is the polarization energy of the positive ion in the liquid.

The simple expressions (1) to (3) suggest a number of ways of selecting and developing ultrasensitive (large $G_{fe}^E$) dielectric liquids/mixtures. Clearly, the larger the $G_{te}$ and $P_{esc}$ are, the higher the $G_{fe}^E$.

Pure Liquids ($V_o < 0$ eV)

The total electron yield $G_{te}$ for pure liquids can be increased if W can be lowered. In view of (3)—and since $P^+$ and $V_o$ are negative quantities—$I_L < I_G$ (see Christophorou and Siomos, 1984; Christophorou, 1988; Schmidt, 1984; Freeman, 1987; Kunhardt et al., 1988; Böttcher and Schmidt, 1984; Buschick and Schmidt, 1989; Faidas et al., 1989b; Faidas and Christophorou, 1988; Tables 2 and 3) and thus, $W_L < W_G$ (Christophorou and Siomos, 1984) and $(G_{te})_L > (G_{te})_G$. This is certainly the case for liquid Ar and Xe (Column 4, Table 3).

While the total electron yield $G_{te}$ can be larger in the liquid than in the corresponding gas, the free electron yield $G_{fe}^E$ is smaller in the liquid—by an amount which depends on the applied electric field—even for the very fast liquids (Column 5, Table 3). This is especially the case for densely ionizing particles (e.g., $\alpha$-particles; Column 6, Table 3) due to the very low values of $p_{esc}$. It should be noted that $p_{esc}$ increases with increasing electron drift velocity w; the w—as the electron thermalization length—increases with decreasing electron scattering cross section of the liquid.

For pure liquids ($V_o < 0$ eV), then, a low $I_L$ and large values of w and E are desirable for a large $G_{f}^E e$.

Dielectric Liquids ($V_o < 0$ eV) with Molecular Additives

Clearly the free electron yield can be considerably increased by increasing $G_{te}$ and $P_{esc}$ in liquid rare gas-molecule mixtures. Traces of nonelectron-attaching additives with low $I_L$ in rare gas liquids lower the $W_L$ of the mixture via Penning ionization and other photoionization processes and thus, increase $G_{te}$. A profound increase in $G_{fe}^E$ can be realized (Fig. 12A, B,; Anderson, 1986; Suzuki et al., 1986) by the use of an additive X to liquid Ar (or Xe) which can absorb efficiently the recombination luminescence which is abundantly produced in rare gas

Table 3. $I_L$, $I_G$, and Free Electron Yields for Some Efficient Liquids

| Liquid | $I_L$(eV) | $I_G$(eV) | Electron Yield (Electrons/100 eV) $G_{te}(e, \gamma)^a$ | $G^o_{fe}(e,\gamma)^a$ | $G^E_{fe}(\alpha)^b$ |
|---|---|---|---|---|---|
| Ar | ~14.1[c] | 15.755[d] | 4.4[e] | 2.3[f] (4.3)[f,g] | 0.45[f,g] |
| Xe | ~8.9[c] | 12.127[d] | (3.8)[h]$_G$ 6.5[e] (4.6)[h]$_G$ | 4.4[i] | - |
| $C(CH_3)_4$ | 8.85[j] | 10.23[k] | 4.30[l] | 1.1[f] (1.8)[f,g] | 0.036[f,g] |
| $Si(CH_3)_4$ | 8.1[j] | 9.65[k] | - | 0.74[f] (1.19)[f,g] | 0.029[f,g] |

[a]For low-ionization density particles (electrons, $\gamma$-rays).
[b]For high-ionization density particles ($\alpha$-particles).
[c]Christophorou and Siomos (1984), p. 307.
[d]Christophorou (1971).
[e]Christophorou and Siomos (1984), p. 304.
[f]Holroyd and Anderson (1985) (T = 296 K).
[g]For E= $10^4$ V $cm^{-1}$, see Holroyd and Anderson (1985).
[h]Gaseous value determined from the W-values in Christophorou (1971).
[i]Huang and Freeman (1977).
[j]From Table 2.
[k]Levin and Lias (1982).
[l]György and Freeman (1987).

liquids, see Doke (1981), and be efficiently ionized. For a liquid Ar, X system these processes can be written as

$$Ar^+ + Ar \longrightarrow Ar_2^+$$

$$Ar_2^+ + e \longrightarrow h\nu_E + Ar + Ar$$

$$h\nu_E + X \xrightarrow{\sigma_{ax}} X^* \xrightarrow{\eta_x} X^+ + e$$

where $h\nu_E$ is the liquid argon excimer (E) recombination luminescence which peaks at ~ 9.55 eV and $\sigma_{ax}$ and $\eta_x$ are, respectively, the absorption cross section and ionization efficiency of $X^*$. To optimize these processes one needs to select an X with an optimum $\sigma_{ax}\eta_x$ product. Such additives (e.g., amines, tetramethylgermanium) (Anderson, 1986; Suzuki et al., 1986) can be added in parts per million levels to binary liquid argon-molecule mixtures already optimized for a maximum electron drift velocity. A large w and a high applied field E will further increase $G^E_{fe}$ by increasing $p_{esc}$ (Fig. 12).

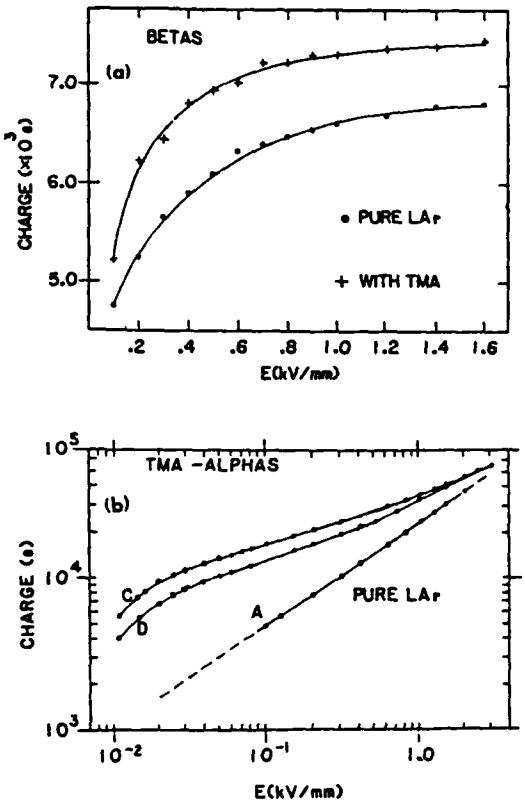


Fig. 12. Charge collected as a function of applied electric field for:
Fig. 12(a): β-particles in pure argon (●) and liquid argon-triethylamine (TEA) mixture.
Fig. 12(b): α-particles in pure argon (A) and in liquid argon-triethylamine mixtures (Curve C: 4.6 x $10^{15}$ molecules $cm^{-3}$; Curve D: 1.1 x $10^{15}$ molecules $cm^{-3}$). From Anderson (1986); see this reference for details and data on other liquid argon mixtures.

The $G_{fe}^{E}$ of fast room temperature dielectric liquids is limited compared to cryogenic liquid rare gases, especially for densely ionizing particles (Table 3). For room temperature liquids the electron thermalization length--and hence $p_{esc}$--are much smaller than for the cryogenic liquids, internal conversion and dissociation processes rapidly deplete excited electronic states which might lead to Penning ionization in room temperature mixtures, and recombination luminescence is too weak or nonexistent to be useful as an additional electron production mechanism in mixtures. However, it might be possible to improve the efficiency of fast room temperature dielectric liquids by employing Penning mixtures where the ionization onset energy, $I_L(X)$, of the impurity X in these fast

liquids is very lov [e.g., the $I_L$ of tetrakis(dimethylamino)ethylene (TMAE) in tetramethylsilane has been reported to be 3.54 eV (Nakato et al., 1974) and 3.66 eV (Holroyd et al., 1985) and that of N,N,N', N'tetramethyl-p-phenylenediamine (TMPD) in the same liquid 4.29 eV (Holroyd, 1972) and 4.45 eV (Bullot and Gauthier, 1977)] and by applying very high electric fields.

ACKNOWLEDGMENTS

Research sponsored by the Office of Health and Environmental Research of the U. S. Department of Energy under Contract No. DE-AC05-84OR21400 with Martin Marietta Energy Systems, Inc. and by the U. S. Department of Energy and the Office of Naval Research under, respectively, Contracts No. DE-AS05-76ER03956 and N00014-89-J-1990 with the University of Tennessee.

REFERENCES

Allen, A. O., 1976, NSRDS-NBS 58, 1.
Anderson, D. F., 1986, Nucl. Instr. Meth. Phys. Res. A242, 254; ibid, A245, 361.
Bakale, G., and G. Beck, 1986, J. Chem. Phys. 84, 5344.
Bakale, G., U. Sovada, and W. F. Schmidt, 1976, J. Phys. Chem. 80, 2556.
Böttcher, E. -H., and W. F. Schmidt, 1984, J. Chem. Phys. 80, 1353.
Brassard, C., 1979, Nucl. Instr. Meth. 162, 29; J. Engler, and H. Keim, 1984, Nucl. Instr. Meth. Phys. Res. 223, 47.
Bullot, J., and M. Gauthier, 1977, Can. J. Chem. 55, 1821.
Buschick, K., and W. F. Schmidt, 1989, IEEE Trans. Electr. Insul. EI-24, 353.
Christophorou, L. G., 1985, Chem. Phys. Lett. 121, 408.
Christophorou, L. G., 1988, "The Liquid State and Its Electrical Properties," E. E. Kunhardt, L. G. Christophorou, and L. H. Luessen, (Eds.), NATO ASI, Series B, Vol. 193, (Plenum Press), New York, p. 283.
Christophorou, L. G., 1971, "Atomic and Molecular Radiation Physics," Wiley-Interscience, New York.
Christophorou, L. G., and H. Faidas, 1989, Appl. Phys. Lett. 55, 948.
Christophorou, L. G., and K. Siomos, 1984, "Electron-Molecule Interactions and Their Applications," L. G. Christophorou, (Ed.), Academic, New York, Vol. 2, Chapt. 4.
Christophorou, L. G., S. R. Hunter, and J. G. Carter, 1989, Intern. J. Radiat. Phys. Chem. 34, 819.
Christophorou, L. G., D. L. McCorkle, and A. A. Christodoulides, 1984, "Electron-Molecule Interactions and Their Applications," L. G. Christophorou, (Ed.), Academic, New York, Vol. 1., Chapt. 6.
Christophorou, L. G., D. L. McCorkle, D. V. Maxey, and J. G. Carter, 1979, Nucl. Instr. Meth. 163, 141; L. G. Christophorou, D. V. Maxey, D. L. McCorkle, and J. G. Carter, 1980, Nucl. Instr. Meth. 171, 491.
Doke, T., 1981, Portgal. Phys. 12, 9.
Döldissen, W., and W. F. Schmidt, 1979, Chem. Phys. Lett. 68, 527.
Faidas, H., and L. G. Christophorou, 1987, J. Chem. Phys. 86, 2505.
Faidas, H., and L. G. Christophorou, 1988, Rad. Phys. Chem. 32, 433.
Faidas, H., L. G. Christophorou, and D. L. McCorkle, 1989a, Chem. Phys. Lett., 163, 495.
Faidas, H., L. G. Christophorou, P. G. Datskos, and D. L. McCorkle, 1989b, J. Chem. Phys. 90, 6619.
Freeman, G. R., (Ed.), 1987, "Kinetics of Nonhomogeneous Processes," Wiley-Interscience, New York.

Gushchin, E. M., A. A. Kruglov, and I. M. Obodovskii, 1982, Sov. Phys. JETP 55, 650.
György, I., and G. R. Freeman, 1987, J. Chem. Phys. 86, 681.
Holroyd, R. A., 1972, J. Chem. Phys. 57, 3007.
Holroyd, R. A., and D. F. Anderson, 1985, Nucl. Instr. Meth. Phys. Res. A 236, 294.
Holroyd, R. A., S. Ehrenson, and J. M. Preses, 1985, J. Phys. Chem. 89, 4244.
Huang, S. S., and G. R. Freeman, 1977, Can. J. Chem. 55, 1038.
Hunter, S. R., J. G. Carter, and L. G. Christophorou, 1988, Phys. Rev. A 38, 5539.
Kubota, S., T. Takahashi, and J. Ruangen, 1982, J. Phys. Soc. Jpn. 51, 3274.
Kunhardt, E. E., L. G. Christophorou, and L. H. Luessen, (Eds.), 1988, "The Liquid State and Its Electrical Properties," NATO ASI, Series B, Vol. 193, (Plenum Press), New York.
Lekner, J., 1967, Phys. Rev. 158, 130.
Levin, R. D., and S. G. Lias, 1982, "Ionization Potential and Appearance Potential Measurements, 1971-1981," U. S. Department of Commerce, NSRDS-NBS-71, NBS.
Miller, L. S., S. Howe, and W. E. Spear, 1968, Phys. Rev. 166, 871.
Nakamura, S., Y. Sakai, and H. Tagashira, 1986, Chem. Phys. Lett. 130, 551; Y. Sakai, S. Nakamura, and H. Tagashira, 1985, IEEE Trans. Electr. Insul. EI-20, 133.
Nakato, Y., T. Chiyoda, and H. Tsubomura, 1974, Bull. Chem. Soc. Jpn. 47, 3001.
Onsager, L., 1938, Phys. Rev. 54, 554.
Robertson, A. G., 1977, Austr. J. Phys. 30, 39.
Schmidt, W. F., 1984, IEEE Trans. Electr. Insul. EI-19, 389.
Shibamura, E., A. Hitachi, T. Doke, T. Takahashi, S. Kubota, and M. Miyajima, 1975, Nucl. Instr. Meth. 131, 249.
Shibamura, E., T. Takahashi, S. Kubota, and T. Doke, 1979, Phys. Rev. A 20, 2547.
Suzuki, S., T. Doke, A. Hitachi, J. Kikuchi, A. Yunoki, and K. Masuda, 1986, Nucl. Instr. Meth. Phys. Res. A 245, 366.
Yoshino, K., U. Sowada, and W. F. Schmidt, 1976, Phys. Rev. A 14, 438.

APPENDIX D

Proceedings of the 10th International Conference on Conduction and Breakdown in Dielectric Liquids, Grenoble, France, September 10-14, 1990, (P. Atten, R. Tobazeon, Eds.) (1990)



# DIELECTRIC-LIQUID PULSED POWER SWITCH[1]

L. G. Christophorou and H. Faidas

Atomic, Molecular, and High Voltage Physics Group, Health and Safety Research Division, Oak Ridge National Laboratory, Oak Ridge, Tennessee 37831, and Department of Physics, The University of Tennessee, Knoxville, Tennessee 37996

## ABSTRACT

Room temperature fast dielectric liquids with electron conduction bands ($V_0$ < 0 eV; e.g., neopentane, tetramethylsilane, 2,2,4,4-tetramethylpentane and their mixtures) are electrically-active insulators and have potential as controlled conduction media in pulsed power switching devices. A concept for a dielectric-liquid pulsed power switch employing flash lamps is outlined.

## INTRODUCTION

A number of new concepts and materials have been proposed for various types of opening and closing pulsed power switches. Some utilize dielectric gases as switching media, and others employ semiconductor wafers [Ref. 1; Fig. 1, paths 1 and 2). A salient feature of these devices is that a laser or an electron beam is employed to ionize the switching medium to initiate and/or to sustain a current flow through the switch (i.e., to close the switch) which is otherwise open due to the very high resistance of the switching medium in the absence of the ionizing energy. While optimization of the materials and the parameters of operation of this type of switches may further improve their performance, there is a continuing need to develop a switching medium that can be made conducting with a conventional energy source and a switch which is easily manufactured and maintained.

In this paper, we explore[2] the possibility of using a dielectric liquid as the switching medium in pulsed power generation and especially the possibility of switching a good dielectric liquid to a good conductor by photo-injecting excess electrons into it using a flash lamp (Fig. 1, path 3).

---

[1]Research sponsored by the Office of Health and Environmental Research, U.S. Department of Energy under Contract DE-AC05-84OR21400 with Martin Marietta Energy Systems, Inc., and by the Office of Naval Research under Contract N00014-89-J-1990 with the University of Tennessee.

## DIELECTRIC LIQUIDS AS ELECTRICAL INSULATORS AND AS CONDUCTORS OF EXCESS ELECTRONS

In Fig. 2 are shown recent measurements[3] of the electron drift velocity, w, for tetramethylsilane (TMS), tetramethyltin (TMT), 2,2,4,4-tetramethylpentane (TMP) and neopentane (TMC), and in Table I are listed values, $w_{max}$, of w at the highest, $E_{max}$, electric field employed in Ref. 3 for the neat liquids and some of their mixtures, along with the $V_0$ values[4] for the neat liquids. Clearly, such liquids are--in the absence of electronegative impurities--good conductors of excess electrons for reasonable values of E; they are also good electrical insulators, withstanding $E \gtrsim 2 \times 10^5$ V cm$^{-1}$. It should be noted, however, that some of these liquids may be unsuitable for this particular application for other reasons; for example, TMT was found[3] to extensively decompose in the event of electrical breakdown.

The photo-injection of excess electrons in the liquid can be accomplished by the use of conventional pulsed light sources. The work function at E = 0, $W_{L,0}$, of a metal immersed in dielectric liquids with $V_0 < 0$ eV is lowered from its vacuum value, $W_V$: $W_{L,0} = W_L + V_0$. At $E > 0$, the work function is lowered further by an amount $\Delta W$ so that $W_{L,E} = W_V + V_0 + \Delta W$. This lowers the minimum photon energy to eject an electron from a metal surface into the liquid[2,6] and conveniently locates it in the optical spectrum of many flash lamps. For example, for Zn in TMS, $W_{L,E} = 3.12$ eV (corresponding to a threshold wavelength $\lambda \simeq 4000$ Å; $E \simeq 10^4$ V cm$^{-1}$) and for Ba in TMS, $W_{L,E} = 1.77$ eV [$\lambda \simeq 7000$ Å; $E \simeq 7 \times 10^3$ V cm$^{-1}$ (Ref. 5)]. For a fixed E, the photoelectron yield increases[6] rapidly with increasing photon energy hν above $W_{L,E}$ and tends toward saturation when $h\nu \simeq W_{L,E} + (1 \text{ to } 2)$ eV.

It is, therefore, possible to employ conventional pulsed-light sources to inject large numbers of excess electrons in dielectric liquids with negative $V_0$, especially when $h\nu - W_{L,E} \gtrsim 2$ eV and E is large, since a large fraction of the electrons injected at the metal/liquid interface returns to the cathode especially at low E.

## DIELECTRIC LIQUID PULSED POWER SWITCH

In Fig. 3 a schematic of such a switch is depicted for the case of inductive energy storage. Its main features are: (1) a dielectric liquid as the switching medium, (2) a light pulse as the ionization source, and (3) a metallic (or semiconducting) film as the photoemissive material. The dielectric liquid can be one of the liquids mentioned above. The light source

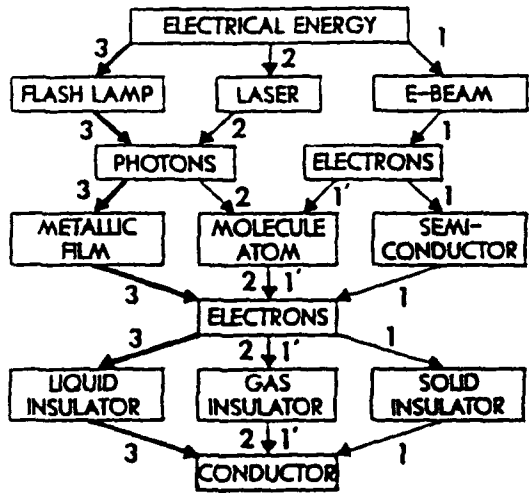


Fig. 1: Principle/ steps of pulsed power switches using flash lamps, lasers or e-beams.

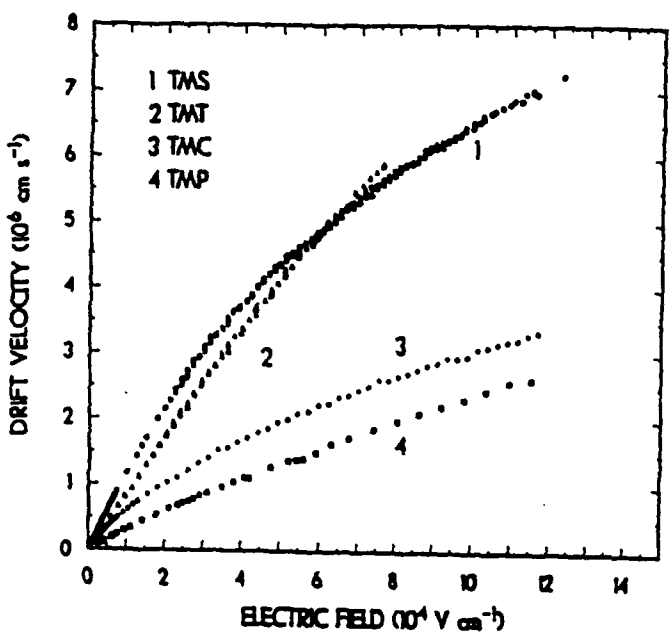


Fig. 2: Electron drift velocity as a function of the applied uniform electric field in a number of fast room temperature dielectric liquids.[3]

TABLE 1: Mole Fraction, $w_{max}$, $E_{max}$, and $V_0$ for Fast Liquids/Mixtures[3].

| Liquid/Mixture | Mole Fraction | $w_{max}$ ($10^6$ cm $s^{-1}$) | $E_{max}$ ($10^3$ V $cm^{-1}$) | $V_0$[a] (eV) |
|---|---|---|---|---|
| TMS | Neat | 7.2 | 125 | -0.62 |
| TMT | Neat | 6.0 | 75 | -0.75 |
| TMC | Neat | 3.3 | 117 | -0.43 |
| TMP | Neat | 2.6 | 115 | -0.36 |
| TMS/TMP | 1.31/1 | 3.2 | 105 | - |
| TMS/n-pentane | 102/1 | 6.8 | 105 | - |
| TMS/n-pentane | 17/1 | 6.8 | 145 | - |
| TMS/n-pentane | 5.6/1 | 4.9 | 145 | - |

[a]Ref. [4].

considered is a gas-filled flash lamp of appropriate geometry generating a UV light pulse of the desired intensity and duration determined by its design, gas selection and gas pressure.[6] The lamp's envelope can be made of a UV transmitting material coated with metallic or semiconducting film and serve as the cathode and the electron injecting material. By proper optimization of the thickness and composition of the coating material one can maximize the photoelectron yield, minimize light transmission, and achieve good electrical conductivity and stability.

Opening switches for inductive energy storage normally require closing ("ON") times in the μs to ms range and opening times < 50 to 100 ns. Since the electron drift times, d/w where d is the drift distance, are of the order of ns, the switch opening time will be determined by the fall time of the light pulse. While many flash lamps, such as Xe flash lamps, can generate kJ light pulses of μs to ms duration, the fall times of these pulses--at least for their UV part--must be short, ~ 100 ns, for those applications requiring short and large amplitude load pulses. (Nanosecond flash lamps normally generate mJ pulses). Preliminary calculations indicate that conduction currents due to excess electrons in the kA range are achievable with reasonable efficiencies. A dielectric liquid pulsed power switch can be cheap, can carry high currents and can sustain high voltages; it can be more efficient (compared to laser or e-beam), more stable (compared to solid state or gas), and more compact (compared to gas).

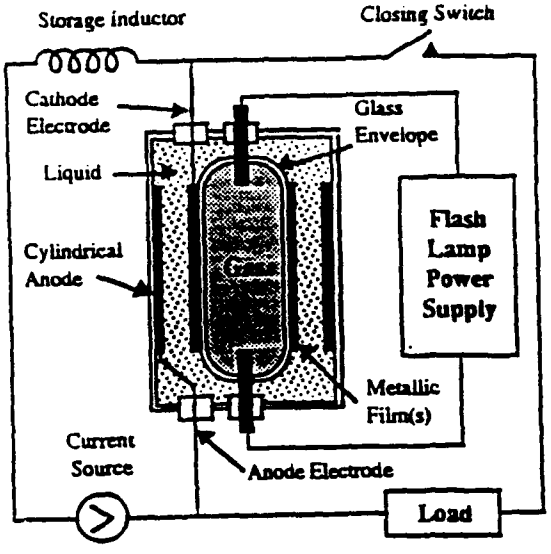


Fig. 3: Schematic diagram of the dielectric liquid pulsed power switch employing a pulsed flash lamp.[2]

While further studies are needed to establish the full potential (and limitations) of dielectric liquids in pulsed power switching, fast liquid conducting and insulating media appear to be powerful new pulsed-power switching materials.

REFERENCES

[1] L. G. Christophorou and D. W. Bouldin, Eds., *Gaseous Dielectrics V* (Pergamon, New York, 1987), Chap. 7; A. Guenther, M. Kristiansen, and T. Martin, Eds., Opening Switches (Plenum, New York, 1987).

[2] L. G. Christophorou and H. Faidas, Appl. Phys. Lett. 55, 948 (1989).

[3] H. Faidas, L. G. Christophorou, D. L. McCorkle, and J. G. Carter, *Nuclear Instruments and Methods in Physics Research (Section A)* (submitted).

[4] L. G. Christophorou and K. Siomos, in *Electron-Molecule Interactions and Their Applications*, edited by L. G. Christophorou, (Academic, New York, 1984), Vol. 2, Chap. 4; W. F. Schmidt, IEEE Trans. Electr. Insul. EI-19, 389 (1984); R. A. Holroyd, S. Tames and A. Kennedy, J. Phys. Chem. 79, 2857 (1975).

[5] R. A. Holroyd and M. Allen, J. Chem. Phys. 54, 5014 (1971).

[6] F. B. A. Früngel, *High Speed Pulse Technology* (Academic, New York); Vol. II (1965); Vol. IV (1980); *Flash Tubes and Related Equipment* (Xenon Corporation, Woburn, Massachusetts, 1989).

APPENDIX E

To be published in: "Linking the Gaseous and Condensed Phases of Matter" L. G. Christophorou, W. F. Schmidt, and E. Illenberger (Eds.), Plenum Press, New York (1993)

# LINKING THE GASEOUS AND THE CONDENSED PHASES OF MATTER: THE SLOW ELECTRON AND ITS INTERACTIONS[1]

Loucas G. Christophorou

Atomic, Molecular, and High Voltage Physics Group, Health and Safety Research Division, Oak Ridge National Laboratory, Post Office Box 2008, Oak Ridge, Tennessee 37831-6122, and Department of Physics, The University of Tennessee, Knoxville, Tennessee, 37996

## ABSTRACT

The interfacing of the gaseous and the condensed phases of matter as effected by interphase and cluster studies on the behavior of key reactions involving slow electrons either as reacting initial particles or as products of the reactions themselves is discussed. Emphasis is placed on the measurement of both the cross sections and the energetics involved, although most of the available information to date is on the latter. The discussion is selectively focussed on electron scattering (especially the role of negative ion states in gases, clusters, and dense matter), ionization, electron attachment and photodetachment. The dominant role of the electric polarization of the medium is emphasized.

## INTRODUCTION

### Interphase and Cluster Studies

The interfacing of the gaseous and the condensed phases of matter requires multidisciplinary and systematic investigations as to how the microscopic and the macroscopic properties of materials and the elementary processes involving electrons, photons, ions, and neutral particles change as one makes the transition from a low pressure gas (isolated-particle behavior) to the condensed phase. There have been two complementary approaches in this endeavor: (i) interphase physics/chemistry and (ii) clusters. In the former approach, a given reaction (or property) is studied as a function of the density and the nature of the medium in which it occurs from the low-pressure gas to the liquid or the solid. Actually, traditionally such studies begin at either end of the density range: from the liquid (solid) density to progressively lower densities and from a low density gas (binary collisions)

[1]Research sponsored by the Office of Health and Environmental Reserach, U.S. Department of Energy, under Contract DE-AC05-84OR21400 with Martin Marietta Energy Systems, Inc., and by the Office of Naval Research under Contract N00014-89-J-1990 with the University of Tennessee, Knoxville, Tennessee, 37996.

to progressively higher densities (multiple scattering regime), and to the condensed phase. Both bridge the density gap between low pressure gases and condensed matter (e.g., see Refs. 1-5 and references therein). In the latter approach, the properties and reactions of a given species (atom or molecule) are studied as a function of its size (increased gradually by clustering), cluster[2] shape and cluster composition. A unique feature of clusters is that they allow studies of the transition from large finite clusters to the bulk and thus determination of the minimum cluster size beyond which the cluster properties no longer vary with size but are essentially similar to those of a macroscopic sample of the material (e.g., see Ref. 6 (and references cited therein) and Refs. 7-12).

## Why Slow Electrons?

Slow electrons are abundant and reactive species in all phases of matter[13]. They are generated in gaseous and condensed matter by a multiplicity of mechanisms: energy transfer from high-energy particles to atoms and molecules; absorption of light by neutrals or negative ions; collisions of excited and unexcited atoms, negative ions with neutrals, electrons with neutrals or ions; injection from surfaces. They lose their energy and slow-down in matter in elastic and a multiplicity of inelastic collisions[14]. They interact before they are thermalized (i.e., during their slowing down) and also after they have reached thermal equilibrium or steady-state conditions (when an applied electric field E is superimposed on the medium). This distinction is significant since the interactions of slow electrons in a dense medium depend on the "state" of the electron itself.

For a low-pressure gas, the electrons are normally free and the collision (interaction) mean free path $l$ is much longer than the electron de-Broglie wavelength. In a dense medium (high pressure gas, liquid or solid) $l$ is smaller than the de-Broglie wavelength and as the medium density increases the electrons become localized or delocalized into conduction bands. In the former case, their mobilities are low and their kinetic energies are thermal and in the latter case their mobilities are high and their kinetic energies (under an applied electric field) can exceed considerably thermal energies[3].

The reactions of slow electrons in dense matter often differ greatly from those in a low-pressure gas. They are unique in that they help us unravel the structure of atoms and molecules, probe the structural and dynamical changes with the density and the nature of matter, and quantify the energetics and dynamics of basic reactions in matter.

## This Lecture

In this lecture we discuss the behavior of key reactions--as studied by interphase and cluster researches--involving slow electrons either as reacting initial particles or as products of the interactions themselves. We emphasize measurement of both cross sections and energetics, although most of the available information to date is on the latter. We selectively focus on electron scattering (especially the role of negative ion states in gases, clusters, and dense matter), ionization, electron attachment and photodetachment and emphasize the dominant role of the electric polarization of the medium on the reaction energetics. The comparison between the gaseous and the liquid phase measurements is restricted to dielectric

[2]Normally the term cluster is used to describe finite aggregates of 2 to $10^4$ particles (atoms or molecules).

liquids with conduction bands[3] where the excess electrons are quasi-free--not localized as, say, in polar media--and the connection between the electron behavior in the two phases is more apparent. Finally, the general nature of this lecture unavoidably touches on aspects of the theme of this meeting that will be covered by subsequent lecturers. We hope that it will enhance the value of and the anticipation for these upcoming and in-depth lectures.

## DIRECT AND INDIRECT ELECTRON COLLISIONS

Slow electrons lose their energy and slow down in matter in elastic and (a multiplicity of) inelastic collisions. Such collisions are either direct or indirect (*Fig. 1*). *In a direct* - glancing - collision the electron is scattered at a distance from the target, the duration of the collision is short, and the cross section for the collision--whether elastic or inelastic--is appreciable over a broad range of incident electron energies. In contrast, in indirect collisions the electron is temporarily captured by the target forming a transient anion whose

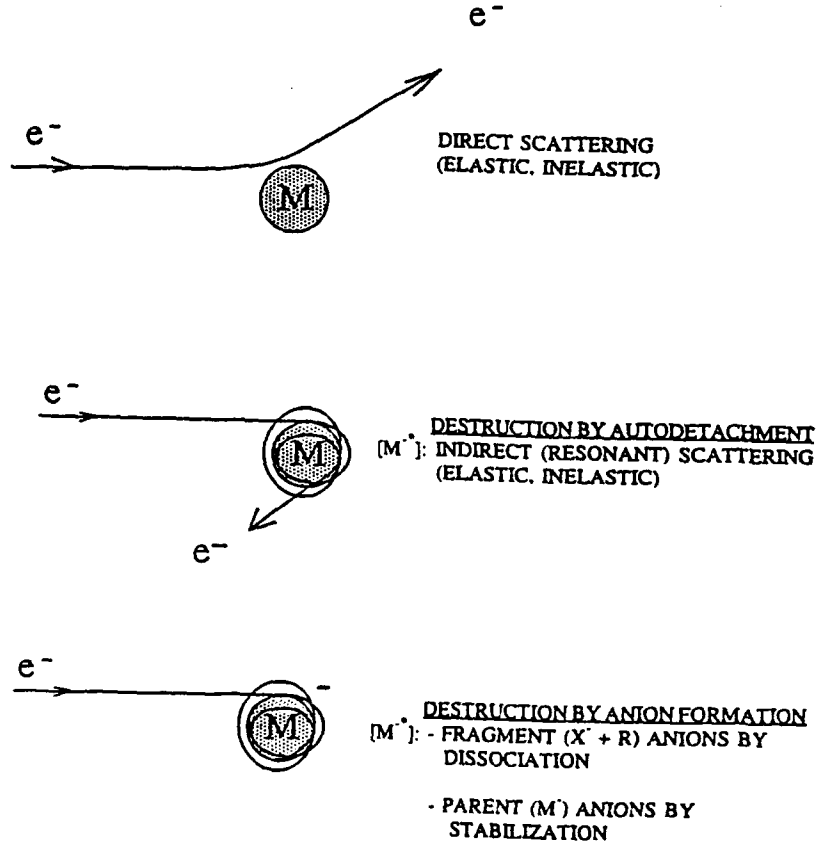


**Figure 1.** Schematic pictures depicting direct and indirect electron-molecule collisions; $M^{-*}$ indicates a transient negative ion with excess energy denoted by the asterisk.

---

[3]These are dense media whose $V_o < 0$ eV; $V_o$ is the energy of the excess electron at the bottom of the conduction band. It is defined as $V_o = W_M - W_{vac}$ where $W_M$ and $W_{vac}$ are, respectively, the work functions of a metal immersed in the dense medium and in vacuum.

lifetime can vary from ~ $10^{-15}$ to > $10^{-3}$ s (Refs. 13-15). Such collisions are resonant, i.e., they occur over a limited energy range--where empty orbitals exist for electrons to enter into and be temporarily retained. Subsequent to its formation the transient anion $M^{-*}$ is destructed by autodetachment (i.e., indirect elastic or inelastic electron scattering) or by "permanent" negative ion formation: fragment anions by dissociation and parent anions by stabilization. These processes are of general occurrence in nature. An example of an indirect collision leading only to elastic and inelastic scattering is shown in Fig. 2 for $N_2$ (no permanent $N_2^-$ or $N^-$ ions are formed since the electron affinities of $N_2$ and $N$ are negative). The pronounced peak in the momentum transfer cross section $\sigma_m$ and in the total vibrational cross section at ~ 2.3 eV--pointed to by the arrows in Fig. 2--is due, respectively, to the elastic and the inelastic scattering of electrons via the decay of the transient anion $N_2^{-*}$ formed by the temporary capture by $N_2$ molecules of ~ 2.3 eV electrons. Examples of the formation of "permanent" fragment negative ions via indirect (resonant) collisions are shown in Fig. 3. Clearly, these negative ion resonances occur abundantly in the energy range below ~ 20 eV and their cross sections increase as their energy positions are lowered.

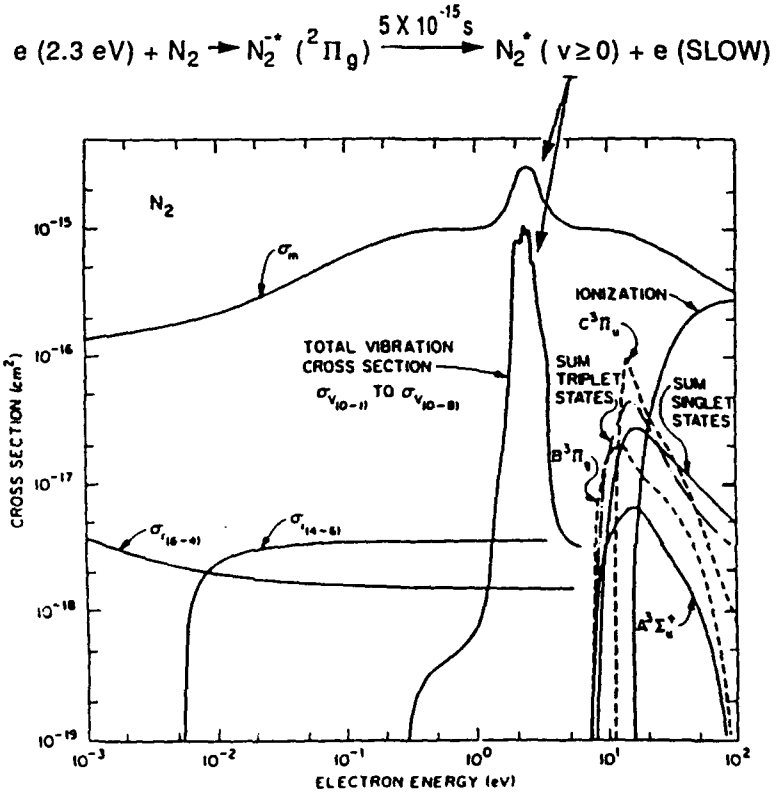


**Figure 2.** Cross sections for various electron scattering processes in $N_2$ as a function of electron energy (see the text) (based on Fig. 51 of Ref. 14, Vol. 2, p. 194).

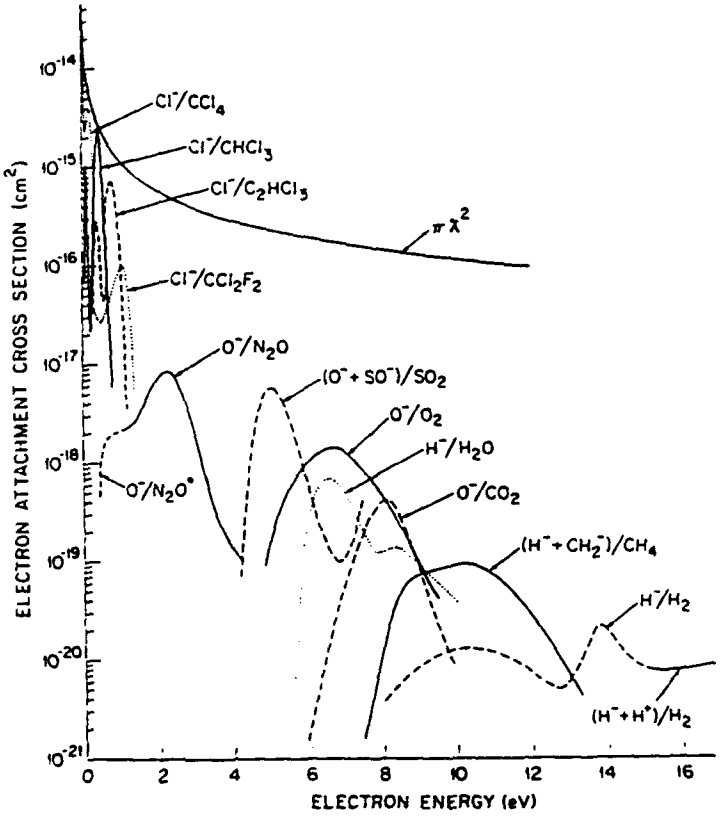


**Figure 3.** Dissociative electron attachment cross sections as a function of electron energy for a number of molecules (from Ref. 14, Vol. 1, p. 559).

Indirect collisions forming transient anions occur in condensed matter as well, but as we shall see their "isolated species" properties, energetics, and effects on other processes involving slow electrons are modified in dense matter by the nature and the density of the medium in which they occur. We shall try to understand some of these changes by considering knowledge from selected investigations on condensed phase and clusters.

## ELECTRON SCATTERING

In Table 1 are listed examples of the effects of phase on various electron energy loss processes and cross sections (see also Refs. 16,17). Let us illustrate some of these by examining the effect of phase on the differential oscillator strength distribution $f(\varepsilon)$ of water shown in Fig. 4. Clearly one sees a general loss of structure and a shift of $f(\varepsilon)$ to higher energies in going from the vapor to the condensed phase. Interestingly, the main difference is between the vapor and the condensed matter and not between the various forms (liquid, hexagonal ice, amorphous ice) of the latter. These phase effects seem to diminish with excitation energy. Important as this information is, it is still largely indirect[18,19] and limited. It should be noted in this connection that total inelastic cross sections estimated[20] for slow (1-20 eV) electron scattering in amorphous ice compare in magnitude (they are, actually,

Table 1. Examples of Condensed Phase Effects on the Oscillator Strength Spectrum

| |
|---|
| Shift of oscillator strength to higher energies (occurs over wide ranges of excitation energy) |
| Excitation of special modes of motion (plasmons in metals and excitons in molecular and ionic crystals; occur at specific energies) |
| Intermolecular vibrations (vibrational and translational phonons) |
| High Rydberg states (normally absent) |
| Negative Ion Resonances (exist as in single molecules but perturbed by the medium, e.g., their symmetries, lifetimes, selection rules, energetics) |
| Ejected electrons undergo further interactions |
| Scattering affected by correlation (medium structure) effects, nuclear/electronic excitation mode coupling, screening of interaction potential |
| Dissociation processes influenced by fast radiationless transitions and changes in energetics |

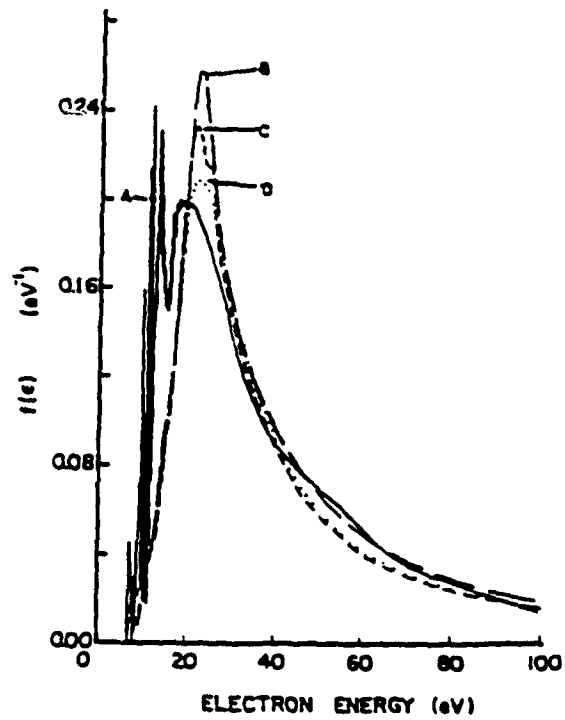


Figure 4. Differential oscillator strength distribution, $f(\varepsilon)$, of water vapor (A), liquid water (B), hexagonal ice (C), and amorphous ice (D) (Refs. 18 and 19).

slightly larger) and general trend with gas phase data (see discussion in Ref. 20); this conclusion, however, requres further scrutiny.

Let us now look at a system, namely xenon, for which scattering cross sections for slow electrons are well-known in the gas[13,14,21] and electron drift velocities as a function of the density, N, reduced electric field E, E/N, have been measured in the low pressure gas[13,14,21], the high pressure gas[2,22], the liquid[2,23], and the solid[2,23]. From the liquid phase electron transport data Sakai et al.[24] deduced two types of scattering cross sections, namely,

a cross section for elastic energy loss (energy transfer to acoustic phonons which is independent of the liquid structure)

$$\sigma_o(\varepsilon) = 2\pi \int_0^{\pi} (1-\cos\theta)\ \sigma(\varepsilon,\theta) \sin\theta\ d\theta, \qquad (1)$$

and a cross section for elastic momentum transfer which depends on the liquid structure through the structure factor S(K)

$$\sigma_1(\varepsilon) = 2\pi \int_0^{\pi} (1-\cos\theta)\ \sigma(\varepsilon,\theta)\ S(K) \sin\theta\ d\theta \qquad (2)$$

where $\sigma(\varepsilon,\theta)$ is the differential scattering cross section, $\theta$ is the scattering angle and $\varepsilon$ is the electron energy. These are compared with the low-pressure gas momentum transfer cross section $\sigma_m$ in Fig. 5. Both $\sigma_o(\varepsilon)$ and $\sigma_1(\varepsilon)$ exhibit a displaced and shallower (relative to the low pressure gas) Ramsauer-Townsend minimum and are much lower in magnitude than $\sigma_m(\varepsilon)$ especially at low $\varepsilon$. As $\varepsilon$ increases, $S(K) \rightarrow 1$ and the gas and liquid cross sections converge. A quantitative determination of the scattering cross section in the liquid is still lacking although the lowering of its magnitude in the condensed phase clearly is due to the screening of the scattering potential by the medium.

The indicated changes in the energy dependence and the magnitude of the scattering cross section in going from the low-pressure gas to the liquid explain nicely the much higher drift velocities, w, of slow electrons in gaseous compared to liquid xenon (Fig. 6). At a fixed E/N, the w(E/N) of slow electrons in solid xenon are about twice those in liquid xenon[22]. While this is consistent with the lower values of the total electron scattering cross section in solid xenon ($\sigma_s$) deduced by Bader et al.[25] (Fig. 7), the behavior of $\sigma_s$ (Fig. 7) is different at high energy from that of $\sigma_1$ or $\sigma_o$ (Fig. 5) in the liquid, probably indicating different scattering processes.

A behavior similar to that in xenon has been reported[26] for the w(E/N) of room temperature liquids with conduction bands [eg. see, Fig. 8][4].

---

[4]See Stephens[27] for a possible relationship between the mobilities of thermal electrons in different pentane isomers and their respective structure functions.

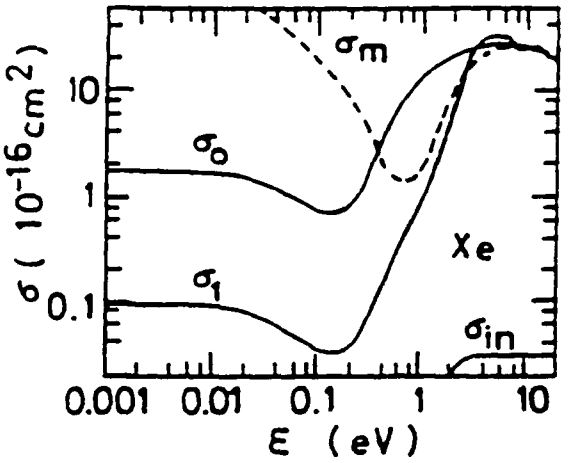


**Figure 5.** Cross sections $\sigma_o(\varepsilon)$ and $\sigma_1(\varepsilon)$ for liquid xenon and $\sigma_m(\varepsilon)$ for gaseous xenon (see the text and Refs. 3 and 24).

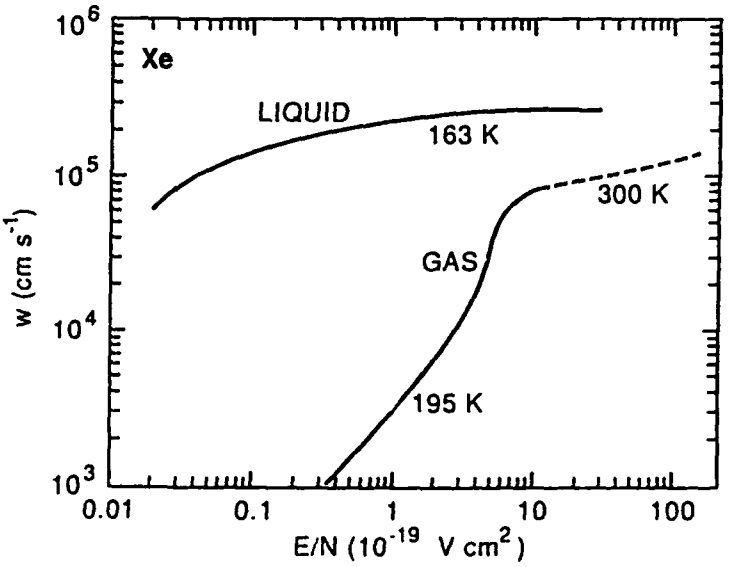


**Figure 6.** Electron drift velocity w as a function of E/N for liquid[23] and gaseous[21] Xe at the indicated temperatures.

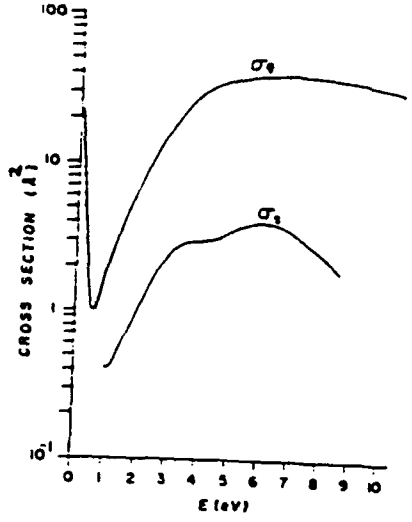


**Figure 7.** Comparison of the total electron scattering cross section for gaseous, $\sigma_g$, Xe and for solid, $\sigma_s$, Xe (17 K deposition on Pt.) plotted as a function of the electron energy (note that the zero energy in the solid is shifted by the $V_0$ value of the solid) (from Ref. 25).

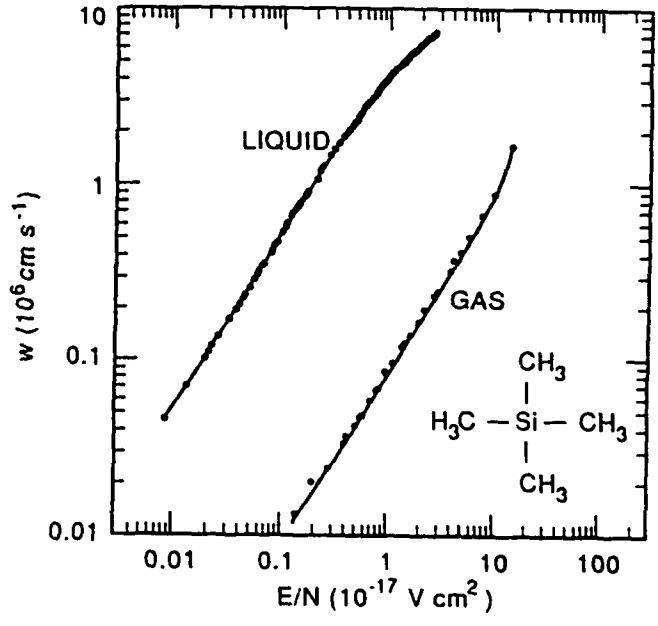


**Figure 8.** *w* vs E/N for gaseous and liquid tetramethylsilane (T = 300 K) (based on Ref. 26).

The cross sections in Figs. 5 and 7 are due to direct electron scattering. In condensed matter--as in low pressure gases--indirect scattering of slow electrons occurs abundantly. It manifests itself through a strong enhancement in the scattering cross section over limited energy regions where the negative ion states (NISs) are located. A prototypical example is shown in Fig. 9 for solid films of $N_2$. The cross section function for excitation of the $N_2$ molecule in solid $N_2$ films in the first (v = 1) vibrational level via its lowest, $N_2^{-*}$ ($^2\Pi_g$), negative ion state has--as in the isolated-molecule case--distinct structure which originates from the vibrational levels of the transient $N_2^{-*}$ ($^2\Pi_g$) state. The position of the first peak in Fig. 9 (first broken vertical line) lies ~ 0.7 eV lower than the corresponding position in the low pressure gas (first solid vertical line in Fig. 9). This lowering of the energy position of the $N_2^{-*}$ ($^2\Pi_g$) state is a general characteristic of the changes in the energetics of the NISs of atoms and molecules embedded in dense matter and is due to the polarization of the medium which surrounds the temporarily localized electron on the molecule. The cross section functions for excitation of $N_2$ in the v = 2, 3, etc. levels exhibit similar behavior[16]. Interestingly, however, while in the solid--as in the isolated molecule--the vibrational excitation increased by ~ 2 orders of magnitude in the region of the resonance, Sanche et al.[16] observed no such enhancement in the elastic scattering channel in the $N_2$ solid film. This is in sharp contrast to the gas where indirect elastic electron scattering is profoundly enhanced. The formation of the NIS in the condensed phase--as in gases--is localized in space and is dominated by the short-range forces. For this reason in the solid--as in the gas--the formation of a NIS leads to intramolecular changes that enhance excitation of individual vibrational levels of the molecular constituents. The decay of the NIS in the condensed phase, however, should differ from that in the gas because it is affected by the medium due to polarization. The intermolecular changes lead to continuous accoustic excitations (phonons) which in essence replace the (low pressure) elastic scattering. This process is very probable due to the large number of such low frequency vibrations (see Refs. 2,16,17,28, and 29). It, thus, seems that the formation of negative ion states in dense matter enhances intramolecular vibrational excitation and intermolecular excitation of phonon modes of the lattice. A theoretical understanding of slow electron interactions in condensed matter in a manner analogous to gases, is, however, still lacking.

The electrons that have been slowed down via the NISs cause (see later) profound changes in the observed electron attachment properties of molecules in dense matter and in clusters.

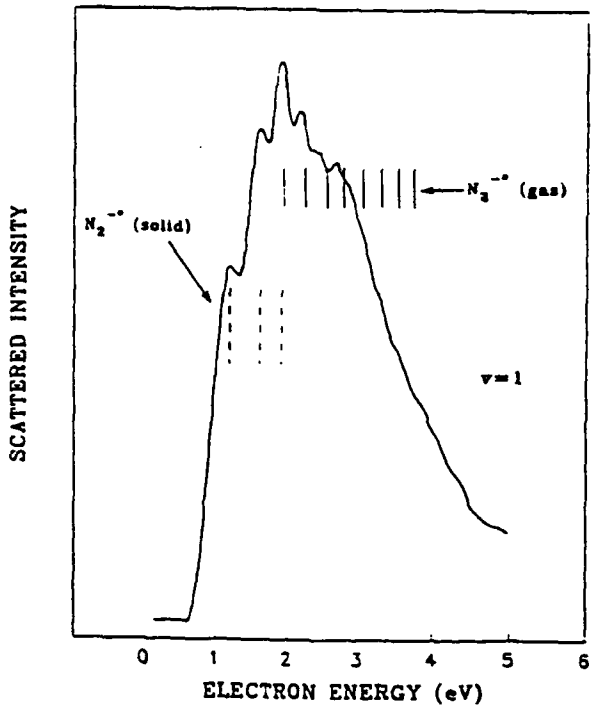


**Figure 9.** Relative cross section for indirect scattering of slow electrons via the $N_2^{-*}$ ($^2\Pi_g$) negative ion state of $N_2$ in solid $N_2$ film leaving $N_2$ excited in the v = 1 vibrational level. Note that the position of the first peak in the cross section function for the solid lies ~ 0.7 eV lower than for the corresponding gas (see the text) (based on Fig. 13b in Ref. 16).

## IONIZATION IN DENSE MATTER AND IN CLUSTERS

### Electron Impact Ionization

Inspite of its basic and applied significance, there appears to be no direct measurement of the electron impact ionization cross section as a function of the electron energy $\sigma_\alpha(\epsilon)$ for any system. There is, however, some limited information on the effective ionization cross section of $H_2$ in $H_2$ clusters as a function of the cluster size (Fig. 10) which indicates that the $\sigma_\alpha(\epsilon)$ for closely packed and interacting $H_2$ molecules is smaller than that for the isolated $H_2$ molecules[30]. There exists, also, some indirect information on media with $V_o < 0$ eV such as xenon. For this medium the electron impact ionization coefficient $\alpha(E/N)$ does not scale with the density N in going from the gas to the liquid[31]. In Table 2 are compared: the total electron yield $G_w$ (e,γ,x) for electrons, γ-rays and x-rays; the energy to produce an electron-ion pair for β particles, $W_\beta$; and the ionization threshold energy for the low pressure gas, $I_G$, and the liquid, $I_L$. The lowering of $W_\beta$ (increase in $G_w$) for the liquid can be attributed to the lowering of I in the liquid compared to the gas (see below). Due to the lower $I_L$, electronic states that would have led to inelastic scattering in the gas lead to ionization in the liquid.

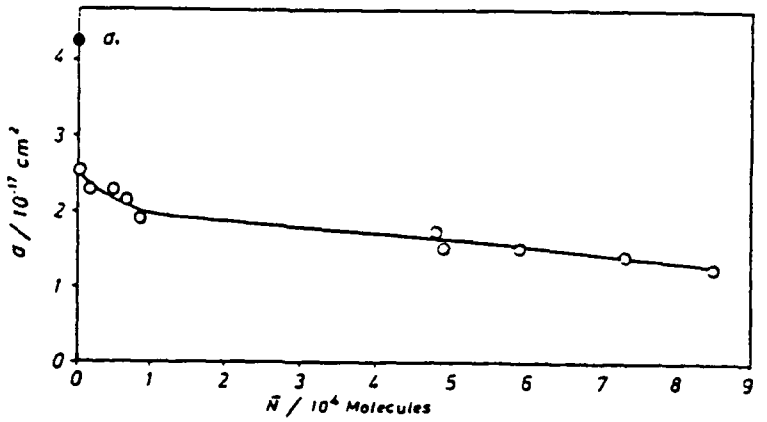


**Figure 10.** Effective electron impact ionization cross section of cluster beams of $H_2$ as a function of the mean cluster size N for 500 eV. The solid point shows the value, $\sigma_1$, of the cross section for uncondensed $H_2$ at the same electron energy[30].

**Table 2.** Comparison of $G_{ie}$ (e,γ,x), $W_\beta$ and I for gaseous and liquid xenon[1]

| Quantity | Liquid | Gas |
|---|---|---|
| $G_{ie}$(e,γ,x) | 6.4 | 4.6 (electrons/100 eV) |
| $W_\beta$ | ~16 | 21.9 (eV/i.p.) |
| I | ~9.0 | 12.13 eV |

[1]See the text and Ref. 1.

### Single and Multiphoton Ionization of Molecules in Fluids

Here again absolute cross section measurements are scarced. However, many studies on pure liquids and solutions quantified the effect of the medium on the energetics of the reaction

$$M_F + nh\nu \ (n \geq 1) \rightarrow M_F^+ + e_F \qquad (3)$$

where F stands for the fluid medium in which the molecule M is embedded and the reaction takes place. If we neglect the small broadening of the valence electron levels in the fluid due to condensation, for liquids [F = L) the measurements showed[1,2,32,33] that

$$I_L = I_G + V_o + P^+ \tag{4}$$

In Eq. (4), $P^+$ is the polarization energy of the positive ion $M_F^+$ and is normally represented by the Born expression

$$P^+ = -\frac{e^2}{2R}\left[1 - \frac{1}{\varepsilon_{opt}}\right] \tag{5}$$

where R is the effective radius of the positive ion cavity and $\varepsilon_{opt}$ is the optical dielectric constant of the medium. For a number of organic molecules in nonpolar liquids[3], $I_L - I_G$ (= $V_o + P^+$) ≈ -1 to -3 eV and $\langle R \rangle$ ~ 2.7 Å. A major uncertainty in the determination of $P^+$ remains the lack of accurate knowledge of R.

The validity of (4) can indeed be seen from measurements (see Ref. 34, Table 3) of $I_L$ of a certain molecule (azulene) in a number of dielectric liquids with different $V_o$ values. Since in this case we are dealing with the same positive ion, $P^+$ may be regarded as constant for these nonpolar liquids and, hence, the $I_L$ should correlate with the $V_o$ of the liquids. Indeed, the linear dependence of $I_L$ on $V_o$ implied under such conditions by Eq. (4) is exhibited by the measurements in Table 3 (see Fig. 11).

**Table 3:** $I_L$ and $I_G$ for Azulene in Dielectric Liquids With Various $V_o$ Values[34]

| Liquid | $I_L$(eV) | $I_G$(eV) | $V_o$(eV) |
|---|---|---|---|
| Tetramethyltin (TMT)[1] | 5.33 | 7.42 | -0.75 |
| Tetramethylsilane (TMS)[1] | 5.45 | | -0.55 |
| 2,2,4,4-Tetramethylpentane (TMP)[1] | 5.70 | | -0.36 |
| n-Pentane (n-Pt)[1] | 6.12 | | +0.01 |
| n-Tridecane | 6.28 | | +0.21 |

[1]Abbreviations used in Fig. 11.

Similarly, for a fluid of number density N the ionization threshold, $I_F(N)$, of a molecule (atom) embedded in the fluid has been found (e.g., Refs. 35,36) to be related to its isolated-molecule value, $I_G$, by

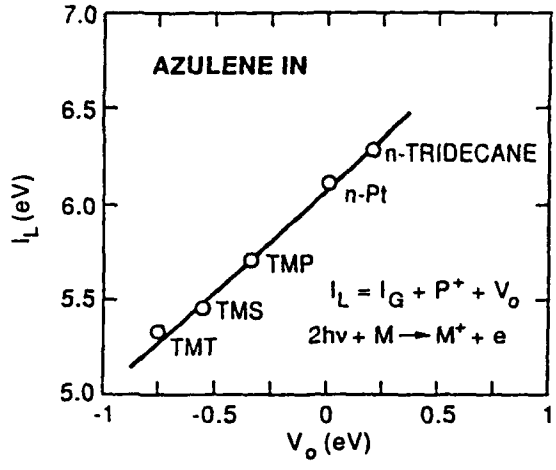


**Figure 11.** $I_L$ vs $V_o$ for the azulene molecule, M, ionized by two photon absorption ($2\ h\upsilon + M_L \rightarrow M_L^+ + e_L$) in a number of nonpolar liquids (Ref. 34; see Table 3).

$$I_F(N) = I_G + P^+(N) + V_o(N) \qquad (6)$$

i.e., by the N-dependence of $P^+$ and $V_o$; the N-dependence of $P^+$ is dominated by the N-dependence of $\varepsilon_{opt}$ while the N-dependence of $V_o$ is more complicated. The $V_o(N)$ has been calculated in a few cases using the Springett, Jortner, and Cohen (SJC) model[35-37]. In Fig. 12 is plotted the $I_F$ of the molecule TMPD (N,N,N',N'-tetramethyl-p-phenylenediamine) in ethane as a function of the ethane density $\rho(M/l)$ from the dilute gas to the liquid. The effect of increasing medium density on $I_F$ is a continuous gradual decrease and a smooth transition to the liquid. The solid lines represent the dependence of $I_F$ on N for the indicated values of the "hard core" radius $\langle \tilde{a} \rangle$ as predicted by the SJC model.

From the experimental investigations to date it appears that the energetics of ionization in dense matter are modified from their values in dilute gases by the charge induced medium polarization energies. The energetics of the process for nonpolar fluids is reasonably well understood and needs to the extended to polar media.

## Photoionization Energetics in Clusters

Many studies have been devoted recently to this topic and subsequent lectures will deal with the subject in more detail. Here we merely lay down a few aspects of the energetics of the process as a background for the other lectures and, also, to integrate our discussion on the kind of knowledge obtained by the two complementary approaches we mentioned in the Introduction. Let us first refer to Fig. 13 which shows schematically[6] the dependence on the cluster size of a cluster property $x(n)$; n is the number of the cluster constitutents. For small n, $x(n)$ exhibits specific cluster size effects (e.g., shell closure effects). For large n, Jortner[6] expressed $x(n)$ as

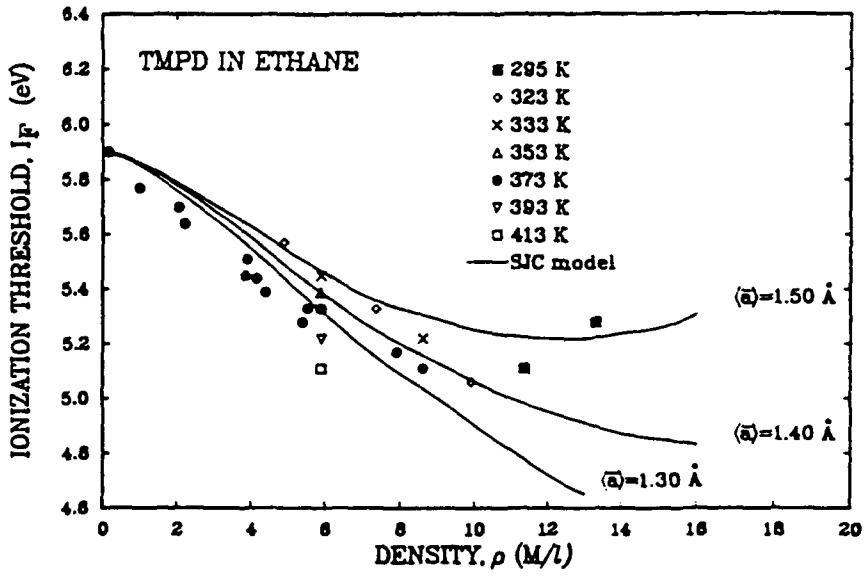


**Figure 12.** Ionization threshold of TMPD (N,N,N'N'-tetramethyl-p-phenylenediamine) in ethane as a function of the ethane density from a dilute gas to the liquid at the indicated temperatures. The data points ■ are measurements made in liquid ethane at 295 K. The solid lines represent the dependence of $I_p$ on N for the indicated values of the "hard core" radius <ā> as predicted by the Springett-Jortner-Cohen (SJC) model[35,37].

$$x(n) = \chi(\infty) + An^{-\beta} \tag{7}$$

namely, in terms of the corresponding bulk value $x(\infty)$ and a correction term $An^{-\beta}$ ($0 \leq \beta \leq 1$) which accounts for the modification of the bulk value in the cluster due to the "excluded volume" outside of it. Expressing Eq. (7) in terms of the cluster radius $R_c$ (taken equal to $R_o n^{1/3}$ where $R_o$ is the effective single particle radius determined from the molecular (atomic) volume using the bulk medium density) we have

$$\chi(R_c) = \chi(\infty) + (A\, R_o^{3\beta})\, R_c^{-3\beta} \tag{8}$$

This "cluster-size equation" attempts to provide a quantitative description of the "smooth" cluster size dependence of $x(n)$ for large clusters and it interpolates to the corresponding bulk value $x(\infty)$ in much the same way as Eqs. (4) and (6) we have discussed earlier.

Let us apply (7) and (8) to the case of the ionization potential I(n) of clusters. We can write

$$I(n) = I_A + P^*(R_c) = I_A + P^*(\infty) + C(R_c) = I(\infty) + C(R_c) \tag{9}$$

where $I_A$ is the ionization potential of the isolated species A, $P^*(\infty)$ is the bulk polarization energy and $C(R_c)$ is the correction for the finite cluster size (i.e., the long-range electrostatic

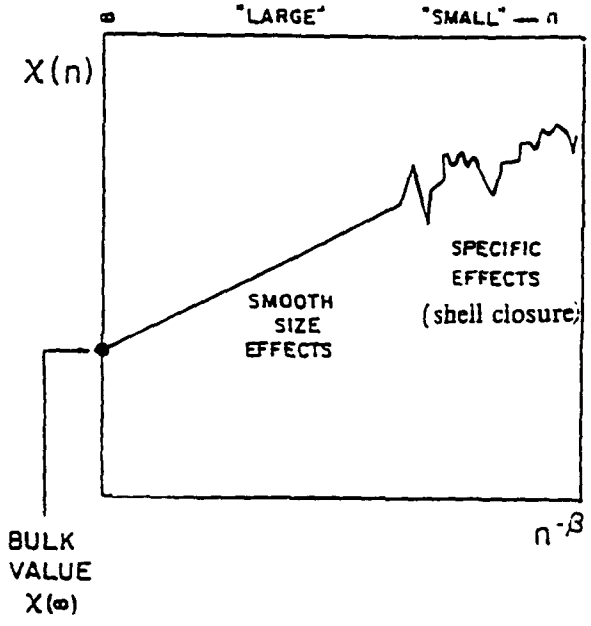


**Figure 13.** Schematic representation of the cluster size dependence of a cluster property $x(n)$ on the number, n, of the cluster constituents (from Ref. 6; see the text).

interaction of the generated charge with the "excluded region"). If we use for $C(R_c)$ the classical electrostatic expression which gives the energy required to remove an electron from a uniformly conducting sphere having the same dimensions as the cluster, namely,

$$C(R_c) = (e^2/2R_c)(1 - 1/\varepsilon_{opt}) = (e^2/2R_o)(1 - 1/\varepsilon_{opt})n^{-1/3} \qquad (10)$$

we have

$$I(n) = I(\infty) + (e^2/2R_o)(1 - 1/\varepsilon_{opt})n^{-1/3} \qquad (11)$$

In Eq. (11), $I(\infty) = I_A + P^+(\infty)$ is the bulk photoelectric threshold for molecular clusters, the top of the bulk valence energy for semiconductor clusters, or the bulk metal work function for metallic clusters.

The validity of Eq. (11) is illustrated in Fig. 14 for the rare gas and mercury clusters[8]. The results of Rademann et al.[8] for mercury clusters show in addition the gradual transition from van der Waals-type to metallic properties; on the basis of their data in Fig. 14 this transition occurs in the cluster size range of ~ 70 atoms. In cluster energetics as in interphase studies energetics a major uncertainty in applying relations such as Eqs. (4), (5), and (11) is the proper knowledge of R.

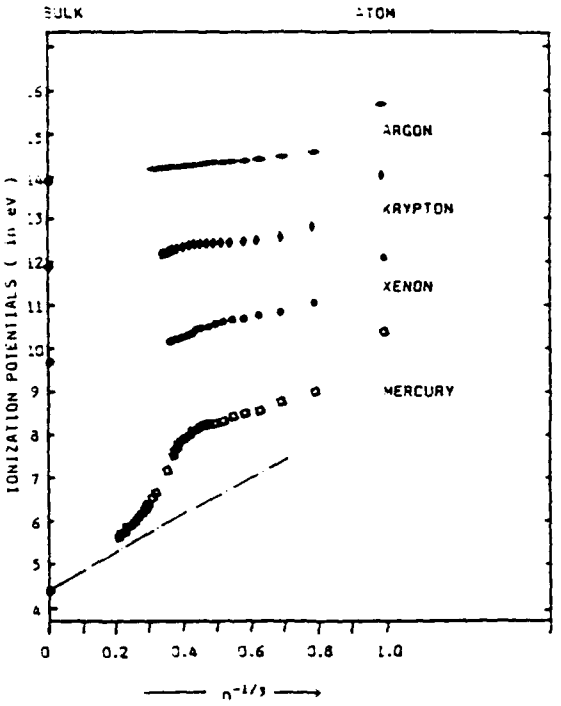


**Figure 14.** Ionization potential (in eV) vs $n^{-1/3}$ for Ar, Kr, Xe, and Hg clusters (from Ref. 8) (see the text).

## ELECTRON ATTACHMENT

Subsequent lectures will--most assuredly--discuss the effect of the state and the nature of the medium on the attachment of slow electrons to molecules. We, also, elaborated on interphase studies of electron attachment and the relevance of electron attachment processes in gases to those in the condensed phase earlier (e.g., Refs. 1-3). We shall, thus, be brief. In Fig. 15, the rate constant for the dissociative electron attachment reaction

$$e + N_2O \rightarrow N_2O^{-*} \rightarrow O^- + N_2 \qquad (12)$$

as measured in gaseous argon, $(k_a)_G$, and in liquid argon, $(k_a)_L$, is plotted as a function of respective values of the mean electron energy, $\langle\varepsilon\rangle_G$ in gaseous argon and $\langle\varepsilon\rangle_L$ in liquid argon. In spite of the large uncertainty in $\langle\varepsilon\rangle_L$, the comparison of $(k_a)_G$ ($\langle\varepsilon\rangle_G$) with $(k_a)_L$ ($\langle\varepsilon\rangle_L$) in Fig. 15 shows three rather distinct features: (i) the dissociative attachment resonant reaction (12) occurs in liquid argon as it occurs in the argon buffer gas, (ii) the position of the dissociative attachment resonance shifts to lower energy as a result of the polarization of the medium around the transient $N_2O^{-*}$, and (iii) the rate constant for the reaction is higher in the liquid than in the gas largely because of the lowering of the energy of the negative ion state.

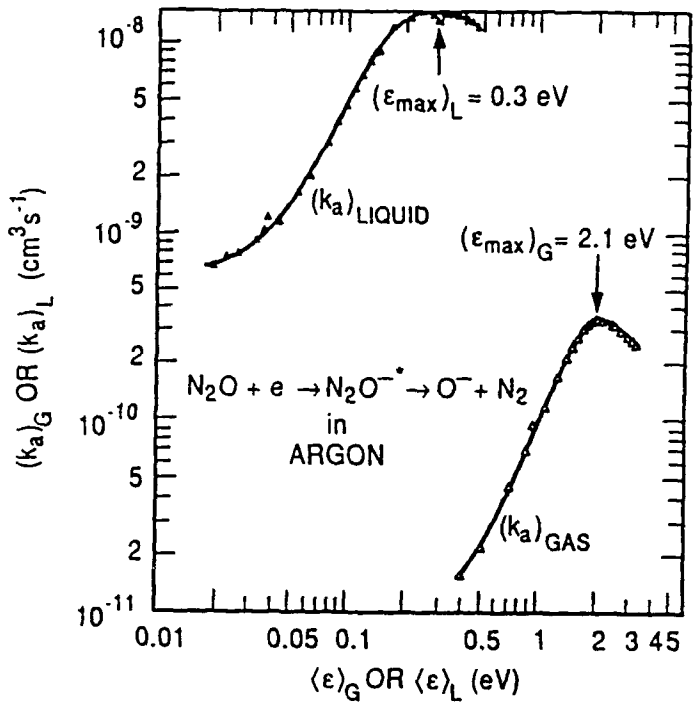


**Figure 15.** Electron attachment rate constant for $N_2O$ in gaseous ($(k_a)_G$) and liquid ($(k_a)_L$) argon plotted as a function of the respective, $\langle\varepsilon\rangle_G$ and $\langle\varepsilon\rangle_L$, mean electron energies (the data for liquid argon are from Ref. 38).

Studies of electron attachment to molecules in clusters and in solid films generally showed similar changes: the perturbation from the isolated-molecule case of the formation of the transient anion and its decay channels by the medium. Thus, as is shown in Fig. 16a, the negative ion resonance that produces $O^-$ from $O_2$ and peaks at ~ 6.7 eV in the gas exists in solid films of mixtures of $O_2$ in Ar, but it is shifted to lower energies by ~ 0.7 eV. Additionally, the yield of $O^-$ from $O_2$ from the solid shows (Fig. 16a)--in contrast to the isolated $O_2$ case--enhanced $O^-$ production at ~ 8 and ~ 14 eV. These enhancements ("peaks") in the $O^-$ yield have been attributed by Sanche and collaborators (e.g., see Ref. 16) to the transitions

$$O_2(^3\Sigma_g^-) + e \rightarrow O_2^{-*}(^2\Sigma_g^+) \rightarrow O^- + O \qquad (13)$$

and

$$O_2(^3\Sigma_g^-) + e \rightarrow O_2^{-*}(^2\Sigma_u^+) \rightarrow O^- + O \qquad (14)$$

which are symmetry forbidden in the isolated molecule case, but become allowed in the solid because of the perturbation by the medium. Observation of $O^-$ via dissociative electron attachment to $O_2$ in $O_2$ clusters as a function of cluster size showed similar evidence. This is indicated by the enhancement in the $O^-$ yield around 8 and 14 eV in Fig. 16c with increasing stagnation pressure from 1 to 3.5 bar (the cluster size distribution increases with increasing stagnation pressure).

From these rather limited studies it can be inferred that in going from the gaseous to the condensed phase additional negative ion states contribute to indirect energy loss and dissociative electron attachment processes.

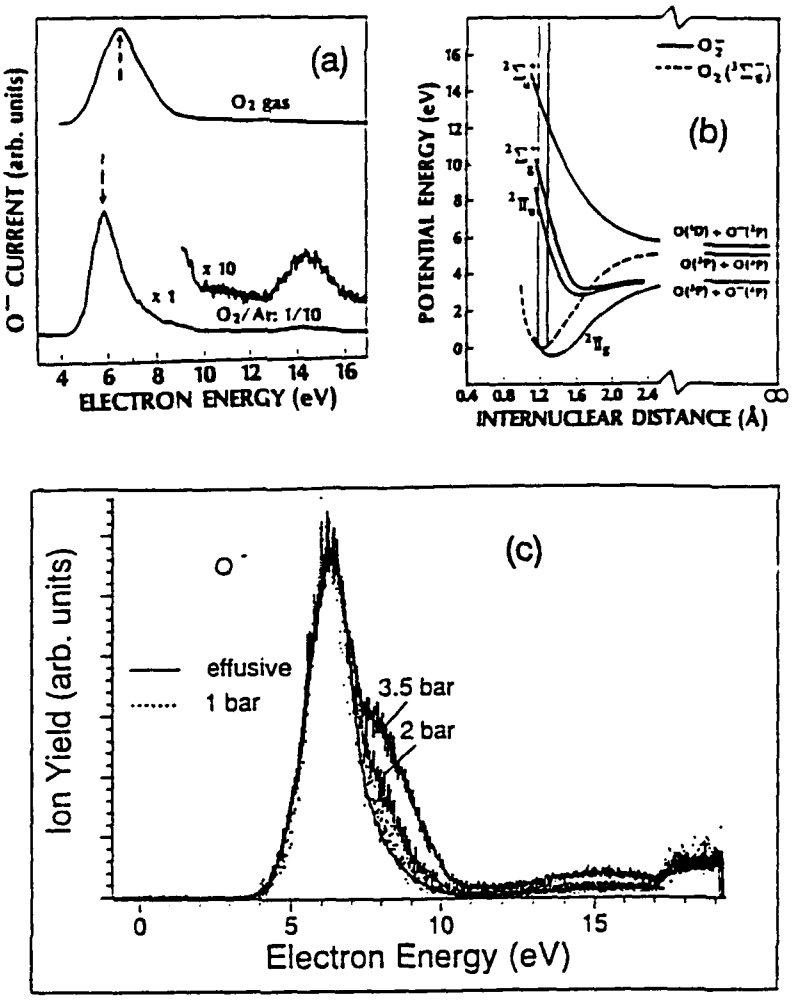


**Figure 16.** a. $O^-$ from $O_2$ in $O_2$ gas (upper curve) and $O_2$/Ar (1/10 mixture), solid film.
b. Schematic potential energy curves for $O_2(^2\Sigma_g^-)$ (---) and $O_2^-$ ($^2\Pi_g$, $^2\Pi_u$, $^2\Sigma_g^+$, $^2\Sigma_u^+$) (——).
c. Yield of $O^-$ from $O_2$ clusters at 1, 2, and 3.5 bar stagnation pressure normalized at the lowest maximum to the yield of $O^-$ from $O_2$ at low pressure (effusive ——). (a and b from Ref. 16; c from 39).

Besides these changes, the proximity of collision partners within the condensed medium or the cluster will enhance the production of parent negative ions (e.g., $O_2^-$). Furhermore, the negative ion properties of single molecules or clusters with strong "zero" or "near-zero" nondissociative electron attachment resonances are strongly influenced by inelastic electron scattering by the cluster constituents. This is beautifully illustrated in Fig. 17 where the production of $(O_2)_2^-$ in $O_2/N_2$ mixed clusters is strongly influenced by the inelastic electron scattering by $N_2$, especially by the inelastic electron scattering via the 2.3 eV negative ion resonance $N_2^{-*}$ ($^2\Pi_g$). The yield of this ion exhibits a strong resonance at ~ 2.3 eV in the case of the $O_2/N_2$ clusters (Fig. 17b) which is absent in the homogeneous clusters of $O_2$ (Fig. 17a). The profound effect of inelastic electron scattering (especially via NIRs) by the cluster constitutents on the intensity and energy dependence of the anions formed in clusters by the capture of "near-zero" energy electrons indicates that such processes can be employed to probe electronic and negative ion states of molecules in clusters.

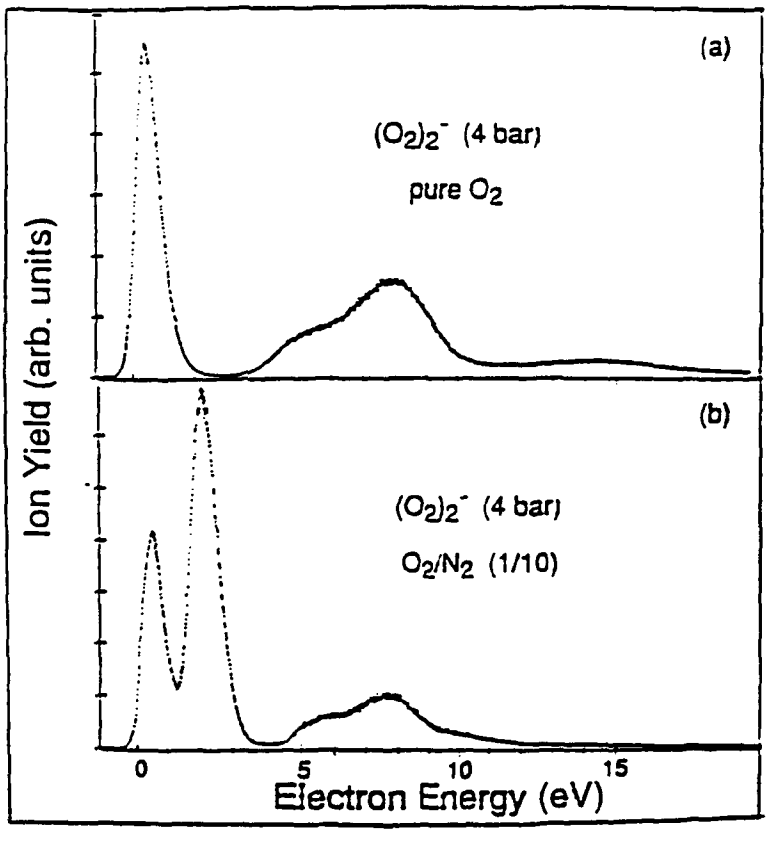


**Figure 17.** Yield of $(O_2)_2^-$ from (a) pure $O_2$ clusters and (b) $O_2/N_2$ clusters ($O_2/N_2$ gas mixture ratio 1/10). The stagnation pressure was 4 bar[40]. The pronounced additional resonance in (b) at ~ 2.3 eV is due to the formation of $(O_2)_2^-$ by capture of electrons inelastically scattered to near-zero energy via the 2.3 eV $N_2^{-*}$ ($^2\Pi_g$) resonance of $N_2$.

## PHOTODETACHMENT IN GASES, LIQUIDS, AND CLUSTERS

The photodetachment of electrons from negative ions in low-pressure gases is well-understood and the relation of the photodetachment threshold $E_{th}$ to the electron affinity, EA, of the electron attaching species is well-established (e.g., see Ref. 13). Near threshold, the photodetachment cross section, $\sigma_{pd}$, is predicted[41,42] to vary as

$$\sigma_{pd}(E) = BE(E-E_{th})^{(2l+1)/2} \propto k^{2l+1}, \tag{15}$$

where B is a constant, E = hυ is the photon energy, and k and *l* are the linear and angular momenta of the ejected electron. For atoms, A, the value of the $E_{th}$ for the process

$$A^- + h\nu \rightarrow A + e \tag{16}$$

is equal to the electron affinity EA(A) of A, which in turn, is equal to the "vertical detachment energy" (VDE). For molecules, M, the relation of $E_{th}$ for the process

$$M^- + h\nu \rightarrow M + e \tag{17}$$

to the electron affinity, EA(M), of M and the VDE is complicated by possible differences in the structural parameters of M and $M^-$. If we define the VDE for (17) as the minimum energy required to eject the electron from the negative ion in its ground electronic and molecular state without changing the internuclear separations, then the VDE is related to the EA and $E_{th}$ by

$$E_{th} = VDE = EA + \Delta E, \tag{18}$$

i.e., the VDE for (17) exceeds the EA by ΔE; the magnitude of ΔE depends on the relative positions of the potential energy curves (surfaces) of M and $M^-$.

The photodetachment of electrons from negative ions in dense gases, liquids and clusters has been studied--and the energetics of the process have been related to their gas-phase values--for only a limited number of cases (e.g., see Refs. 43-46). Even more limited seem to be the measurements of the photodetachment cross sections. Experimental studies are in progress at the author's laboratory to determine the photodetachment energetics and cross sections as a function of medium density from a low-pressure gas to the liquid. Establishing the energetics and the cross sections for photodetachment as a function of the nature and density of the medium is significant because it gives a direct measure of the stability of the anion in dense matter and because it provides a basic input for understanding electron transfer mechanisms in dense matter.

In dense gases, liquids and clusters, the photodetachment process for molecular negative ions is complicated by the effect of the medium on $E_{th}$ and the potential energy curve (surface) of $M^-$. Rewriting reaction (17) for, say, the liquid as

$$M_L^- + h\upsilon \rightarrow M_L + e_L \tag{19}$$

and assuming that $(EA)_L = (EA)_G + V_o - P^-$ (Refs. 1,44) we have

$$(E_{th})_L = (VDE)_L = (EA)_L + (\Delta E)_L$$

$$= (EA)_G + V_o - P^- + (\Delta E)_L \tag{20}$$

where $V_o$ and $P^-$ are the polarization energies of the electron and the negative ion in the medium, and $(EA)_L$ and $(EA)_G$ are the values of the electron affinity of M in the liquid and the gas phase.

Among the few studies of photodetachment of negative ions in liquids is that on $C_6F_6^-$ (Refs. 43,44). Let us, then, by way of example, refer to the method of Faidas et al. [44] which utilizes a two-laser photoconductivity technique suitable for photodetachment studies in dense fluids and the results they obtained on $C_6F_6^-$ photodetachment in liquid TMS using this method. A schematic of their experimental arrangement and an outlay of the principle of their technique is shown in Fig. 18. A cell--with appropriate light windows and feedthroughs--contains the molecule ($C_6F_6$) under study disolved in the liquid (TMS) at an appropriate concentration. Two counter-propagating coaxial laser beams traverse the interaction volume in the liquid cell with a time delay of ~ 5 μs. The first laser beam from

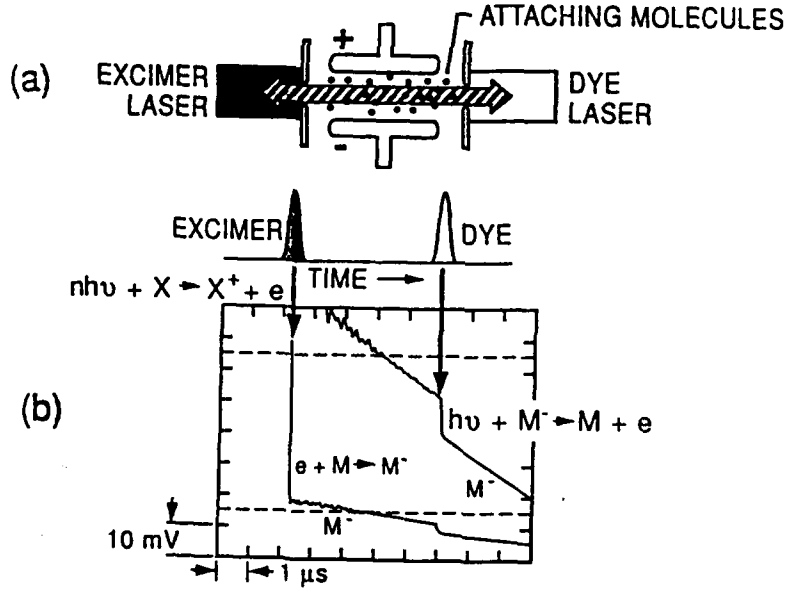


**Figure 18.** Schematics of the two laser photodetachment technique and an oscillogram of the conductivity signal (see the text and Ref. 44).

an excimer laser ($\lambda$ = 308 nm; *f*whm = 15 ns) ionizes biphotonically the liquid and produces electrons which give rise to a fast signal (initial drop in Fig. 18b identified by $\downarrow$ and the process $nh\upsilon + X \rightarrow X^* + e$). These electrons quickly (within < 1 ns) attach to $C_6F_6$ forming $C_6F_6^-$ (process $e + M \rightarrow M^-$ in Fig. 18b); the slow falling portion of the signal (indicated by $M^-$ in Fig. 18b) after the initial steep fall is due to these slow-moving anions. At the preset time delay (~ 5 $\mu$s), the second laser pulse (tunable dye laser, *f*whm = 0.6 ns) detaches the electron from $C_6F_6^-$ (when $h\upsilon > (E_{th})_L$) and produces a second transient signal (step drop in Fig. 18b identified with $\downarrow$ and $h\upsilon + M^- \rightarrow M + e$), followed by a slow drop when the detached electrons attach to $C_6F_6$ again forming slow moving $C_6F_6^-$.

The basis for determining the photodetachment cross section $\sigma_{pd}(E)$ as a function of the photon energy E can be seen by referring to Fig. 19. The first (excimer) laser pulse has an essentially flat intensity profile $I_e(r)$ for distances $r < \alpha$ where $\alpha$ is the radius of the cross sectional area of the interaction volume (Fig. 19a). This pulse generates electrons uniformly in the interaction volume with a density distribution $n_{ei}(r) \propto I_e^2(r)$. Under the experimental conditions employed by Faidas et al. all these electrons were captured by $C_6F_6$ within 1 ns and the resultant negative ions $C_6F_6^-$ were essentially stationary with an ion density distribution $n_i(r) = n_{ei}(r) \propto I_e^2(r)$ when the second (tunable dye) laser pulse arrived ~ 5 $\mu$s later. The intensity profile $I_d(r)$ of the dye laser pulse was Gaussian and lay well within $\alpha$ (Fig. 19c). The density distribution, $n_{ed}(r)$, of the photodetached electrons is

$$n_{ed}(r) = \sigma_{pd}(E)\, n_i(r)\, I_d(r) \tag{21}$$

Under the experimental conditions employed, $n_{ed}(r) << n_i(r)$, the $I_e(r)$, $n_i(r)$, and $I_d(r)$ were virtually constant along the axis of the interaction volume, and

$$\sigma_{pd}(E) = \frac{N_{ed}}{N_i}\,\frac{\pi\alpha^2}{I_t} \tag{22}$$

Thus, $\sigma_{pd}(E)$ can be determined from a measurement of the ratio $N_{ed}/N_i$ of the total number of photodetached electrons, $N_{ed}$, to the total number of negative ions $N_i$, a measurement of the total number of photons in the dye laser pulse $I_t$ and a knowledge of $\alpha$ and the intensity profiles of the two laser beams.

In Fig. 20 is shown the $\sigma_{pd}(E)$ for $C_6F_6^-$ in TMS (T = 298 K) determined by this technique. The cross section $\sigma_{pd}(E)$ exhibits two well-defined maxima at 2.58 and 3.15 eV due presumably to excited negative ion states of $C_6F_6^-$. The photodetachment threshold $(E_{th})_L$ was determined by fitting the experimental measurements near threshold to

$$(\sigma_{pd}/E)^{1/n} = B[E-(E_{th})_L] \tag{23}$$

with $n = 1/2(2l+1)$. The best fit was obtained for n = 3/2 (i.e., $l$ = 1, see Eqs. (15) and (23)) and $(E_{th})_L$ = 1.51 eV. Using this value, Eq. (20), and literature values of $(EA)_G$ Faidas et al. concluded that the electron affinity of $C_6F_6$ is lowered in liquid TMS by ~ 0.4 eV compared to its isolated-molecule value.

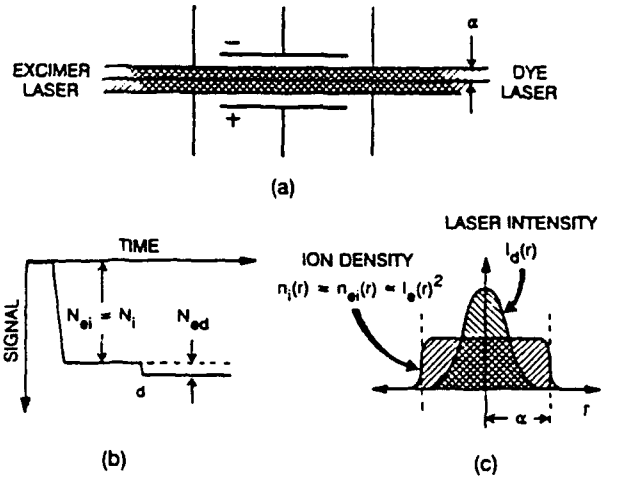


**Figure 19.** Schematics of the photodetachment technique illustrating: (a) the laser interaction region, (b) the type of signal measured, and (c) the laser intensity and negative ion density profiles (see the text and Ref. 44).

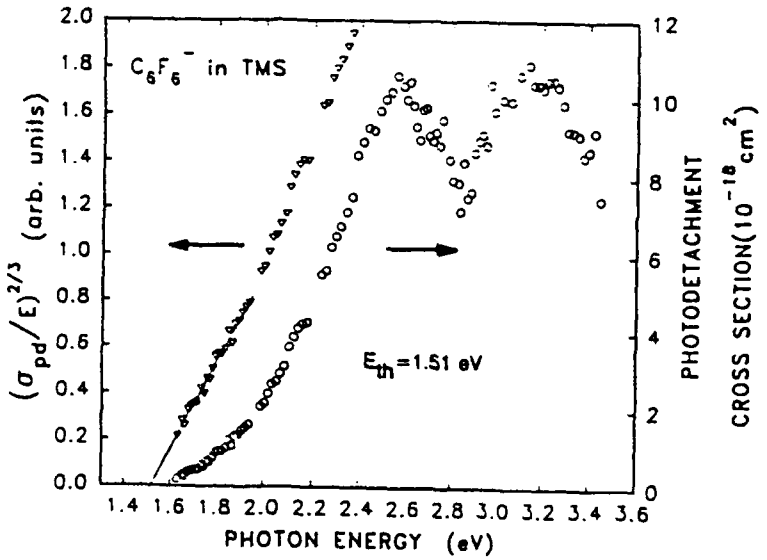


**Figure 20.** The absolute photodetachment cross section $\sigma_{pd}(E)$ (right-hand side Y axis) of $C_6F_6^-$ in tetramethylsilane as a function of the photon energy, E, and a linear least squares fit of $(\sigma_{pd}/E)^{2/3}$ (left-hand side Y axis) for E < 1.95 eV. The intercept with the X axis gives a threshold energy $E_{th}$ of 1.51 eV (Ref. 44).

Finally, photodetachment studies on a number of cluster negative ions aided considerably our understanding of the energetics of the process. Experimental studies on the vertical values of EA (photodetachment thresholds; e.g., see Refs. 45,46) revealed the existence of the expected (Fig. 13, and Refs. 6 and 11) specific size variations and the smooth (increase) transition to the bulk property as the cluster size is increased. This is clearly shown in Fig. 21 where the measured EA values of $Cu_n$ clusters are plotted as a function of cluster size[45]. Odd copper clusters are seen to have substantially lower EA than adjacent even clusters and this continues at least through $Cu_{17}$. It was pointed out[45] that the LUMO (lowest unoccuppied molecular orbital) of the even clusters would be expected to be strongly antibonding and the corresponding negative ion more weakly bound than if the electron were to be placed in the half-filled nonbinding HOMO of an odd cluster.[5]

The electron affinity, EA(n), of the larger clusters would be predicted to increase as [e.g., see Ref. 6)

$$EA(n) = EA(R_c) = EA(\infty) - a\,\frac{e^2}{R_c} \qquad (24)$$

where $EA(\infty)$ is the bulk band energy and a = 1/2 for the polarization and a = 5/8 for the metal droplet model of negative metal clusters. The predictions of (24)--as in the case of (5), (10), and (20) we have seen earlier--depend on the accuracy of $R_c$.

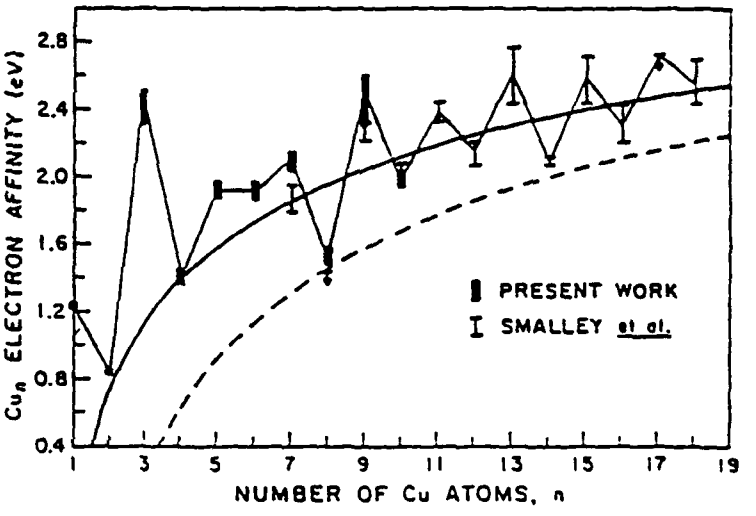


**Figure 21.** Experimental electron affinities for $Cu_n$ compared with predictions of the classical spherical drop model ■ (Ref. 45); I (Ref. 47); --- and —— predicted using Eq. (24) and a = 5/8, EA (∞) = 4.65 eV, $R = n^{1/3} r_s$ (----) and $R = n^{1/3} r_s + \Delta r$ (—— ) with $r_s$ (half the average distance between the atoms in the bulk) = 1.41 Å and Δr (correction for orbital overlap among bounded atoms) = 0.53 Å (from Ref. 45).

[5]An opposite alternation is exhibited by the ionization threshold energy I (i.e., $I_{odd} < I_{even}$) (e.g., see Ref 11).

## REFERENCES


1. Christophorou, L. G., and Siomos, K., Interphase Physics: Linking Knowledge on Electron-Molecule Interactions in Gases to Knowledge on Such Processes in Condensed Matter, in "Electron-Molecule Interactions and Their Applications," Christophorou, L.G., Ed., *Academic Press*, Orlando, 1984, Vol. 2, Chapt. 4.

2. Christophorou, L. G., Gas/Liquid Transition: Interphase Physics, in "The Liquid State and Its Electrical Properties," Kunhardt, E. E., Christophorou, L. G., and Luessen, L. H., (Eds.), *Plenum Press*, New York, 1988, pp. 283-316.

3. Christophorou, L. G., Radiation Interactions in High-Pressure Gases, in "Physical and Chemical Mechanisms in Molecular Radiation Biology," Glass, W. A. and Varma, N. M., Eds., *Plenum Press*, New York, 1991, pp. 183-230.

4. Kunhardt, E. E., Christophorou, L. G., and Luessen, L. H., (Eds.), "The Liquid State and Its Electrical Properties," *Plenum Press*, New York, 1988.

5. Freeman, G. R., (Ed.), "Kinetics of Nonhomogeneous Processes," *Wiley-Interscience*, New York, 1987.

6. Jortner, J., Cluster Size Effects, Z *Phys. D* 24:247 (1992).

7. Kappes, M. M., Schär, M., Radi, P., and Schumacher, E., On the Manifestation of Electronic Structure Effects in Metal Clusters, *J. Chem. Phys.* 84:1863 (1986).

8. Rademann, K., Reactivity and Electron Structures of Isolated Clusters, Ber. Bunsenges. *Phys. Chem.* 94:1295 (1990); Photoelectron Spectroscopy and UV/VIS-Photoabsorption Spectroscopy of Isolated Clusters, Z*Phys. D* 19:161 (1991).

9. Leopold, D. G., Ho, J., and Lineberger, W. C., Photoelectron Spectroscopy of Mass-Selected Metal Cluster Anions. I. $Cu_n^-$, n = 1-10, *J. Chem. Phys. 86:1715 (1987).*

10. Märk, T. D., Free Electron Attachment to van der Waals Clusters, *Intern. J. Mass Spectr. Ion Proc.* 107:143 (1991).

11. Bonačić-Koutecký, V., Fantucci, P., and Koutecký, J., Quantum Chemistry of Small Clusters of Elements of Groups Ia, Ib, and IIa: Fundamental Concepts, Predictions, and Interpretation of Experiments, *Chem. Rev.* 91:1035 (1991).

12. Illenberger, E., Electron Attachment Reactions in Molecular Clusters, *Chem. Rev.* 92:1589 (1992).

13. Christophorou, L. G., "Atomic and Molecular Radiation Physics," *Wiley-Interscience*, New York, 1971.

14. Christophorou, L. G. (Ed.), "Electron-Molecule Interactions and Their Applications," *Academic Press*, Orlando, 1984, Vols. 1 and 2.

15. Christophorou, L. G., The Lifetimes of Metastable Negative Ions, *Adv. Electr. Electron Phys.* 46:55 (1978).

16. Sanche, L., Primary Interactions of Low Energy Electrons in Condensed Matter, in "Excess Electrons in Dielectric Media," Ferradini, C., and Jay-Gerin, J.-P., Eds., *CRC Press*, Boca Raton, 1991, pp. 1-42.

17. Inokuti, M., How is Radiation Energy Absorption Different Between the Condensed Phase and the Gas Phase?, in "Radiation Effects and Defects in Solids," Gordon and Breach, U.K., 117, (1991), pp. 143-162.

18. LaVerne, J. A. and Mozumder, A., Effect of Phase on the Stopping and Range Distribution of Low-Energy Electrons in Water, *J. Phys. Chem.* 90:3242 (1986).

19. Ashley, J. C., Stopping Power of Liquid Water for Low-Energy Electrons, *Rad. Research* 89:25 (1982).

20. Michaud, M. and Sanche, L., Total Cross Sections for Slow-Electron (1-20 eV) Scattering in Solid $H_2O$, *Phys. Rev. A* 36:4672 (1987).

21. Hunter, S. R., Carter, J. G., and Christophorou, L. G., Low-Energy Electron Drift and Scattering in Krypton and Xenon, *Phys. Rev. A* 38:5539 (1988).

22. Dmitrenko, V. V., Romanyuk, A. S., Suchkov, S. I. and Uteshev, Z. M., *Sov. Phys. Tech. Phys.* 28:1440 (1983).

23. Miller, L. S., Howe, S. and Spear, W. E., "Charge Transport in Solid and Liquid Ar, Kr, and Xe," *Phys. Rev.* 166:871 (1968).

24. Sakai, Y., Nakamura, S., and Tagashira, H., Drift Velocity of Hot Electrons in Liquid Ar, Kr, and Xe, *IEEE Trans. Electr. Insul.* , EI-20:133 (1985).

25. Bader, G., Perluzzo, G., Caron, L. G., and Sanche, L., Elastic and Inelastic Mean-Free Path Determination in Solid Xenon from Electron Transission Experiments, *Phys. Rev. B*, 26:6019 (1992).

26. Faidas, H., Christophorou, L. G., McCorkle, D. L., and Carter, J. G., "Electron Drift Velocities and Electron Mobilities in Fast Room-Temperature Dielectric Liquids and Their Corresponding Vapors," *Nucl. Instr. Meth. Phys. Res.* A294:575 (1990).

27. Stephens, J. A., "Comment on Electron Mobility in the Liquid Isomeric Pentanes," *J. Chem. Phys.* 84:4721 (1986).

28. Fano, U., Studies of Slow Electron Action on Condensed Media, *Radiat. Phys. Chem.* 32:95 (1988); Short- and Long-Range Interactions of Slow Electrons in Condensed Matter: Effects of Reflection and Transmission, *Phys. Rev.* B36:1929 (1987).

29. Mills, D. L., Resonant Scattering of Slow Electrons in Molecular Solids: Suppression of the Elastic Beam, *Phys. Rev. B* 45:36 (1992); Resonant Scattering of Electrons in the Presence of Coupling to Phonons, *Phys. Rev. B* 45:13221 (1992).

30. Henkes, W. and Mikosch, F., The Effective Cross Section for Ionization by Electrons of Molecules in Hydrogen Clusters, *Int. J.Mass Spectr. Ion Phys.* 13:151 (1974).

31. Derenzo, S.E., Mast, T. S., Zaklad, H., and Müller, R.A., *Phys. Rev.* A9:2582 (1974).

32. Schmidt, W. F., Electron Conduction Processes in Dielectric Liquids, *IEEE Trans. Electr. Insul.* EI-19:389 (1984).

33. Raz, B. and Jortner, J., Energy of Quasi-Free Electron State in Liquid and Solid Rare Gases, *Chem. Phys. Lett.* 4:155 (1969).

34. Faidas, H. and Christophorou, L. G., "Laser Multiphoton Ionization of Aromatic Molecules in Nonpolar Liquids," *Rad. Phys. Chem.* 32:433 (1988).

35. Faidas, H., Christophorou, L. G., Datskos, P. G., and McCorkle, D. L., "The Ionization Threshold of N, N, N',N'-Tetramethyl-p-phenylenediamine in Dense Fluid Ethane; Effects of Fluid Density and Temperature," *J. Chem. Phys.* 90:6619 (1989).

36. Steinberger, I. T., Photoconductivity, Conduction Electron Energies, and Excitons in Simple Fluids, in Ref. 4, p. 235.

37. Springett, B. E., Jortner, J., and Cohen, M. H., Stability Criterion for the Localization of an Excess Electron in a Nonpolar Fluid, *J. Chem. Phys.* 48:2720 (1968).

38. Bakale, G., Sowada, U., and Schmidt, W. F., *J. Phys. Chem.* 80:2556 (1976).

39. Jaffke, T., Hashemi, R., Christophorou, L. G., and Illenberger, E., Mechanisms of Anion Formation in $O_2$, $O_2$/Ar, and $O_2$/Ne Clusters; the Role of Inelastic Electron Scattering, *Z. Phys. D* 25:77 (1992).

40. Hashemi, R., Jaffke, T., Christophorou, L. G., and Illenberger, E., Role of Inelastic Electron Scattering by $N_2$ in the Formation of $(O_2)_n^-$ Anions in Mixed $O_2$/$N_2$ Clusters, *J. Phys. Chem.* 96:10605 (1992).

41. Christophorou, L. G., Electron Attachment and Detachment Processes in Electronegative Gases, *Contrib. Plasma Physics* 27:237 (1987).

42. Geltman, S., Theory of Threshold Energy Dependence of Photodetachment of Diatomic Molecular Negative Ions, *Phys. Rev.* 112:176 (1958).

43. Sowada, U., and Holroyd, R. A., Laser Photodetachment Spectra of $C_6F_6^-$ in Nonpolar Liquids, *J. Phys. Chem.* 84:1150 (1980).

44. Faidas, H., Christophorou, L. G., and McCorkle, D. L., Laser Photodetachment in Liquids: $C_6F_6^-$ in Tetramethylsilane, *Chem. Phys.* 193:487 (1992).

45. Leopold, D. G., Ho, J., and Lineberger, W. C., Photoelectron Spectroscopy of Mass-Selected Metal Cluster Anions I. $Cu_n^-$, n=1-10, *J. Chem. Phys.* 86:1715 (1987).

46. DeLuca, M. J., Han, C.-C., and Johnson, M. A., Photoabsorption of Negative Cluster Ions Near the Electron Detachment Threshold: A Study of the $(O_2)_n^-$ System, *J. Chem. Phys.* 93:268 (1990).

47. Zheng, L.-S., Karner, C. M., Brucat, P. J., Yang, S. H., Pettiette, C. L., Craycraft, M. J., and Smalley, R. E., Photodetachment Studies of Metal Clusters: Electron Affinity Measurements for $Cu_n$, *J. Chem. Phys.* 85:1681 (1986).